Studies on

some chiral liquid crystal mixtures

A Thesis

Submitted for the Award

of the Degree of

DOCTOR OF PHILOSOPHY

By

Shikha Kapila

Roll No. 9051501

School of Physics and Materials Science
Thapar University
Patiala – 147 004 (INDIA)

June 2010

Jai Sai Ram

With the blessings of Sai Baba ji

This thesis is dedicated to

Er. Ashok Kumar Kapila

My Father, my mentor, my idol, my hero, my family's leader and by far the wonderful and coolest person I will have ever known. We will miss you every moment and will always try to make you proud.

For all the love and happiness, you showered on us

……. *Thanks Papa!*

CERTIFICATE

This is to certify that the thesis entitled **"Studies on Some Chiral Liquid Crystal Mixtures"** which is being submitted by **Ms. Shikha Kapila** in fulfillment of the requirement for the award of the degree of Doctor of Philosophy in the School of Physics and Materials Science, Thapar University, Patiala, is a record of candidate's own work carried out by her under my supervision and guidance. The matter presented in this thesis has not been submitted in part or full for the award of any degree in any other University or Institute.

Prof. K. K. Raina
Deputy Director and Dean (Faculty Affairs)
Distinguished Professor of Physics and Materials Science
Thapar University
Patiala-147004, Punjab

Date:

Place: Patiala

Acknowledgement

The process of scientific research is fraught with ups and downs and success is made possible by the support and assistance of many others, some share a high level of scientific knowledge and offer guidance in the research process, others are kind enough to offer the use of their facilities and some lovingly provide the love and compassion necessary to sustain the researcher through the most difficult of times. I would like to thank all those who have helped make my research fruitful.

First and foremost I would like to express my sincere gratitude to my research supervisor ***Prof. K. K. Raina****, Deputy Director and Dean (Faculty Affairs), Distinguished Professor of Physics and Materials Science, Thapar University, Patiala, who has been a fantastic supervisor and mentor. Thanks to him for greatly enriching my knowledge with his exceptional insights into the rich world of liquid crystals. I had a great experience to learn from his enormous knowledge related not just in liquid crystal & materials science but also in the wide scenario of attitude of living. Despite the numerous demands on his time Prof. Raina always made himself available to discuss research results and offer guidance. In addition he allowed me the independence to explore this area for myself enriching my understanding of research process, bolstering my confidence thus helping me mature as a student and a scientist. His level of commitment to the well being of his students in and outside the laboratory has greatly enhanced my research experience at* Thapar University.

I am thankful to ***Prof. Abhijit Mukherjee****, Director, Thapar University, Patiala, for providing me the entire necessary infrastructure to carry out the experimental work in the School of Physics and Materials Science, financial assistance and lot of opportunity for the interaction with national and international scientists in the various conferences and seminars held during my Ph.D years.*

I am deeply thankful to ***Dr. Susheel Mittal****, Dean, Research & Sponsored Projects, Thapar University, Patiala, for his needful help during my research work.*

I am profoundly obliged to ***Prof. O. P. Pandey****, Head, School of Physics and Materials Science, Thapar University, Patiala for his whole-hearted and tangible*

support during the various stages of my work, which paved the path for successful completion of this research work.

Special thanks go to ***Dr. Kulvir Singh****, Associate Professor, School of Physics and Materials Science, for his constructive suggestions and encouragement in his own amiable way.*

I would like to convey my sincere thanks to ***Prof. N. K. Verma****,* ***Dr. Manoj Sharma****,* ***Dr. Sunil Kumar****,* ***Dr. Puneet Sharma****,* ***Dr. D. P. Singh*** and ***Dr. S. P. Tiwari*** *for their extended help during my tenure as teaching assistant in School of Physics and Materials Science, Thapar University, Patiala.*

My special appreciation and gratitude goes to ***Dr. G. Sumana****, Scientist C, NPL, New Delhi, for her encouragements, technical and scientific advice, constructive suggestions and whole hearted support during my initial years at Thapar University.*

I am thankful to **Dr. S. S. Bawa**, *Scientist G, National Physical Laboratory,* New Delhi, **Dr. S. Krishna Prasad**, *Scientist,Centre for Liquid Crystal Research, Bangalore and* ***Dr. R. Dhar****, Associate Professor and Coordinator, Centre of Material Sciences, University of Allahabad, Allahabad for their valuable technical suggestions during the experimental work.*

I would like to thank all members, former and present, of Liquid crystal group, Material research laboratory, Thapar University. I will never forget their companionship.

I am also grateful for the support of colleagues and friends near and far, who have always been there when I needed them, special thanks to ***Dr. Pankaj****,* ***Mr. Vishal Choudhary****,* ***Dr. Zinki Jindal****,* ***Mr. Ravi K Shukla****,* ***Mr. Sanjeev****,* ***Dr. J. K. Kushwaha****,* ***Ms. Shefali Kanwar****,* ***Ms. Kamalpreet Kaur****,* ***Ms. Neeraj*** *and* ***Ms. Jasmeet****.*

Thanks to our M. Tech. (Materials Science) students (present and past) in Material research lab *for their cheerful company, special thanks and wishes goes to* ***Mr. Sumit Bhardhwaj****,* ***Ms. Sunita****,* ***Mr. Ishan*** *and* ***Mr. Pankaj Chamolli*** *for their great company during my period of thesis writing.*

I also extend my appreciation to ***Parveen Ma'm****,* ***Mr. S. P. Verma****,* ***Mr. Jant Singh****,* ***Mr. V. Kothari*** *and* ***Mr. Indermani Kumar*** *for letting my stay at* School of Physics and Materials Science, Thapar University, Patiala*, a pleasant and memorable experience.*

I would like to acknowledge all the faculty, staff and research students of School of Physics and Materials Science who stood by me in my most challenging moments of life.

In addition, I wish to express my sincere thanks to my respected auntie ***Mrs. Anju Raina****, for all the moral support and compassionate love she offered to push me up in my down times.*

Above all, I owe special gratitude to my respected and ever dearest, mother ***Mrs. Manu Bala Kapila****, sister* ***Ms. Bindu Kapila*** *(Didi deserves a distinct acknowledgment for all the long years from my pre school days to today, shaping my mind during many technical and non-technical discussions along the way) and brother* ***Mr. Anil Kapila*** *(additional thanks to Bhaiya for helping me in all the drawings and printing of the thesis) for their continual support, never ending love and unceasing care through the years..Without their endurance and understanding I would not have survived.*

There are many more fine people who have selflessly enriched me in ways beyond measure, I thank them all.

(Shikha Kapila)

CONTENTS

LIST OF FIGURES

LIST OF TABLES

LIST OF Schemes

ABBREVIATIONS AND SYMBOLS

LC	Liquid crystal
Cryst	Crystal phase
SmA	Smectic A liquid crystal phase
SmC	Smectic C liquid crystal phase
N*	Chiral nematic liquid crystal phase
SmA*	Chiral smectic A liquid crystal phase
SmC*	Chiral smectic C liquid crystal phase
FLC	Ferroelectric liquid crystal
ELC	Electroclinic liquid crystal
PDLC	Polymer dispersed liquid crystal
PIPS	Polymerisation induced phase separation
SIPS	Temperature induced phase separation
TIPS	Solvent induced phase separation
TGB	Twist grain boundary liquid crystal phase
PSCOF	Phase separated composite films
MOO	Molecular orientational order
PLC	Polymer Liquid Crystal
MCPLC	Main chain polymer liquid crystal
SCPLC	Side chain polymer liquid crystal
HTP	Helical twisting power
ITO	Indium tin oxide
DSC	Differential Scanning Calorimeter
OAD	Optically active dopant
OPM	Optical polarizing microscope
POM	Polarizing optical microtexture
CLC	Chiral liquid crystal
Dv.M	Developable modulation
Gr.M	Growing modulation
RGB	Red-green-blue
HSI	Hue-Saturation-Intensity
CNT	Carbon nanotubes
SWCNT	Single walled carbon nanotubes
MWCNT	Multiwall carbon nanotubes
GM	Goldstone mode
SM	Soft mode
T_{NI}	Nematic to isotropic transition temperature
T_{C^*-A}	SmC*- SmA transition temperature
ΔT	Reduced temperature
n	Anisotropy of refractive index
	Anisotropy of the polarizability
	Dielectric anisotropy
	Dielectric strength
C_{air}	Air capacitance

C_s	Stray capacitance
C_{eff}	Effective capacitance
d	Thickness of LC film
p	Pitch of chiral LC
E_{th}	Threshold field for fingerprint texture
E_{uw}	Threshold field for homeotropic texture
k_{22}	Elastic constant for twist deformation
k_{33}	Elastic constant for bend deformation
$_r$	Rise time
$_d$	Decay time
	Dielectric anisotropy
$'$	Dielectric permittivity
$''$	Dielectric loss
ε_0	Static frequency dielectric constant
ε_∞	Infinite frequency dielectric constant
γ_1	Rotational viscosity
Ps	Spontaneous polarization

Overview

This chapter reviews the properties of liquid crystal systems in general and chiral liquid crystal in particular. We have tried to review the impact of chirality on the structure property relationship in liquid crystal mixtures. Induction of phases with helical ordering, phases which can only exist with chirality and induction of polar properties due to induced chirality are all discussed in detail. The technical applications of chiral liquid crystal mixtures are tabulated to quantify the need of basic and applied research in the chiral liquid crystal mixtures. Aim of the present research work is presented at the end of this chapter.

1.1 Liquid crystals

Liquid crystal is a phase of matter intermediate between ordered solid phase and disordered liquid phase. It shows anisotropy in some of its physical properties, while flows like a liquid [1].

1.1.1 Historical background

Austrian botanist, Friedrich Reinitzer in 1888, accidently discovered the liquid crystal phase, which has now grown enormously to become a fascinating, rich interdisciplinary area of study [1]. Some of the historical landmarks in the liquid crystal research are given in Table 1.1.

Table 1.1 Overview of developments in chiral liquid crystal research

Year	Landmarks in LC research	Contributors
1888	Discovery of this intermediate phase	F. Reinitzer [1]
1889	Liquid crystal nomenclature	O. Lehmann [2]
1922	Classification of thermotropic system as nematic, smectic and cholesteric phase	Friedel [2]
1933	Frederiks Transitions	V. Frederiks [8]
1963	Electro hydrodynamic instabilities	R. Williams [9]
1968	Electro optic liquid crystal device	G.H. Heilmeier [10]
	Nematic guest host effect	Heilmeir and Zanoni [10]
	Field induced cholesteric-nematic phase change effect	Wysocki et.al. [11]
1971	Twisted nematic effect	M. Schadet, W. Helfrich and J. Fergason [12]
1972	The analogy between the nematic to smectic A transition in LC and normal to superconductor transition in metals	P. G. de Genes [13]
1975	Ferroelectricity in chiral smectic phase	R. B. Meyer et.al. [14]

1977	The Electroclinic Liquid Crystal (ELC) in smectic A phase	Garoff and Meyer [15]
1977	Discotic phase	S. Chandershekhar et.al. [16]
1979	Electro optic properties proposed in polymer LC gels	P. G. de Gennes [4]
1980	Surface stabilized ferroelectric LC	N. A. Clark and S.T. Lagerwall [17]
1984	Electro optic effect in PDLC system	J. Fergason [18]
1985	Phase separation methods: PIPS, SIPS, TIPS	J. W. Doane [19]
1988	Theoretical model for TGB phase	Renn and Lubensky [20]
1989	Antiferroelectricity in LC	Chandani et.al. [21]
1999	Phase separated composite films (PSCOF)	S. Kumar et.al. [22]
2002	New TGBC structure based on splayed polarization and twisted director structures adopted by SmC in planar align cells proposed	M. Brunet et.al. [23]
	Organizing Carbon Nanotubes with LC	M. D. Lynch and D. L. Patrick [24]
2003	Induced Blue phases by achiral dopant	H. Takezoe et.al. [25]
2004	Liquid crystal–carbon nanotube dispersions	I. Dierking, G.Scalia et.al. [26, 27]
2005	Induction and stabilization of Blue phase on UV Irradiation	A. Chanshvill, G. Chillaya, G. Petriashvili and P. J. Collings [28]
2006	Amplification of chirality in liquid crystals	R. Eelkema and Ben L. Feringa [29]
	Formation of periodic stripe patterns in nematic liquid crystals doped with functionalized gold nanoparticles	Hao Qi and T. Hegmann [30]
2007	Nanoparticles in Liquid Crystals: Synthesis, Self-Assembly, Defect Formation and Potential Applications	Torsten Hegmann et.al. [31]
2008	Chiral photochemical induction in liquid crystals	Teresa Sierra et.al. [32]
	Optically isotropic-nanostructured liquid crystal composite with high Kerr constant	Hirotsugu Kikuchi [33]
2009	Electro-optics of polymer-stabilized blue phase liquid crystal displays	Shin-Tson Wu [34]
	Dispersions of Carbon Nanotubes in Cholesteric LC	L. N. Lisetski et.al. [43]

1.1.2 Classification of liquid crystals

Liquid crystals can be classified on the basis of their structure, phase transition, molecular shape and molecular arrangement as shown in fig. 1.1.

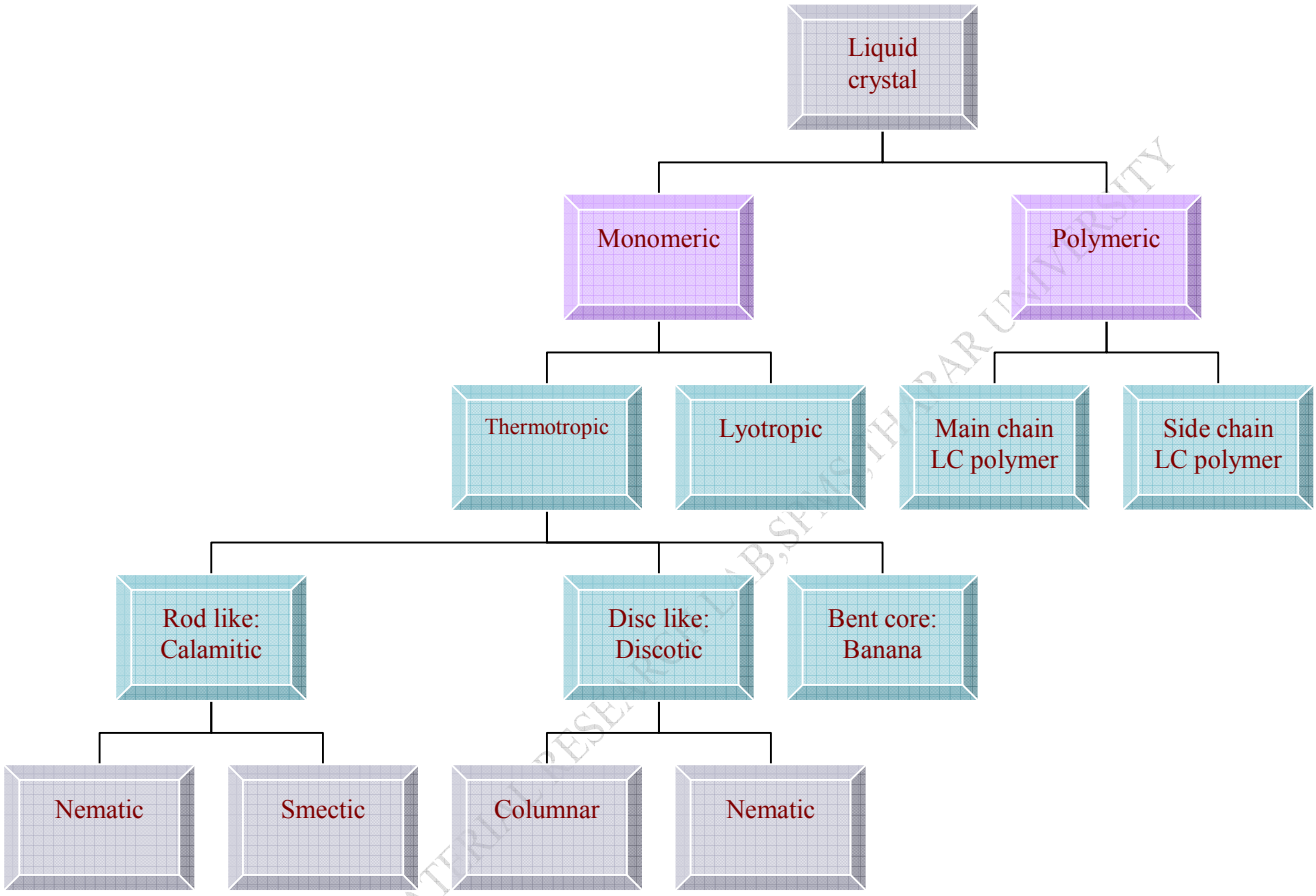

Fig. 1.1 Classification of liquid crystal

The liquid crystals also exist as monomer and polymer forms and depending upon the way of phase transition they can be either thermotropic (in which mesophase transition is temperature dependent) or lyotropic liquid crystal (which categorize liquid crystal with solvent dependent phase transitions) [2]. Their molecules are rod, disc or bent shaped usually and accordingly named as Calamitic, discotic and banana liquid crystal.

Calamitic liquid crystal

In calamitic liquid crystal, the molecular axis is much longer than the other two. The important property for a calamitic or rod like liquid crystal is that the molecule should be rigid for at least some portion of its length, since it must maintain an elongated shape in order to produce interactions that favors alignment [4]. A general molecular structure template for calamitic liquid crystal is shown in fig. 1.2.

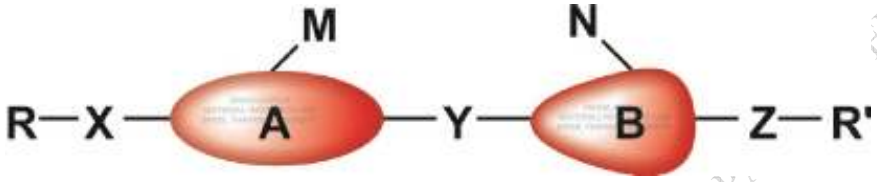

Fig. 1.2 A general structural template for generating single compound calamitic liquid crystal [3]

- A and B are core units, which are some times linked by linkage group (Y) but more often a direct link is used
- The terminal chains (R and R') can be linked to the core, with the groups X and Z but usually the terminal chains are directly linked to the core
- Lateral substituent (M and N) are often used to modify the mesophase morphology and the physical properties of liquid crystal to generate enhanced properties for applications

Nematic phase is the least ordered, having only molecular orientational order (MOO). It differs from the isotropic liquid in that the molecules are spontaneously oriented with their long axes in a preferred direction, known as director ($\hat{n}$) as shown in fig. 1.3. This mesophase owes its high degree of fluidity to the ease with which the molecules slide past one another while still retaining their parallelism [5].

Mesophase	Molecular packing	Molecular order	POM texture
Nematic	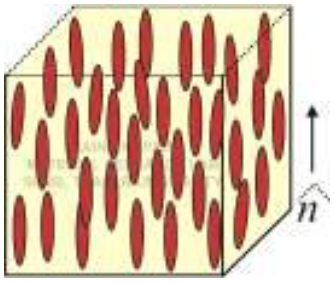	MOO	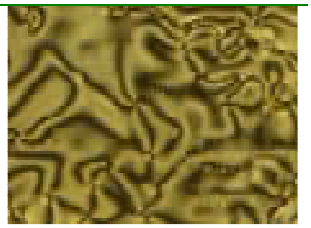 BL036 showing schlieren texture
Smectic A	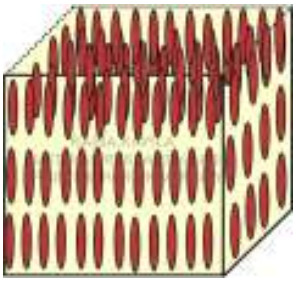	MOO + 1d positional order	 S3 showing fan like texture

Fig. 1.3 Molecular packing in nematic and smectic A liquid crystal mesophase

In smectic phase, the molecules are arranged in stratified structure. It possesses Molecular orientational order (MOO) with the additional positional order. Unlike the nematic phase, the smectic phase exhibits polymorphism [1]. The detailed structure of various smectic phases is shown in fig. 1.4.

Molecular packing	Remarks
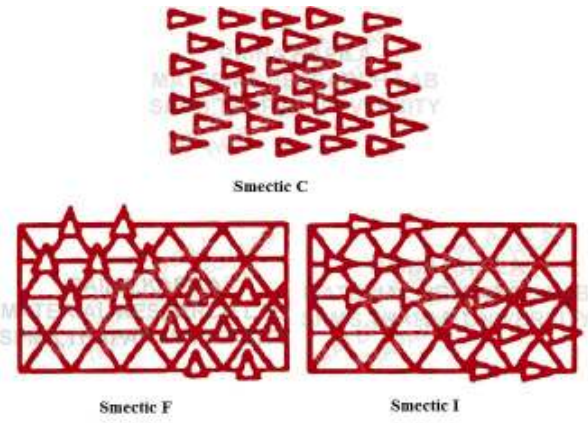	Tilted phases with short range periodic order
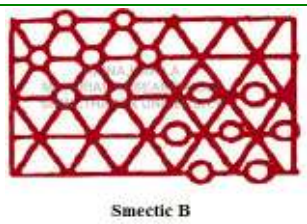	Orthogonal phase with short range periodic order
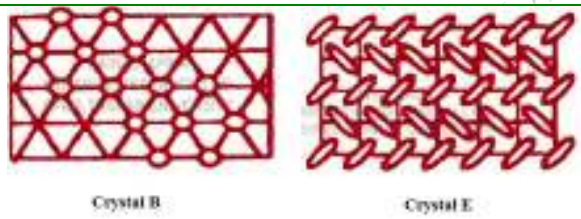	Orthogonal phase with long range periodic order
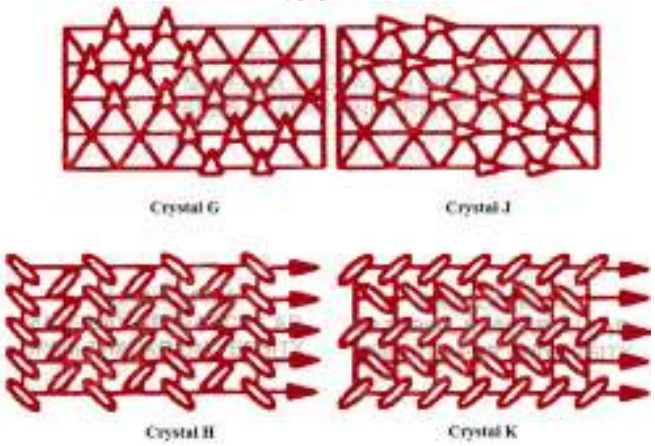	Tilted phases with long range periodic order

Fig. 1.4 Structures of various smectic liquid crystal mesophase [6].

Discotic liquid crystal

In 1977 it was reported by Chandrasekhar that disc like molecules, namely molecules with one molecular axis much shorter than the other two, also form liquid crystal phases [15]. Structurally, most of them fall into two distinct categories, the columnar and the nematic.

Mesophase	Molecular packing	POM texture
Discotic columnar		
Discotic Nematic		

Fig. 1.5 Structure of the disc like molecules [5, 41]

The columnar phase in its simplest form consists of discs stacked one on top of the other aperiodically to form liquid like columns, the different columns constituting a two dimensional lattice shown in fig. 1.5. The nematic phase has an orientationally ordered arrangement of discs without any long range translational order as shown in fig. 1.6 [5].

Polymer Liquid Crystal

Polymer liquid crystals (PLC) combine the properties of liquid crystal and polymer [3]. These hybrids show the same mesophases characteristic of ordinary liquid crystals, yet retain many of the useful and versatile properties of polymers. For normally flexible polymers to liquid crystal display characteristics, rod-like or disk-like elements called mesogens must be incorporated into their chains. The placement of the mesogens plays a significant role in determining the type of PLC that is formed. Main chain polymer liquid crystals (MCPLC) are formed when rigid elements are incorporated into the backbone of normally flexible polymers. These stiff regions along the chain allow the polymer to orient in a manner similar to ordinary liquid crystals exhibiting display liquid crystal characteristics.

Conversely, side chain polymer liquid crystals (SCPLC) are formed when the mesogens are connected as side chains to the polymer by a flexible "bridge" (called the spacer). The molecular arrangement of both MCLCP and SCLCP are shown in fig. 1.6.

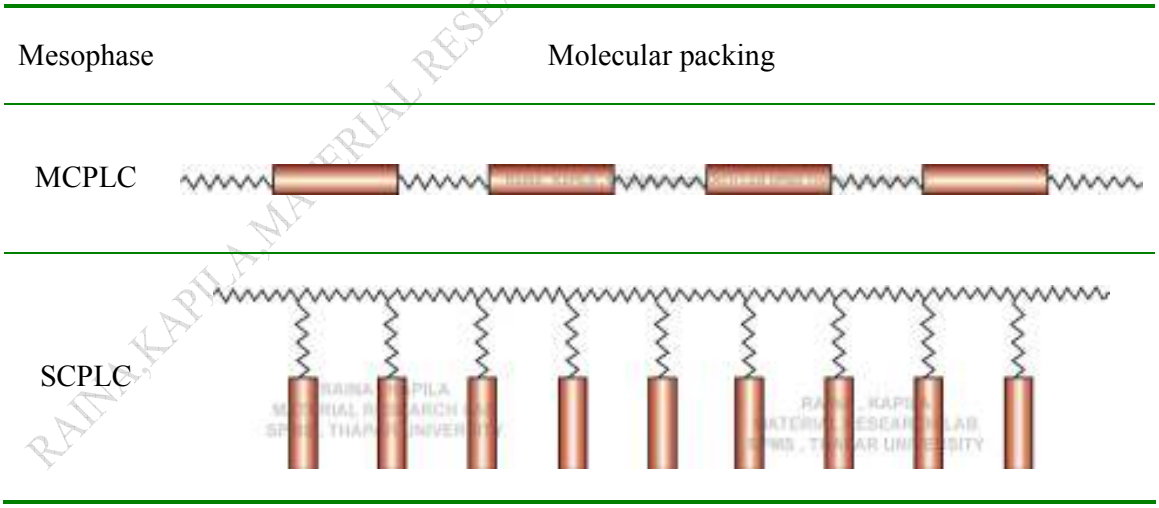

Fig. 1.6 Structure of the polymer liquid crystal [3]

1.2 Chirality

Interest in chiral molecules has continued unabated since last 150 years. The term chirality (originated from Greek vocabulary χείρ (hand)) was first coined by Lord Kelvin:

> "*I call any geometrical figure, or group of points, chiral and say it has chirality if its image in a plane mirror, ideally realized, cannot be brought to coincide with itself.*"

The chirality can be found in systems of all length scales, from elementary particles to macroscopic systems. Due to collective behaviour of the molecules in liquid crystals, molecular chirality has a particularly remarkable influence on the macroscopic physical properties of these systems [6].

1.3 Impacts of chirality in liquid crystals

Chirality is a fascinating subject for liquid crystal research. Molecular chirality is transferred to macroscopic chirality and the resulting effects are:

- ✧ induction of new phases with helical ordering, which are continuously miscible with non-chiral phases
- ✧ new phases, which can only exist with chirality
- ✧ polar properties without changing the phase type

1.3.1 Induction of new phases with helical ordering

A chiral dopant in a nematic phase perturbs the molecular ordering resulting in formation of helical structure. It is also known as chiral nematic (N*) phase. It appears in organic compounds which consist of elongated molecules without mirror symmetry (chiral molecules). The chiral nematic phase occurs in pure chiral compounds and mixtures of achiral nematic with optically active mesogenic or non-mesogenic dopant. Locally it is very much similar to nematic, however the direction of the preferable orientation of the molecules $\hat{n}$ varies periodically in space as shown in fig. 1.7.

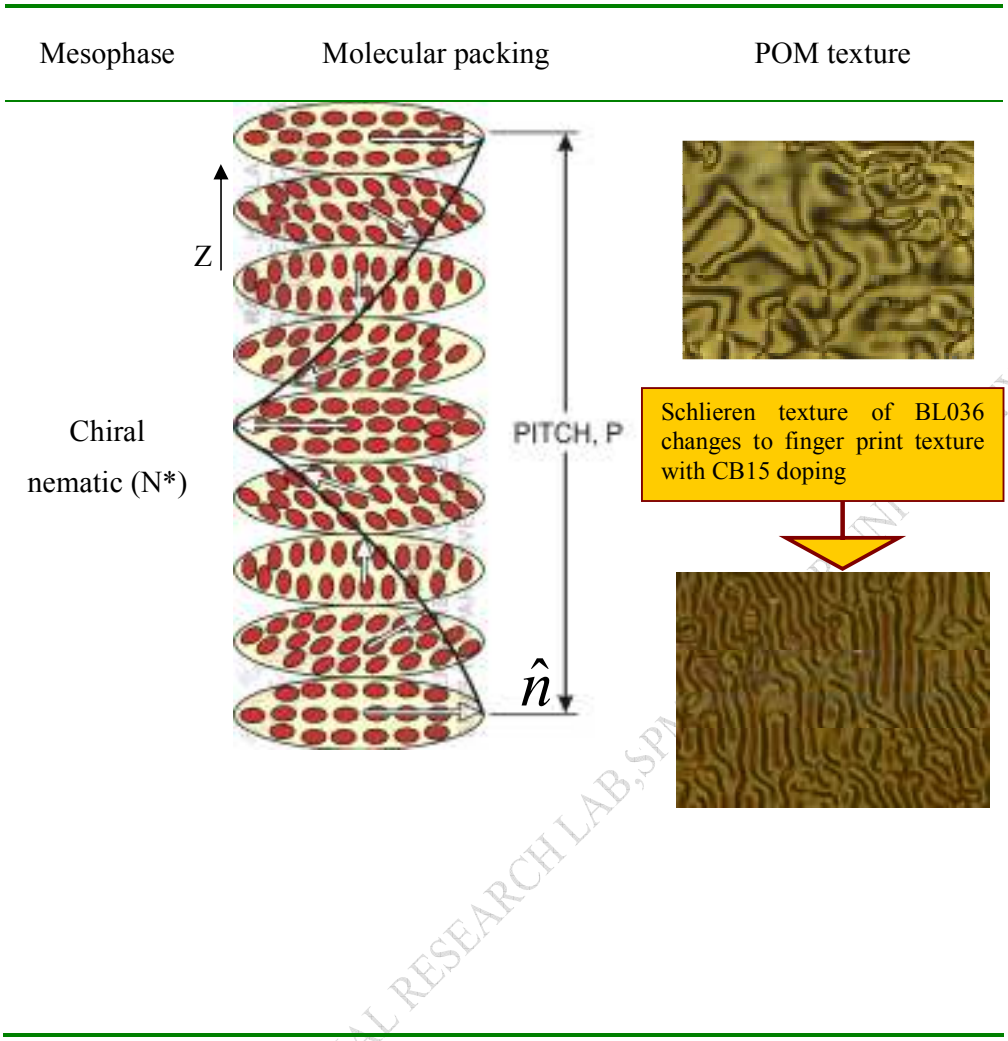

Fig. 1.7 Molecular packing in chiral nematic liquid crystal mesophase [35]

If the helical axis is oriented along z, the director $\hat{n}$ is given as

$$n_x=\cos\theta \quad n_y=\sin\theta \quad n_z=0 \tag{1.1}$$

$$\theta = q_o z + \text{constant} \tag{1.2}$$

helical twist, $q_o = 2$ /p, p is helix pitch.

Structure is periodic along z, with spatial period /q_o. The helix may be right or left handed. In case of chiral liquid crystal, obtained by doping chiral material into nematic liquid crystal, pitch of the mixture is related to concentration of chiral dopant as, 1/p = (HTP) Xc, as given by de Gennes and Prost [2], [where HTP is Helical twisting power and Xc is concentration of chiral dopant]. The helical twisting structure of chiral nematic liquid crystal possesses many interesting optical properties. The temperature

dependence of helical pitch length and thus of selective reflection of light has led to the generation of materials, suitable for encapsulated thermochromic and electrochromic applications, e.g. low cost thermometers, battery testers, textile, inks, paints etc [1].

Similarly when a smectic C phase is formed by chiral molecules, a helical structure appears. The helix is formed by a precession of the director, $\hat{n}$ around the layer normal z, the azimuthal tilt direction changes by a small amount when going from layer to layer as is shown scemetically in fig. 1.8.

Mesophase	Molecular packing	POM texture
Chiral smectic c (SmC*)	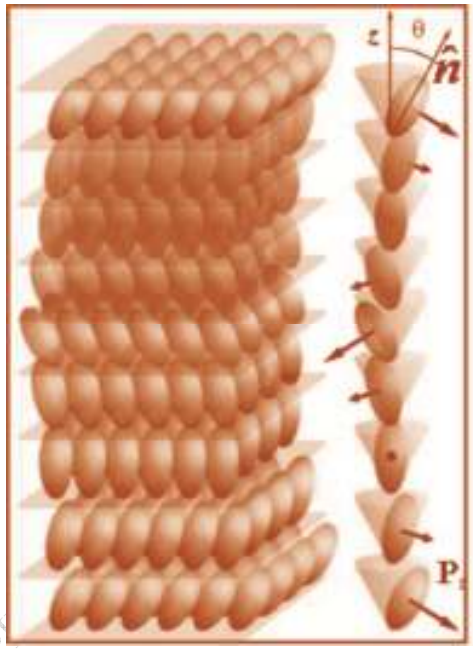	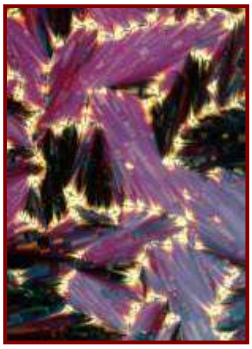

Fig. 1.8. Schematic representation of the periodic helical structures of layers in the smectic C* phase. The pitch of the helix corresponds to the rotation of the director through 360°. The direction of the spontaneous polarization indicated by arrows is orthogonal to the local director. [35]

The director field in such a case is:

$$n_x = \text{Sin}\ \ \text{Cos} \qquad n_y = \text{Sin}\ \ \text{Sin}\ \ , \ \ n_z = \text{Cos}$$

$$\frac{2\ Z}{p_0} \tag{1.4}$$

where p_0 is the pitch (2 rotation) of the helix and the layer normal is along z-direction. There is spontaneous electric polarization Ps in each layer, averaging to zero in macroscopic sample; this phenomenon has great technological implications for very fast-switching ferroelectric light shutters and display devices [6].

1.3.2 New phases, which can only exist with chirality

A chiral dopant can also induce a blue phase from a nematic phase that can only be found for chiral molecules. Blue phases are distinct thermodynamic phases that appear over a narrow temperature range (~1^{o}C) at the helical-isotropic boundary of highly chiral liquid crystals, and sometimes it may be super cooled in chiral nematic phase and observed for the temperature range of more than 10^{o}C. In the absence of electric fields, there can be three blue phases: BPI and BPII, both of which have cubic symmetry and BPIII, which possesses the same symmetry as the isotropic phase. Molecular packing and POM of Blue phase liquid crystal are shown in fig. 1.9(a,b).

Molecular packing	Remarks
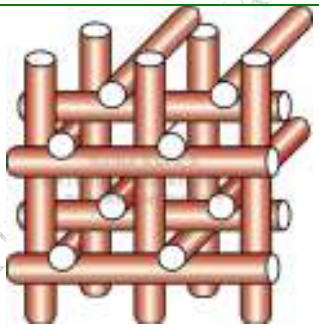	BPI, the cylinders pack into a face-centered cubic structure
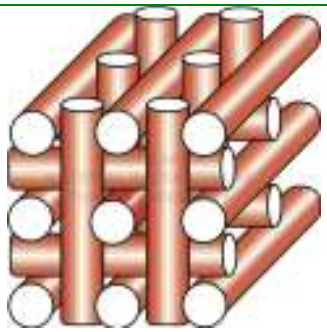	BP II, the cylinders pack into a simple cubic structure

Fig. 1.9 (a) Molecular packing in Blue phase liquid crystal [6]

Fig. 1.9 (b) Blue phase textures viewed under a microscope

Several other blue phases of different cubic symmetry exist but only in the presence of external electric field [6]. Quite recently, there has also been experimental evidence for a smectic blue phase (just like the normal blue phases, but with a smectic-like translational symmetry of the molecular mean positions where the smectic "sheets" are not perfect planes, but instead are hypothetically rotated about an axis, as in a screw) [36] in compounds that lack a helical phase.

Similarly chirality of the system is an essential precondition for the occurrence of twist grain boundary (TGB) phases. TGB phases usually appear in the temperature range between a chiral nematic phase (N*) with short pitch and a smectic phase, typically SmA or SmC*. In particular, they are expected to appear close to a N*/SmA/SmC* triple point [20]. One of their remarkable properties is the selective reflection of circularly polarized light showing the director field has a helical structure similar to the N* phase [37]. On the other hand, X-ray investigations of TGB phases indicate a layer structure as occurring in smectic phases [38]. Fig 1.10 shows the structure of TGB_A phase proposed by Renn and Lubensky, clearly showing a local smectic order and a helical director field at the same time.

Structure	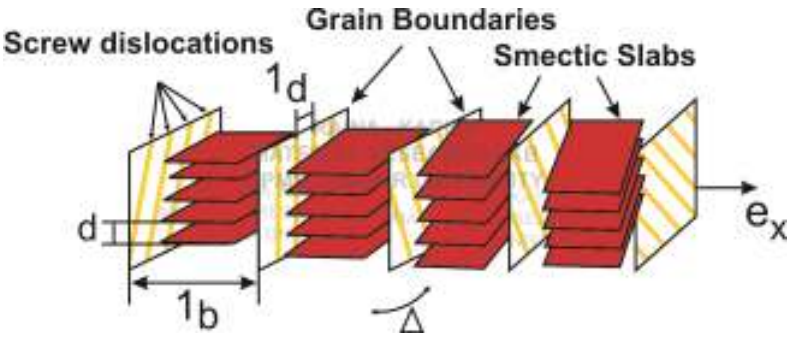
Remarks	Slabs of Sm*A* material of thickness l_b are regularly stacked in a helical fashion along an axis $\mathbf{e}_x$ parallel to the smectic layers. Adjacent slabs are connected by a twist grain boundary made of parallel screw dislocation of average separation l_d

Fig. 1.10 Structure of TGB_A phase proposed by Renn and Lubensky [6]

1.3.3 Polar properties without changing the phase type

Another fundamental type of consequence of chirality is appearance of polar physical properties. A very important property of this type is spontaneous polarization Ps which gives rise to ferroelectric properties of some liquid crystal phases and their electro optical applications. SmC liquid crystals have the following point symmetries:

a) mirror symmetry in the tilt plane of the molecules
b) two fold rotational symmetry about the axis perpendicular to the tilt plane of the molecules, either exactly between layers or exactly mid-layer.

This combination corresponds to the C_{2h} point symmetry group, and also excludes the existence of any net spontaneous polarization in the SmC liquid crystalline phase. However, in the chiral version of the SmC phase, the mirror symmetry is no longer present and only the rotational symmetry remains.

The symmetry group is reduced to C_2. It allows the existence of the spontaneous polarization P_S along the C_2 axis of each smectic layer. The net spontaneous polarization arises due to the lack of rotational degeneracy of the molecules about their

long axes within the smectic layer. Meyer et al, predicted that SmC* liquid crystals are ferroelectric [14].

The chirality of the molecules causes a macroscopic helical structure, such that the C_2 axis (and hence the polarization direction) precesses slowly from one layer to the next. Thus on a macroscopic level there is no net polarization and phase is therefore helielectric. However, in a confined cell geometry the helical structure is suppressed (surface stabilization), and then the system is truly ferroelectric [6].

Smectic A phase of chiral compounds may show electroclinic effect. It is observed in chiral SmA* liquid crystals due to the soft mode [15]. In the SmA* phase, the molecules form parallel layers which are perpendicular to the boundary plates, but they do not have spontaneous tilt. The term "electroclinic" arises because the application of an electric field induces this tilt. These are also called soft-mode ferroelectric – effect liquid crystals. When liquid crystal is cooled down to the SmA*-SmC* phase transition, one of the elastic constants vanishes, softening the restoring force which keeps the molecules perpendicular to the smectic layers. When an electric field is applied the molecules tilt in the plane of the substrate rather than around a tilt cone. The direction of the induced molecular tilt is a function of the polarity of the applied field [8]. The desirable characteristics of the electroclinic liquid crystals are that they exhibit a fast response time, linear response to an electric field and there is absence of the hysteresis of the electro-optical response, which results in continuous grey scale capabilities of the electroclinic light modulators.

1.4 Chiral mesophases with nonchiral Bent-Core molecules

It has been recently shown that nonchiral molecules are capable of forming chiral mesophases. Molecules with a bent core ("banana shaped") can build polar and chiral liquid crystal structures. Bent core molecules form a variety of new phases (B1-B7), which differ from the usual smectic and columnar phases. As a consequence of the polar arrangement, antiferroelectric –like switching was observed in B2 phase formed by bent core molecules. Some POM of mesophases formed by bent core molecules are shown in fig. 1.11.

Matsunaga and co-workers synthesized some banana liquid crystal materials and found that they can form smectic liquid crystal but they did not pay any attention to the electrical properties [39]. Watanable et al. reported that a ferroelectric smectic phase with C_{2v} symmetry might be formed for some chain types of LC polymers, if two different aliphatic spacers with odd numbers of carbons are incorporated into the backbone in regularly

alternating fashion and they segregate into different mono domains [40]. They prepared homologous series of banana shaped molecules, which form the SmAb, HexBb and smectic blue phase in order of decreasing temperature, and then discovered the ferroelectricity in the SmAb and HexBb phases. They reported spontaneous polarization more than 150 nC/cm^2, even in the higher order smectic phase below the SmAb phase, and concluded that this phase is also ferroelectric. Another remarkable property of the nonchiral bent core molecules is the appearance of phases which probably possess some kind of helical super structure [41].

POM texture	Remarks
	The intercalated smectic (B_6) phase growing from the nematic phase
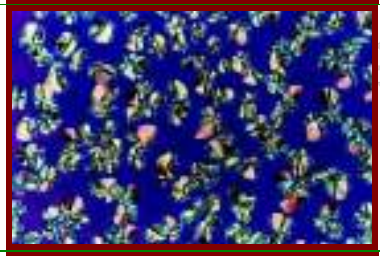	The antiferroelectric B_2 phase growing from the well aligned nematic phase
	The electro-optically switchable B_7' phase developing from the isotropic phase

Fig. 1.11 POM of mesophases formed by bent core molecules [42]

1.5 Technical applications of chiral liquid crystal:

Chirality in liquid crystal has been the subject of intense research in recent years, and is directly responsible for important technological applications, namely the thermo chromic effect of chiral nematic liquid crystal, the ferroelectric and anti ferroelectric switching of smectic liquid crystals. Some of the key applications of chiral liquid crystal are tabulated in Table 1.2, however many more uses of these systems is being explored for display devices.

Table 1.2 Applications of chiral liquid crystals [1-8]

Display	Medical	Optical data processing	Industry	Art
PC	Thermometer	Light Valves	Non destructive testing	T-Shirts
Projection display	Cancer Screening	Shutters	Refrigerators	Pots
Mobile	Mood Rings	Deflectors	Aero plane Wings	Cards
Large Area Inf. Board	BP Indicators	Spatial Light Modulators	Temperature sensors	Paintings
Laptops	Tumor	Logic Elements		Enamels
Handy Cam	Screening	Optical filters		Jewelry
Palmtop				
Stereoscopic systems				

1.6 Aim of the present research work:

Chiral LCs is one of the fastest growing areas of research in liquid crystal science and technology. The exciting nature of the chirality induced liquid crystal mixtures constantly motivates a chemist to synthesize optically pure novel materials from pro chiral substrates. A physicist needs to investigate the cause of appearance of them on the basis of various physical parameters. Although chiral liquid crystal systems have been studied in great detail but several questions are still unanswered. Very little effort has gone into understanding the behaviour of interactions of chiral molecules with host and how it influences the electro-optic performance of the material. Similarly the interactions of carbon nanotubes with chiral liquid crystal mixtures are still in its infancy period. The present research work is formulated on such gaps to find appropriate answers to some of these questions. The electro-optic, dielectric and thermochromic analysis of chirality induced liquid crystal mixture has been performed in detail to understand the basic facts. The effect of carbon nanotubes on the morphological and dielectric spectra of chiral liquid crystal mixture composite has been investigated to answer some of these questions.

The satisfaction of the scientific appetite for this complex and challenging area of the condensed matter physics was the main aim to precede this research work.

References:

[1] P. J. Colling and M. Hird, *Introduction to Liquid Crystal: Chemistry and Physics*, Taylor and Francis Ltd (1997)

[2] P. G. de Gennes, *The Physics of Liquid Crystal*, Oxford University Press (1975)

[3] P. J. Colling, *Liquid Crystal: Nature's Delicate Phase of Matter,* Pricenton: University Press (1990)

[4] P. S. Pershan, *Structure Of Liquid crystal Phases*, World Scientific publishing Co. Pt. Ltd. (1988)

[5] S. Chandrasekhar, *Liquid Crystal 2nd Edn. Cambridge*: Cambridge University Press (1992)

[6] H. S. Kitzerow and C.Bahr, *Chirality in Liquid Crystals*, Springer (1996)

[7] L. M. Blinov and V.G.Chigrinov, *Electrooptic Effects in Liquid Crystal Materials*, Springer-Verlag (1994)

[8] V. Frederiks and V. Zolina, *Trans. Faraday Soc.* 29, 919 (1933)

[9] R. Williams, *J. Chem. Phys*. 39, 384(1963)

[10] G. H. Heilmeier, L. A. Zanoni and L. A. Barton, *Proc. IEEE* 56,1162 (1968)

[11] J. J. Wysocki, J. Adams and W. Haas, Phys. *Rev. Lett.* 20, 1024 (1968)

[12] M. Schadt, *Liquid Crystals* 5(1), 57 (1989)

[13] P. G. de Gennes, *Solid St. Commun*. 10, 753 (1972).

[14] R. B. Meyer, L. Leibert, L. Strzelecki and P. Keller, *J. Phys. Lett. (Paris)* 36, *Liquid Crystal* 69 (1975)

[15] S. Garoff and R. B. Meyer, *Phys. Rev. Lett*. 38, 848 (1977).

[16] S. Chandershekhar, B.K. Sadashiva and K.A. Suresh, *Pramana* 9, 471 (1977)

[17] N. A. Clark and S. T. Lagerwall, *Appl. Phys. Lett*. 36, 899 (1980)

[18] J. L. Fergason, *SID Digest*, 68-70 (1985)

[19] J. W. Doane, N. A. Vaz, B. G. Wu and S. Zumer, *Appl. Phys. Lett.* 48, 269-71 (1986)

[20] S. R. Renn and T.C. Lubensky, *Phys. Rev. A* 38, 2132 (1988).

[21] D. L. Chandani, Ewa Gorecka, Yukio Ouchi, Hideo Takezoe and Atsuo Fukuda, Jpn. *J. Appl. Phys*. 28(7), 1265 (1989)

[22] S. Kumar and V. Vorflusev, *Science,* 283, 1903 (1999)

[23] M. Brunet, L. Navailles and N. A. Clark, *Eur. Phys. J.E* 7, 5 (2002).

[24] M. D. Lynch and D. L. Patrick, *Nano Lett.* 2, 1197 (2002).

[25] M. Nakata, Y. Takanishi, J. Watanabe and H. Takezoe, *Phys. Rev. E*, 68, 041710 (2003)

[26] I. Dierking, G. Scalia, P. Morales, and D. LeClere, *Adv. Mater. (Weinheim Ger.)* 16, 865 (2004).

[27] I. Dierking, G. Scalia, P. Morales, J. *Appl. Phys.* 97, 044309(2005)

[28] A. Chanishvill, G. Chilaya, G. Petriashvili and P. J. Collongs, *Phys. Rev. E* 71, 051705 (2005)

[29] R. Eelkema and B. L. Feringa, *Org. Biomol. Chem.* 4, 3729(2006)

[30] H. Qi and T. Hegmann, *J. Mater. Chem.* 16, 4197(2006)

[31] T. Hegmann , H. Qi and V. M. Marx , *Journal of Inorganic and Organometallic Polymers and Materials* 17,483(2007)

[32] R. M. Tejedor,a Luis Oriol,a Jose´ Luis Serranob and T. Sierra, *J. Mater. Chem.*18, 2899 (2008)

[33] S. W. Choi, S. I. Yamamoto and Y. Haseba, H. Higuchi and H. Kikuchi, *Appl. Phys. Lett.* 92, 043119(2008)

[34] Z. Ge, S. Gauza, M. Jiao, H. Xianyu, and S. T. Wu, *Appl. Phys. Lett.* 94, 101104 (2009)

[35] J. W. Goodby *J. Mater. Chem.1 (*3), 307(1991)

[36] B. Pansu, E. Grelet, M. H. Li and H. T. Nguyen, *Phys. Rev. E* 62, 658-666, (2000)

[37] J. W. Goodby, M. A. Waugh, S. M. Stein, E. Chin, R. Pindak and J. S. Patel, *Nature* 337, 449(1989)

[38] G. Srajer, R. Pindak, M. A.Waugh, J. W. Goodby and J. S. Patel, *Phys. Rev. Lett.* 64, 1545(1990)

[39] T. Akutgawa, Y. Matsunaga and K. Yasuhara, *Liq. Cryst.* 17,659(1994)

[40] T. Niori, T. Sekine, J. Watanabe, T. Furukawa and H. Takezoe, *J. Mater. Chem* 6, 1231(1996)

[41] G. Heppke and D. Moro, *Science* 279,1872(1998)

[42] Raman Research Institute website

[43] L. N. Lisetski, Mol. *Cryst. Liq. Cryst.,* 510, 43(2009)

Overview

This chapter describes the experimental design and characterization techniques to study the various chiral liquid crystal sample cells and their physical parameters. A thermal polarizing microscope has been used to identify the different mesophases through optical texture. The characteristics of the liquid crystals materials used in the experiments, along with their molecular structures and description of instruments are provided in brief.

2.1 Selection of material:

In the present work, the electro optic, dielectric and thermochromic properties of chirality induced nematic liquid crystal were studied in detail. For this purpose, we used 4-pentyl-4'-cynobiphenyl (commercially available as BL036) as nematic material due to its broad temperature range. Its molecular structure, phase sequence and its main physical properties are tabulated in table 2.1.

Table 2.1 Preliminary data of nematic liquid crystal mixture BL036 [1]

Molecular structure	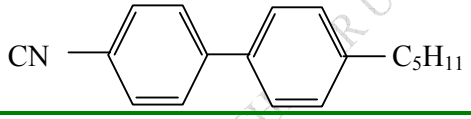	
Phase Sequence	Nematic (N) $\xrightarrow{99\ ^{\circ}C}$ Isotropic (I)	
Optical anisotropy (20^{o}C)	$\Delta n = 0.27$	$n_e=1.79$ $n_o=1.52$
Dielectric anisotropy (20^{o}C)	$\Delta\varepsilon = +17$	$\varepsilon_{ll}=23.10$ $\varepsilon_{\perp}=6.1$

We induced chirality in to this mixture for which the selection of appropriate chiral dopant was an important factor. A good chiral dopant is expected to possess [2]:

- ✧ Mesogenity, stability, solubility, Polarity and Effective mesogenic chirality

Good chiral dopants need to be fitted in most of the above categories. We used the CB15 (Merck, Darmstadt, Germany) as it full filled above characteristics. Its molecular structure and phase sequence is as shown in table 2.2.

Table 2.2 Molecular structure and phase sequence of chiral dopant CB15 [3]

Molecular structure	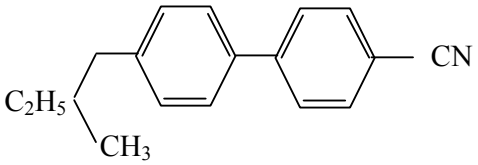
Phase Sequence	Crystal $\xrightarrow{4\ ^oC}$ SmA $\xrightarrow{-54\ ^oC}$ N* $\xrightarrow{-30\ ^oC}$ Isotropic

We also investigated the effects of multiwall carbon nanotubes (MWCNT) on the morphological and dielectric behaviour of chiral liquid Crystal. We used eutectic chiral smectic c liquid crystal mixture (ZLI-4237-100) (E-Merck Darmstadt) as host material and the low concentration of MWCNTs were dispersed in the host chiral smectic C LC to prepare a homogeneous composite system. The material parameters of both chiral smectic c LC mixture and MWCNT are given in Table 2.3.

Table 2.3 Material parameters of chiral smectic c LC mixture and MWCNT [4, 5]

Materials	***Properties***	***Values***
SmC* mixture ZLI-4237-100 (E-Merck) at 20°C	Phase sequence	Crystal $\xrightarrow{-20\ ^oC}$ SmC* $\xrightarrow{61\ ^oC}$ SmA $\xrightarrow{73\ ^oC}$ N* $\xrightarrow{83^oC}$ Isotropic
	Spontaneous Polarization (nC/cm^2) d=5 µm	~ 20
	Tilt angle(°)	~ 24.5
	Pitch (m)	~ 10
MWCNT (M/S Aldrich)	Diameter(nm)	110-170
	Length(micron)	5-9
	Purity (%)	90+

2.2 Cell fabrication technique

2.2.1 Preparation of chiral LC mixture

The mixtures were prepared by doping CB15 in BL036 in different wt/wt ratio in a vial. To ensure proper mixing, the mixtures were first heated to isotropic temperature of the liquid crystal and then shaken to ensure proper mixing and miscibility.

2.2.2 Cell fabrication

The sample cells were made of transparent, conducting indium tin oxide (ITO) coated glass substrates with resistivity of the order of 140-180 ohm-m. The substrates were initially washed with soap solution, rinsed with acetone (purity 99.9%) and distilled water. They were dried in a vacuum chamber and put in dust free (laminar flow) chamber (shown in fig. 2.1) to ensure proper cleaning conditions.

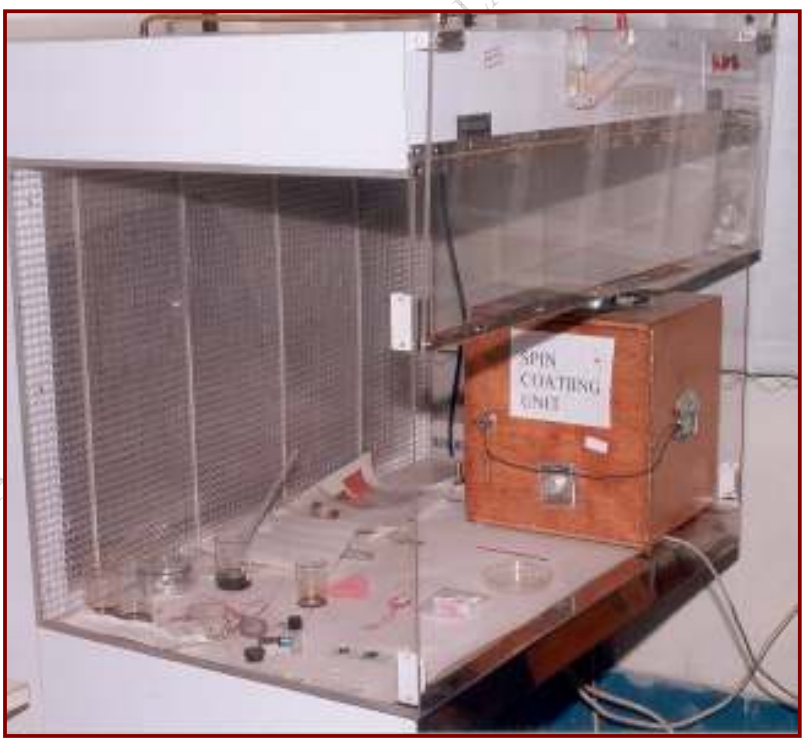

Fig 2.1 Laminar flow chamber

In order to obtain planar alignment, nylon6/6 solution was spin coated on the conducting side of ITO coated glass substrates and then buffed at optimum temperature in an oven for about an hour. The substrates were then rubbed unidirectionally using nylon cloth to induce planer alignment [6-7]. The conducting sides of these ITO coated glass substrates were joined together and separation between the substrates was maintained with the help of mylar spacer (thickness 5-10 μm). The two surface treated glass plates were sealed with optical adhesive (Norland polymer), and cured in presence of UV light. The electrodes were connected at the ITO coated substrate surface of the cell using indium (metal) ingot to obtain better electrical contact. We also used some commercial homogeneous (planar) cells of thickness 5 m, procured from M/S Linkam Instruments, UK.

The CLC mixtures were filled in between ITO coated cells through capillary action by heating the mixture to its isotropic phase in a dust free environment chamber. The cell assembly was then sealed completely to avoid any contaminations. The pictorial view of the cell construction is shown in fig. 2.2.

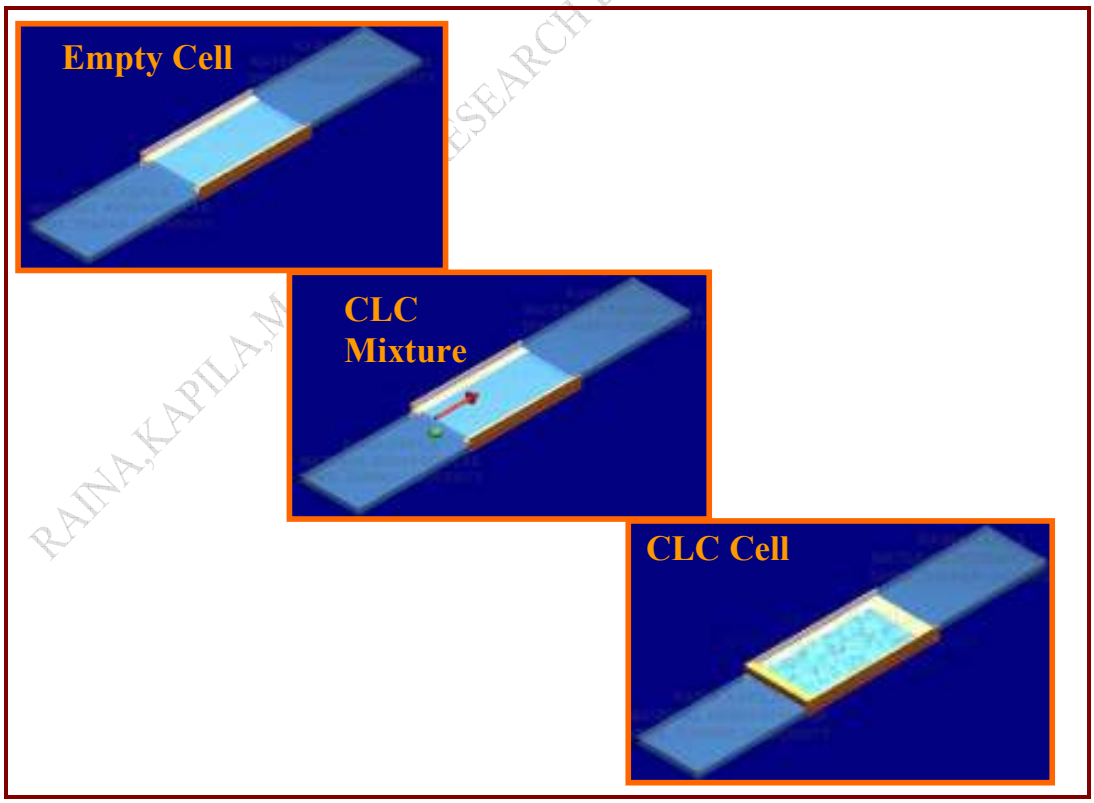

Fig 2.2 Assembled LC Cell

2.3 Method of preparation of MWCNT dispersed SmC* LC

First of all MWCNT dispersed CLC was prepared by mixing CNT in chiral SmC* liquid crystal mixture (ZLI-4237-100) in different wt/wt ratio. The mixture was shaken manually and the homogeneity of the dispersion thus obtained was ensured under polarizing microscope. Fig 2.3 (a) shows optical texture of the SmC* mixture with 0.1% CNT at 10X prepared manually by shaking the compound which clearly indicates need of a homogeneous dispersion method. For achieving homogeneous dispersion and to avoid the agglomeration, the mixture was sonicated at 42 kHz (60^0 C) for about an hour. Fig 2.3 (b), shows 0.1% CNT dispersed composite after sonification, in which we observe a nearly uniform dispersion of CNT. This mixture was filled in a 5μm empty ITO coated cell by capillary action at the isotropic temperature and the sample cell was viewed through the polarizing microscope (OLYMPUS BX-51P) interfaced to LINKAM-TP94 temperature controller and THMS600 hot stage with an accuracy of ±0.1°C.

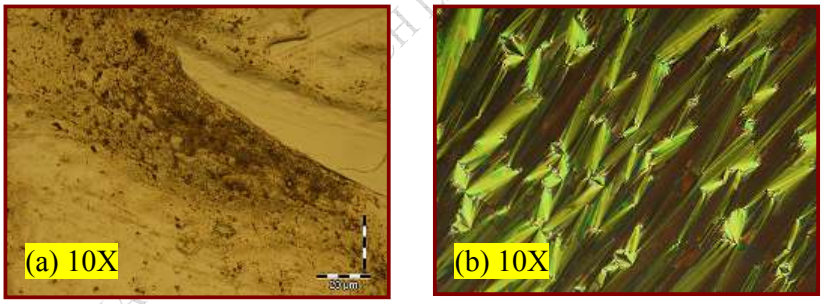

Fig. 2.3 Optical micrographs of 0.1% MWCNT in SmC* (a) with manual shaking (b) after sonication at room temperature.

2.4 Experimental techniques

The liquid crystal texture morphology and phase transition temperatures were noticed using Olympus polarizing microscope (Model- BX51P) fitted with digital camera (DP12). The temperature was controlled through programmer cum hot stage (Linkam Model TP94 and THMS 600) in the wide temperature range -196^0C – 600^0C. The electric field was applied to the sample through Scientech function generator (Model

ST 4060) and Philips function generator (Model FG8002). Electronic Weighing Balance (Sartorius Model CP225D, 0.01 mg –220g) was used for weighing purpose.

A block diagram of our experimental set-up for the investigation of phase behaviour, electro-optic properties and other liquid crystal parameters is shown in fig. 2.4(a). The temperature of the sample cell was controlled using temperature controller interfaced with computer through RS232 port and the output response as a function of field was recorded on a Tektronix Oscilloscope (Model TDS-2024). The snapshot of the experimental set-up to study electro-optical properties is shown in fig. 2.4(b).

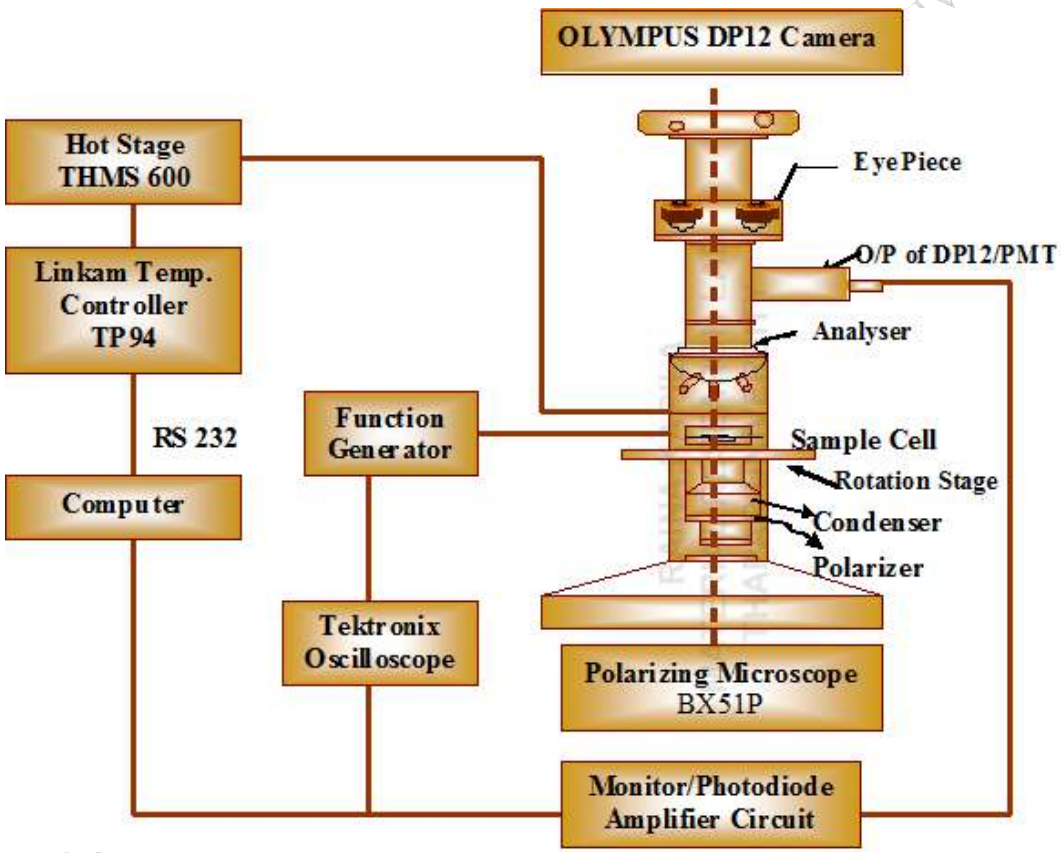

Fig. 2.4(a) Block diagram of experimental set-up for the investigation of optical textures and electro-optic properties of chiral liquid crystal

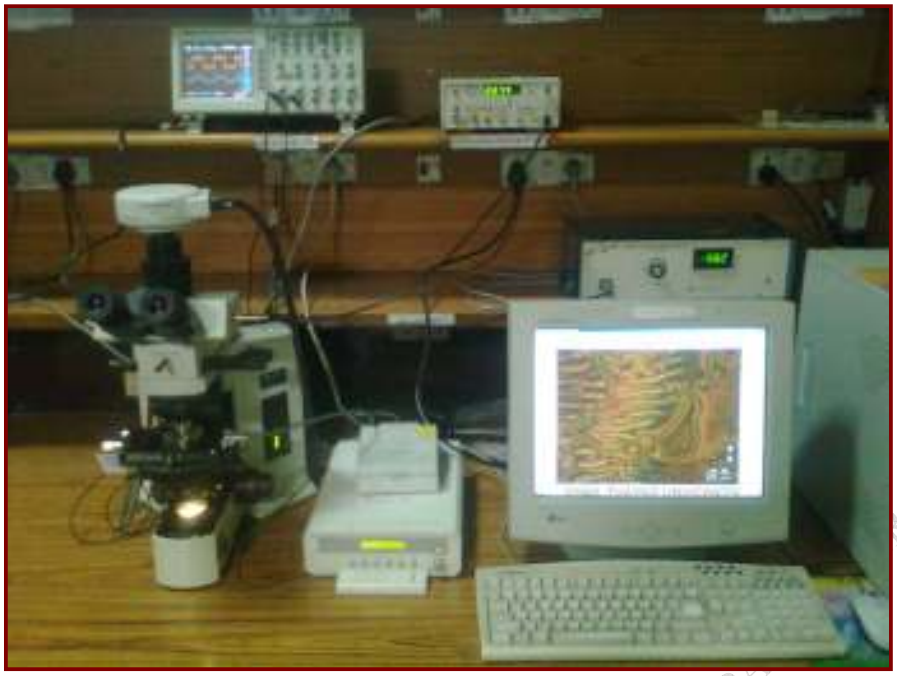

Fig. 2.4(b) Experimental set-up for the investigation of optical textures and electro-optic properties of chiral liquid crystal

2.4.1 Thermodynamical study

Fig 2.5 Differential scanning calorimeter (Lineseis DSC L63)

Thermodynamical parameters of the materials studied were determined with the help of Differential Scanning Calorimeter (Linseis model L63, Germany) shown in the fig. 2.5, controlled by a compatible computer running the LINESEIS DSC instrumental software. The output of this power compensated DSC is a plot of the power difference to the two simple holders, plotted against temperature called a thermogram. The melting of a liquid crystal mixture, an endothermic process is indicated by positive spike on the thermogram.

Prior to taking the measurements, the DSC was calibrated by running a standard material, indium. Each sample was left in the sample pan till we ensured that thermal equilibrium was reached. Then the temperature was allowed to run from room temperature to isotropic of each sample at 5ºC/min. The thermogram thus obtained was used to determine the transition temperatures of liquid crystal mixtures with measurement accuracy of ± 0 to 2 K. It has working temperature range between – 190^{o}C to 700^{o}C, maximum temperature is limited to 600^{o}C due to use of aluminum pans [8].

2.4.2 Temperature programmer and hot stage

In thermal microscopy studies, we used Linkam temperature programmer TP94 and hot stage THMS 600 shown in fig. 2.6. The TP94 is specifically designed for precise temperature control of the Linkam heating/freezing stages with accuracy ± 0.1^{0}C [9].

Fig. 2.6 Linkam temperature programmer TP94 and hot stage THMS 600

The stage sensor is digitally linearized to give accurate temperature readout, the controls and their functions have been carefully chosen for simple and easy operation. The temperature range is –196^{o}C to 600^{o}C. Heating or cooling rates can be changed almost instantly using the three rate keys. The heat ranges are

- from 0.1 to 0.9^{o}C/min at 0.1 degree intervals
- from 1.0 to 9.0^{o}C/min at 1.0 degree intervals
- from 10^{o}C to 90^{o}C/min at 10 degree intervals

A varying dc signal is used to control the stage and results in an even application of power that avoids the bursts seen with conventional burst fire ac techniques. An optional remote control gives single key control of three programmable heating/cooling rates and the HEAT, COOL and HOLD functions. The three programmable heating/cooling rates are held in memory when power is switched OFF. The temperature and limit values can also be stored and recalled using the remote control facility.

2.4.3 Optical polarizing microscopy

The optical studies in sample cells were investigated in transmission mode using an Olympus optical polarizing microscope (Model BX51P) fitted with digital camera (DP12) at 10X magnification under crossed polarizer using long working distance objective lens at 10X. The optical micro-textures of LC materials were also investigated as a function of temperature, voltage and other physical parameters.

2.4.4 Pitch measurement:

The pitch of the CLC sample was measured using OLYSIA BioReport software through the finger print texture measurements [10-12] and using bowed reverse twist disclination lines [13].

For the measurement, the textures of the CLC sample were recorded using an Olympus optical polarizing microscope (Model BX51P) fitted with digital camera (DP12), at 10X magnification under crossed polarizer.

2.4.5 Dielectric studies

Block diagram of experimental setup for the dielectric measurements in the frequency range 50 Hz to 1 MHz is shown in fig. 2.7. The setup consists of hot stage cum programmer temperature controller, Fluke PM 6306 RCL meter and a polarizing microscope (Olympus BX-51P). Using this setup, the real and imaginary parts of the complex dielectric permittivity have been studied as a function of frequency, temperature and external bias.

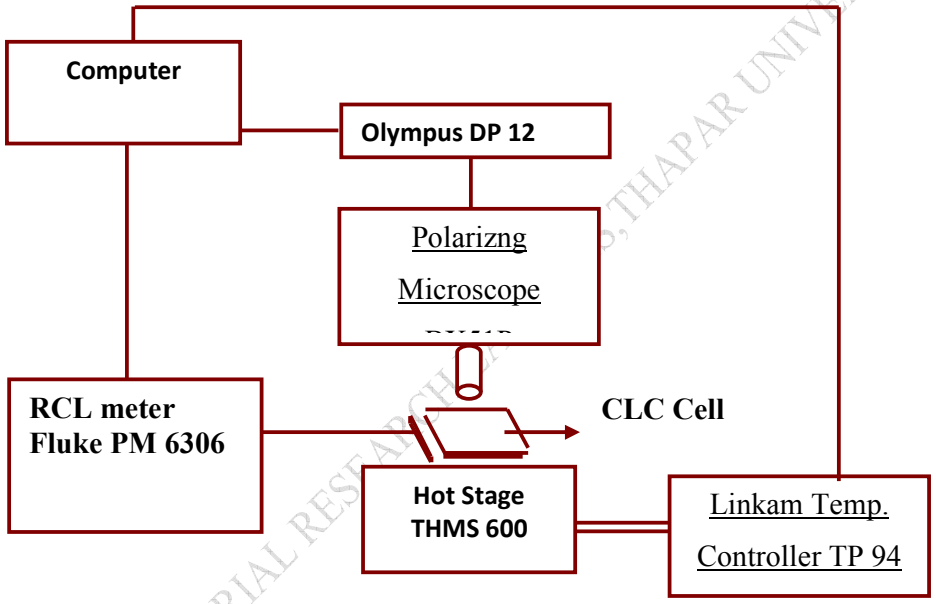

Fig 2.7 Block diagram of experimental set-up for the investigation of dielectric properties of chiral liquid crystal

2.4.5. (a) RCL Meter

The complex dielectric permittivity was carried out using a Fluke PM 6306 programmable automatic RCL meter. It is fully automatic, high performance test instrument designed to measure wide range of impedance parameters capacitance (C) dissipation factor (D), impedance (Z), inductance (L), resistance (R), Q = 1/D, conductance as well as gain, phase angle and group delay. Frequency range of measurement is from 50 Hz to 1 MHz. The measurement display section provide direct read out of the selected measurement parameters along with the appropriate units. Oscillator signal of the RCL meter is adjustable between 5 mV to 1 Vrms values. An

internal dc bias can also be applied from 0V to ± 10V. RCL meter is based on the principle of auto balancing bridge. The measurement Range of RCL meter (Fluke PM 6306) is given in Table 2.4.

Table 2.4 Measurement Range of RCL meter (Fluke PM 6306) [14]:

Parameter	Measurement Range	Max. Resolution
C	0.00 pF to 1/(× 0.1 m), f 50 KHz 0.00 pF to 1/(× 0.1 m), f > 50 KHz	0.01 pF
D	0.000 - 1000	0.001
L	0.00 H - 200 /	0.01 F

2.4.5. (b) Calibration of the dielectric cells

Our dielectric cell consists of a parallel plate capacitor connected with relatively short leads. When condenser was filled with the air as a medium (C_{air}), it has a contribution from the capacitance of the active area of the plates. The stray capacitance (C_s) arises from the leads and the non-homogeneities of the field lines at the edge of the active area. The spacer does not contribute to the capacitance because they are placed outside the active area. In this case, C_{air} can be written as:

$$C_{air} = C_{eff} + C_s \quad (2.1)$$

Where, C_{eff} is the effective capacitance of the empty cell.

To determine the C_{eff} , standard liquids (pure benzene) with known dielectric permittivity has been used. The capacitance of the cell filled with benzene as a medium (having dielectric permittivity $'_B$) is

$$C_B = {}'_B\, C_{eff} + C_s \tag{2.2}$$

from Equation (2.1) and Equation (2.2) C_{eff} can be calculated.

$$C_{eff} \quad \frac{C_B \quad C_{air}}{{}'_B \quad 1} \tag{2.3}$$

We have also estimated C_{eff} from the geometry of the parallel capacitor (cell). The values of Ceff determined from measurement made on the standard liquids agree within 1% with estimated value. Values of capacitance (C_{air}) and loss (D_{air}) with air when subtracted from the capacitance (C_m) and loss (D_m) with the liquid crystal material as dielectric medium at corresponding frequency and temperature give the dielectric permittivity (${}'_m$) and dielectric absorption (${}''_m$) of the liquid crystal material according to equations,

$${}'_m \quad \frac{C_m \quad C_{air}}{C_{eff}} \quad 1 \tag{2.4}$$

and

$${}''_m \quad \frac{C_m D_m \quad C_{air}\, D_{air}}{C_{eff}} \tag{2.5}$$

where ${}'_m$ and ${}''_m$ are the real and imaginary component of the complex permittivity of the liquid crystal material.

REFERENCES

[1] Merck data sheet of BL036

[44] H. S. Kitzerow and C. Bahr, *Chirality in Liquid Crystals*, Springer (1996)

[45] Merck data sheet of CB15

[46] Merck data sheet of ZLI-4237-100

[47] Aldrich data sheet of MWCNT

[48] J. K. Ahuja and K. K. Raina, *Jpn. J. Appl. Phys*., **39** (2000) 4076

[49] J. K. Ahuja, Ph.D Thesis, Thapar Institute of Engineering and Technology (2000)

[50] Manual of Differential scanning calorimeter (Lineseis DSC L 63)

[51] Manual of Linkam temperature programmer TP94 and hot stage THMS 600

[52] P. J. Colling and M. Hird, *Introduction to Liquid Crystal: Chemistry and Physics*, Taylor and Francis Ltd (1997)

[53] S. Chandrasekhar, *Liquid Crystal 2nd Edn. Cambridge:* Cambridge University Press (1992)

[54] P. G. De Gennes, *The Physics of Liquid Crystal:* Oxford University Press (1975)

[55] E. P. Raynes, *Liq. Cryst.* 2006, **33**, 1215 – 1218.

[56] Manual of RCL meter (Fluke PM 6306)

Overview

This chapter describes the studies carried out on the electro-optic and thermo-chromic responses of chiral nematic liquid crystal mixtures. The role of chiral dopant on helix dynamics under electric field has been discussed in detail, via dynamic pattern formation. The results show that the gratings form in two distinct ways depending upon thickness to pitch ratio, d/p i.e chiral dopant concentration. For a d/p = 0.62 the formed cholesteric gratings belong to the Dv.M type. For d/p = 1.56 the Dv.M and Gr.M types appear simultaneously but the latter initiating near the edges and surface defects, before elongating in the direction of rubbing, dominated. The concentration of chiral dopant has been varied to improve cell performance and determine the most appropriate electro-optic response in terms of parameters, such as optical transmission, threshold voltage, response time and decay time as a function of temperature, applied voltage and chiral dopant concentration. Our result indicates decrease in decay time and rise time by almost 2 fold with addition of 10% chiral dopant.

The effect of chiral dopant in room temperature nematic liquid crystal mixture on its thermo-chromic responses in terms of RGB, hue and intensity of transmitted beam has also been discussed. The samples were calibrated over their active range using light transmission characteristics. It was observed that 1% chiral doping showed active response over the wide temperature range starting from 30^{o}C to 94^{o}C among the other samples. The sample showed that it can sustain colour over the period of 2 years and these colours were stable during this period.

3.1 Introduction

Investigation of chirality in liquid crystals is an exciting area of liquid crystal science [1-4]. Dissolution of small amounts of chiral dopant in nematic liquid crystals is known to result in the formation of the chiral nematic mesophase, characterized by the preferred orientation of the long axes of the anisometric molecules (i.e. director n, rotating along the helix axis) showing very distinctly that molecular structure have a profound effect on cooperative behaviour and phase structure [4-6]. The question of how molecular chirality is translated into bulk chirality of the phase is a fundamental issue in liquid crystal science and a macroscopic measure of this chirality transfer is the helical pitch. The optical properties of the chiral nematic liquid crystal thus depend specifically on the pitch, arrangement of the axis of the helix and the polarization of the incident light. In an external field, changes occur both in the direction of the helix axis (texture transitions) and in its pitch (untwisting of the helix) [1-5]. A combination of these leads to unique optical properties of chiral nematic liquid crystals that respond to the external environment in a peculiar and special way. The response of electric field to the chiral nematic system has fielded in them wide range of applications e.g. in twisted nematic displays, medical thermography and imaging, linear and non linear optics, sensors and in novel electro- and magneto-optic devices and detectors [5-8]. There is still a growing scientific and practical interest in these systems [9-13].

In this chapter, we discuss the effects of chiral dopants on the phase transition behaviour, electro-optic and thermo-chromic responses in room temperature nematic liquid crystal mixture.

3.2 Results and discussion:

3.2.1. Effects of temperature

The composition of the investigated materials and their phase sequence is tabulated in table 3.1 (N-Nematic LC phase, N*-Chiral Nematic LC phase, Is-Isotropic phase and Cr-Crystal phase). Their thermal profiles are shown in Fig.3.1.

Table 3.1 Composition and abbreviation of samples studied

S.No	*Composition*	*Abbreviation*	*Phase sequence*
1	BLO36	NLC	Cr $\xrightarrow{30^{o}C}$ N $\xrightarrow{99^{o}C}$ Is
2	BLO36 +1%CB15	CLC1	Cr $\xrightarrow{30^{o}C}$ N* $\xrightarrow{97^{o}C}$ Is
3	BLO36 +5%CB15	CLC2	Cr $\xrightarrow{30^{o}C}$ N* $\xrightarrow{91^{o}C}$ Is
4	BLO36 +10%CB15	CLC3	Cr $\xrightarrow{30^{o}C}$ N* $\xrightarrow{86.5^{o}C}$ Is
5	BLO36 +15%CB15	CLC4	Cr $\xrightarrow{30^{o}C}$ N* $\xrightarrow{84^{o}C}$ Is

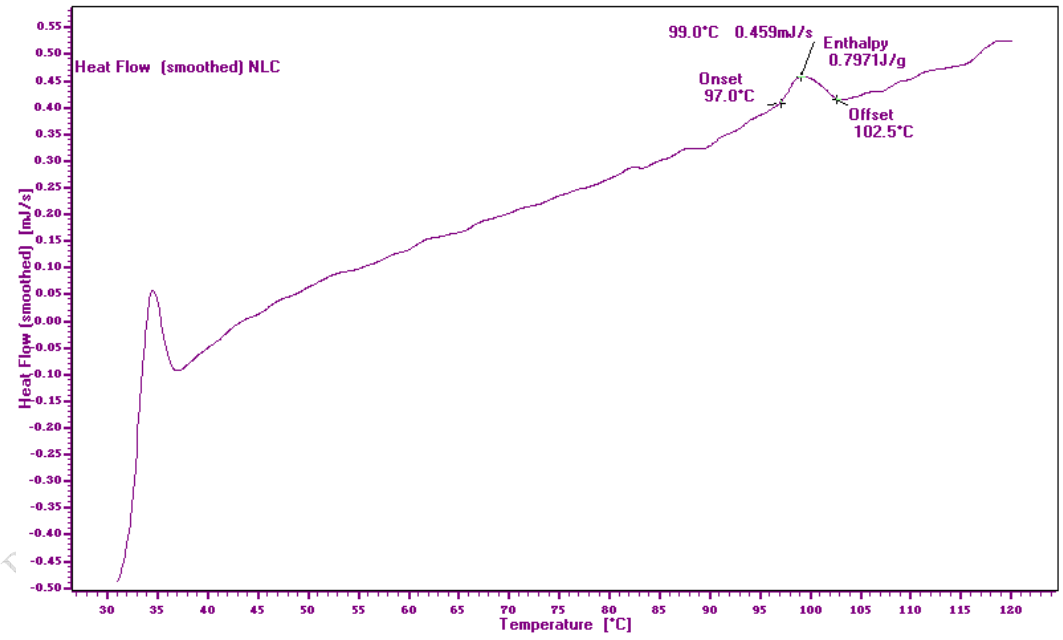

(a)

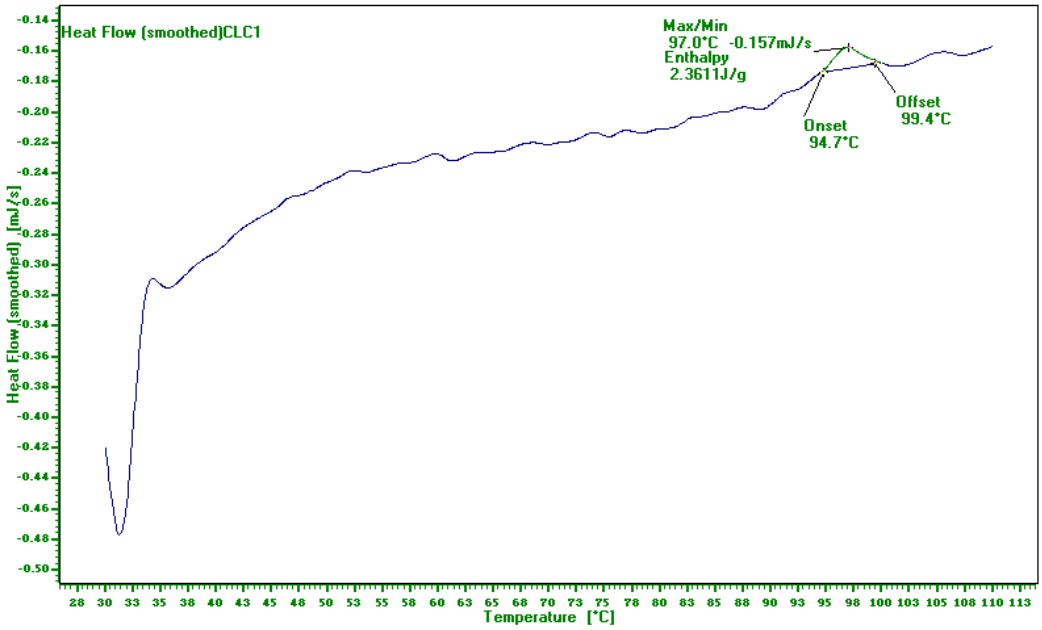
Heat Flow (smoothed)CLC1
Max/Min
97.0°C -0.157mJ/s
Enthalpy
2.3611J/g
Onset
94.7°C
Offset
99.4°C
Heat Flow (smoothed) [mJ/s]
Temperature [°C]

(b)

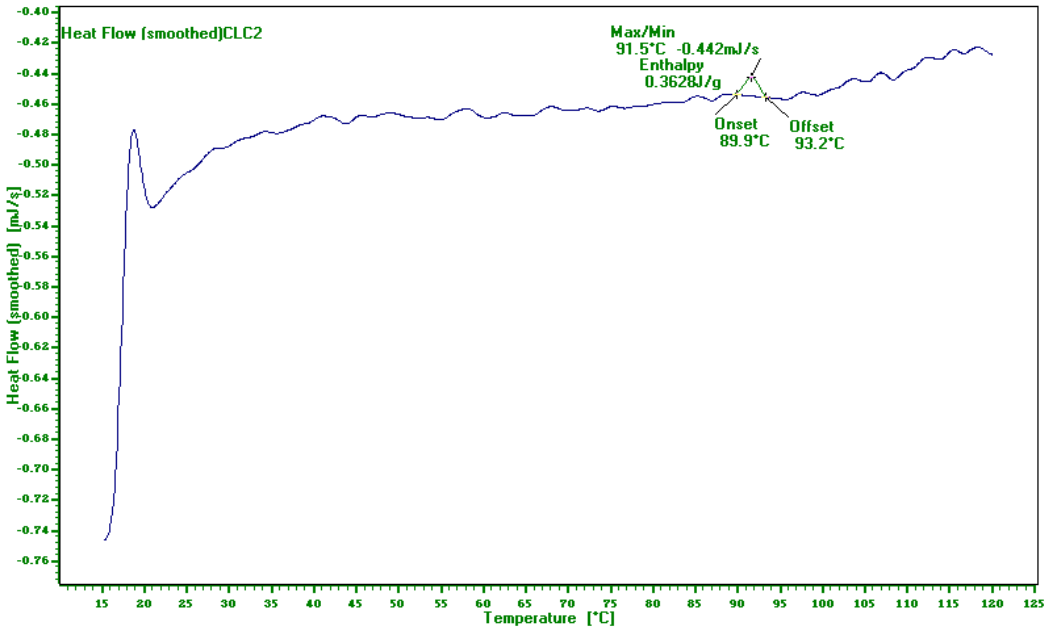
Heat Flow (smoothed)CLC2
Max/Min
91.5°C -0.442mJ/s
Enthalpy
0.3628J/g
Onset
89.9°C
Offset
93.2°C
Heat Flow (smoothed) [mJ/s]
Temperature [°C]

(c)

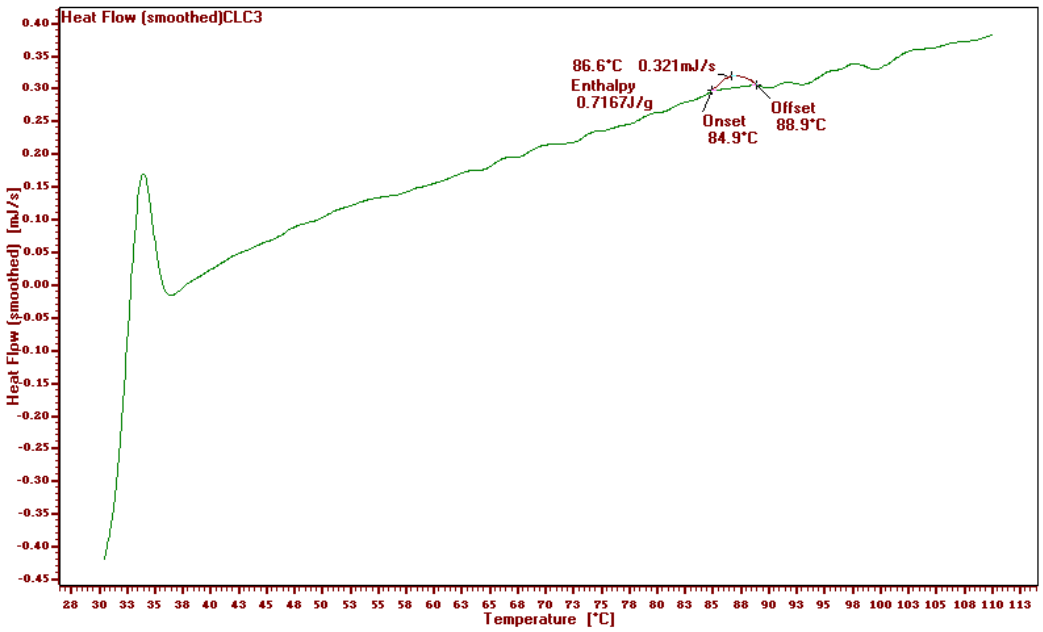

(d)

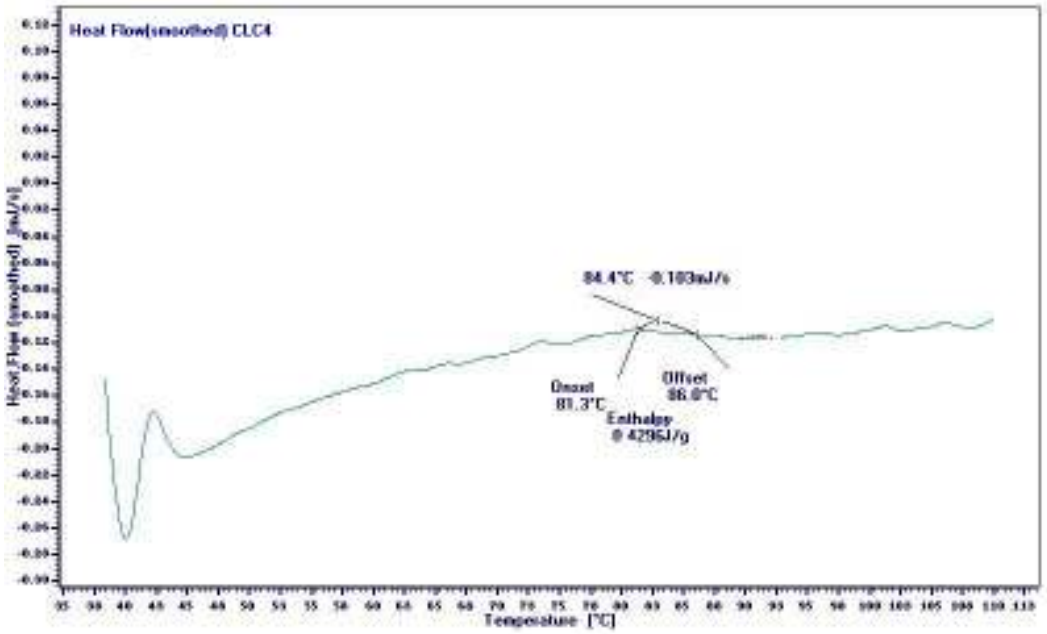

(e)

Fig. 3.1 DSC profiles of (a) NLC (b) CLC1 (c) CLC2 (d) CLC3 (e) CLC4.

The microtexture of NLC sample (~10μm thickness) viewed under crossed polarizers is shown in fig. 3.2. The schilieren texture with four and two brushes of strength, s = ±1 and s = -1/2 respectively, typical of uniaxial nematic liquid crystal, the circular brushes connecting two neighboring disinclinations of equal and opposite strength is clearly seen in the upper right hand side corner of the fig. 3.2(a). These brushes are the regions where the director is either parallel or perpendicular to the plane of polarization of the incident light. The polarization is unchanged by the material in these regions and is therefore extinguished by the crossed analyzer. The positions of points from where the brushes originate, remains unchanged on rotating the crossed polarizer but the brushes themselves rotate continuously showing that the orientation of the director changes continuously about the disinclinations [4]. The rate of this rotation is equal to that of the polarizer when the disinclination has 4 brushes and is twice as fast when it has only 2. In NLC, disinclinations of opposite signs are seen to attract each other and coalesce at temperatures close to T_{NI}.

At the onset of transition to isotropic phase, the BL036 mixture show scintillation type effect with rainbow (Fig. 3.2 (b)) due to fluctuation of director. With increasing temperature, increase in thermal agitation increases the orientation motion of the director, ultimately leading to complete isotropic phase at 99°C.

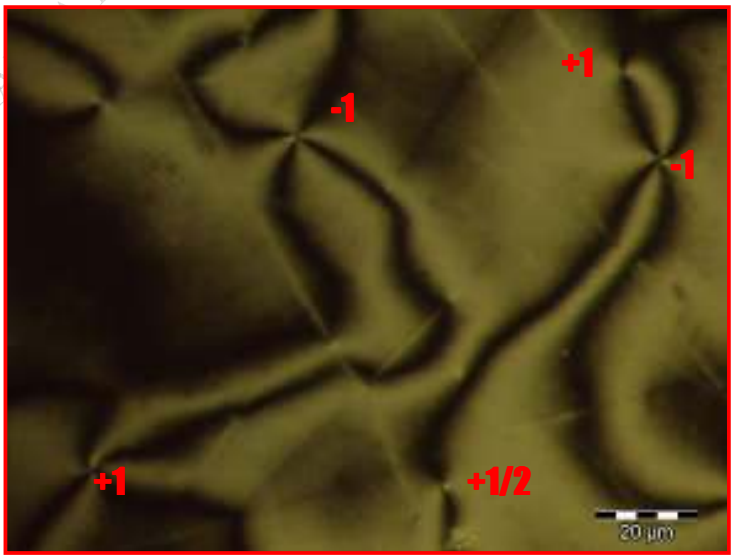

(a)

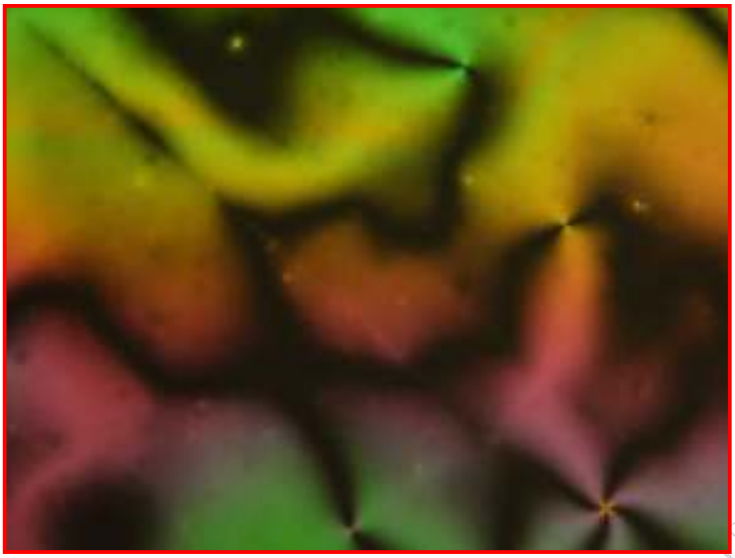

(b)

Fig. 3.2 Microtexture of NLC sample at (a) 30^{o}C (b) 98^{o}C. Defects are clearly seen.

Fig. 3.3 shows the effects of the induced chirality on the schlieren texture of observed NLC samples under crossed polarizers. We noticed the dechiralization lines with variable pitch as a function of chiral dopant concentration at room temperature. The chiralization lines in the domains are clearly observed at 50X (fig. 3.4) for CLC2. The optical morphology of the chiral phase changes with increasing temperature.

As the temperature is increased the constriction in the domains and chiralization lines was observed. We noticed in Fig. 3.5 that the focal conic domains become dominant with mosaic pattern as the temperature is increased. The focal conic domains couldn't be observed for samples CLC3 and CLC4 possibly due to the competition between increased intrinsic chirality of the liquid crystal and the frustrating effects of the thermal agitation. The optical patterns near the transition are shown in fig. 3.6.

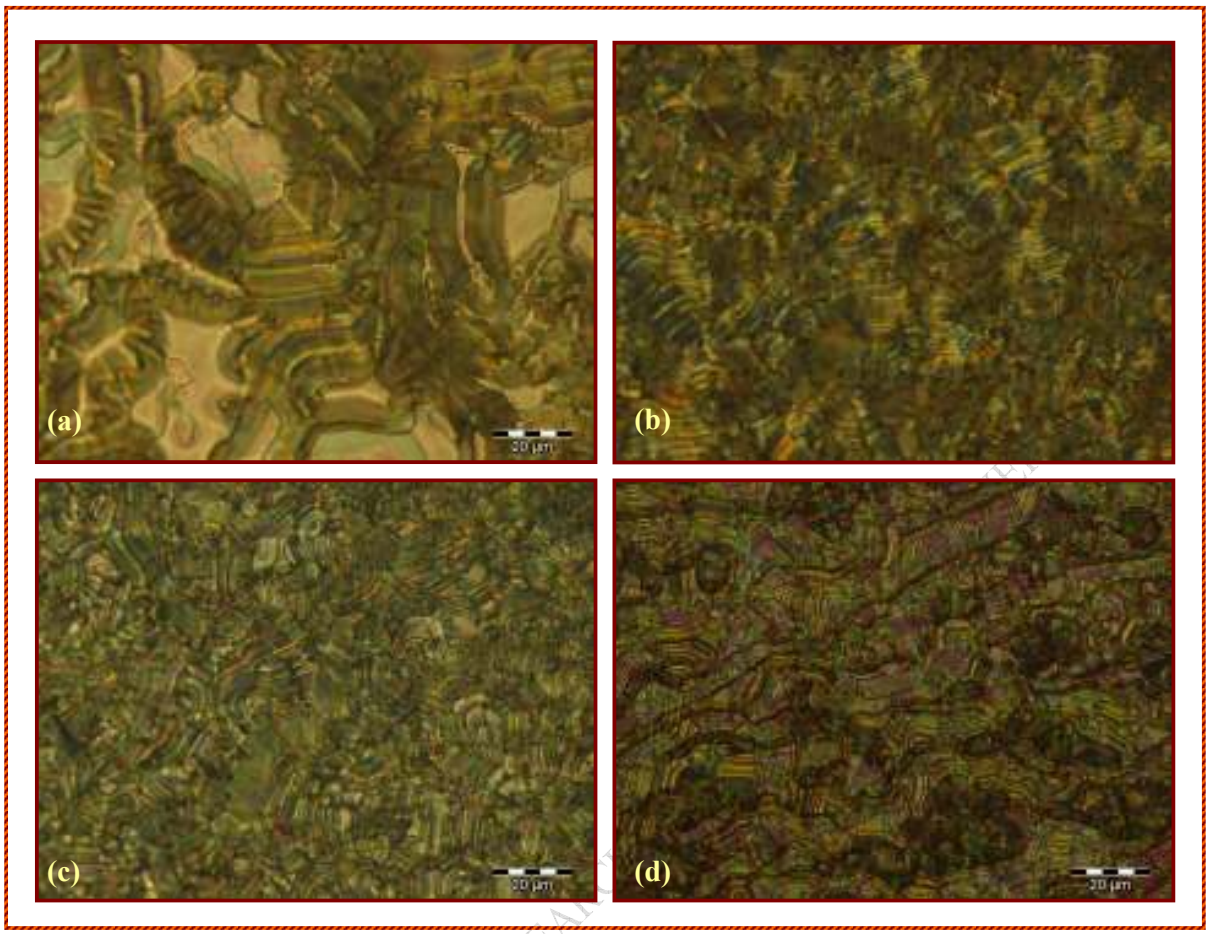

Fig. 3.3 Optical texture of chiral nematic phase at 10X at 30^{o}C, as a function of doping concentration (a) CLC1 (b) CLC2 (c) CLC3 (d) CLC4

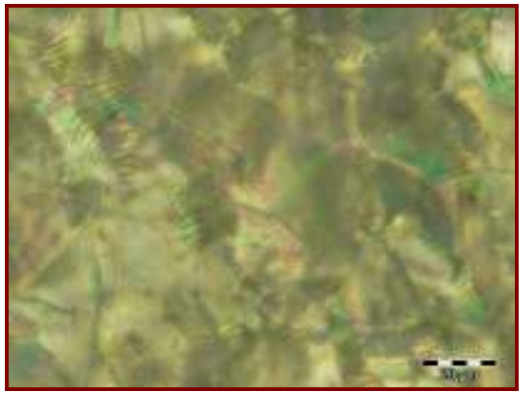

Fig. 3.4 Dechiralization texture of CLC2 at 50X, 30^{o}C

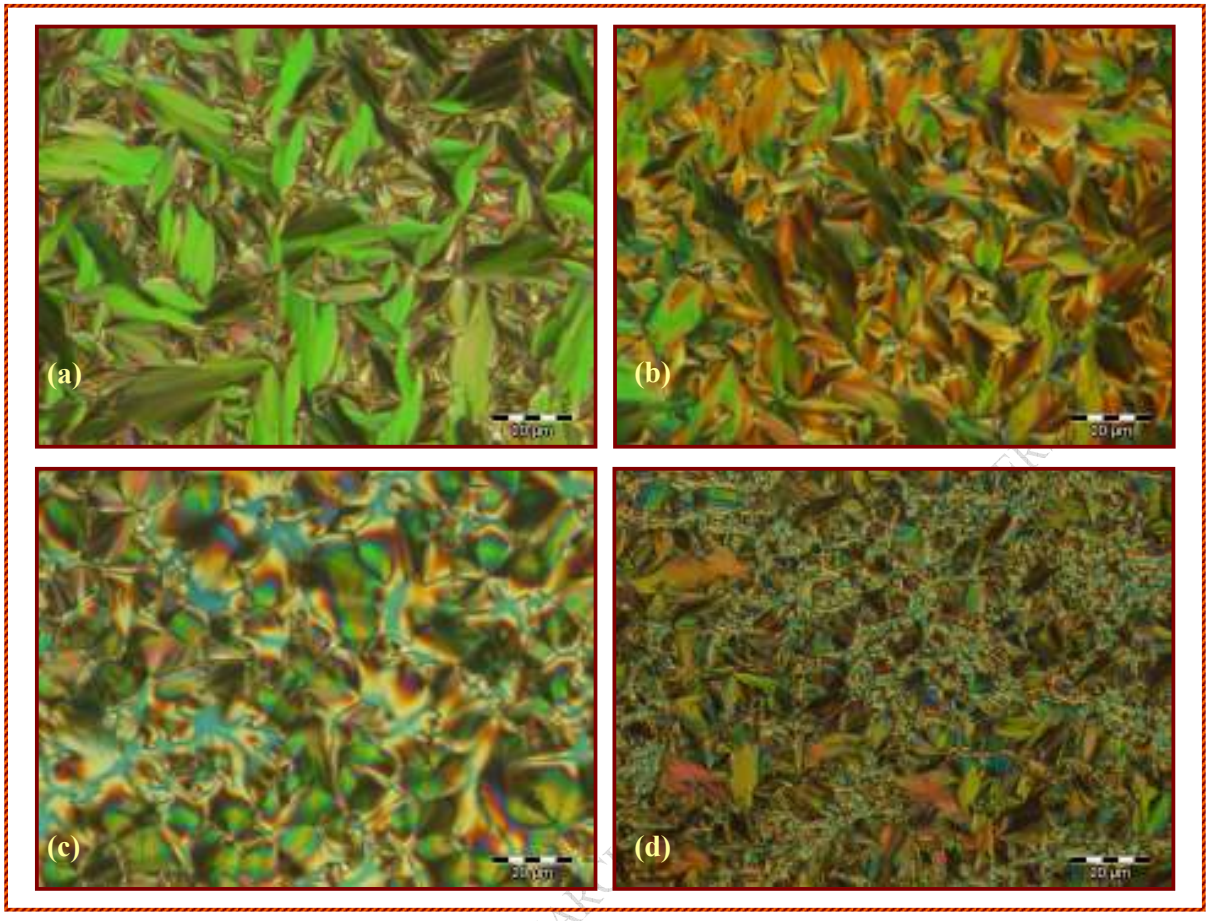

Fig. 3.5 Texture of CLC samples at 80^{o}C (a) CLC1 (b) CLC2 (c) CLC3 (d) CLC4

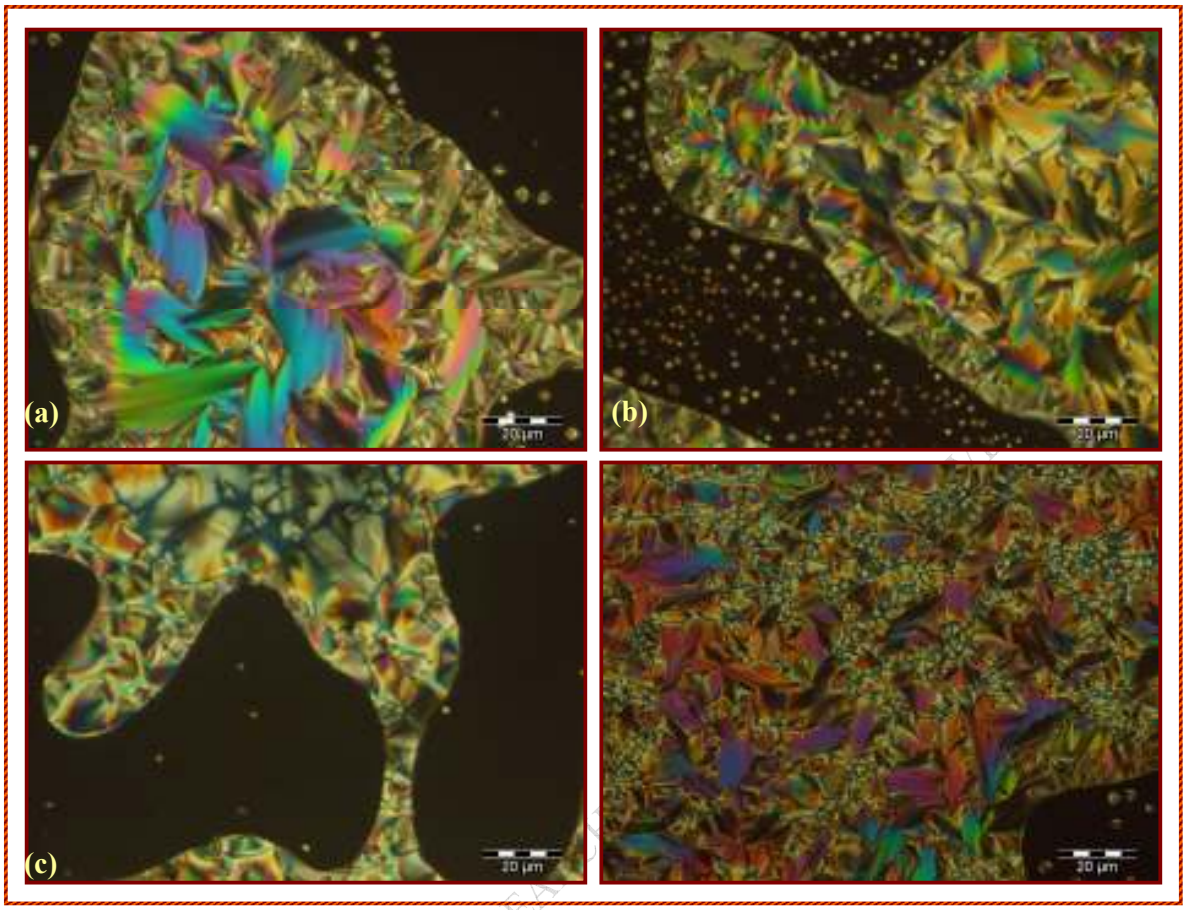

Fig. 3.6 Micro textural changes near melting point (T~0.2^{o}C) of CLC samples (a) CLC1 (b) CLC2 (c) CLC3 (d) CLC4

3.2.2. Electric field effects:

The distortions in the planar chiral nematic structure induced by an applied field have been extensively studied, both theoretically and experimentally [1-2, 14]. Subacius et al.[15-17] described a cholesteric diffraction grating in a fingerprint texture on applying an electric field parallel to the helical axis of a planar texture film. They classified the fingerprint texture into two types, according to the formation of the grating. (**i**) developable modulation (Dv.M) type and the (**ii**) growing modulation (Gr.M) type. In the former, the stripes appear simultaneously all over the domain. These modulations develop by enhancing the optical contrast rather than by propagation in space. In our experiments we observed that the contrast of the stripes increased with time during formation, whereas in the latter type, the stripes were initiated near the edges and the defects on the surface before getting extended over to the whole sample, slowly along the rubbing direction.

In this section, we present the results on the effect of electric field on both nematic and CLC samples. While for the NLC, the orientation of director along the field leads to change in colour with increasing field strength but for the CLC samples, the electric field shows pronounced effects in terms of field induced rotation of helical axis. When electric field was applied perpendicular to the walls of NLC cell, the director orientation changes along the field direction, showing colour variation due to electric controlled birefringence effects. At saturation voltages, the dark texture was observed due to complete alignment of director along the applied field i.e. perpendicular to the cell walls.

Dynamic pattern formation:

On application of the electric field normal to the CLC cell, the director of cholesteric sample tends to align along the field direction due to dielectric anisotropy switching the material into the fingerprint texture [5] (helical axis is parallel to the substrates). The micrographs of the CLC samples at 0V at 10X are shown in Fig. 3.7 and on the application of electric field normal to CLC cell, they switch over to the patterns of the fingerprint texture as shown in Fig. 3.8. We show that the gratings form in two distinct ways depending upon thickness to pitch ratio (d/p i.e. chiral dopant concentration). For d/p = 0.62 (CLC1), the cholesteric gratings pertaining to the Dv.M type where as for d/p = 1.56 (CLC4), the Dv.M and Gr.M types appeared simultaneously (Fig. 3.8) but

the latter initiating near the edges and the surface defects, before elongating along the rubbing direction dominated, (Fig. 3.9). The stripes of the gratings were found to be parallel to the rubbing direction for CLC1 and CLC4, thereby minimizing the free energy of the system. For d/p = 0.90 (CLC2) and 1.09 (CLC3), the fingerprint texture is not uniform (Fig. 3.8).

The threshold field strength for fingerprint texture, E_{th} is given by

$$E_{th} \quad \frac{8\ ^{3}(6k_{22}k_{33})^{1/2}}{(\ \ pd)}^{1/2} \qquad (3.1)$$

Where, k_{22} = Elastic constant for twist deformation, k_{33} = elastic constant for bend deformation, ε = dielectric anisotropy, p = helix pitch length (at E=0) and d = cell thickness

The planar layers are observed to deform periodically in this case and the stripes are perpendicular to the director of the middle layer [17-19]. Therefore, stripes of a cell with d/p ratio 1/2 and d/p ratio 1 are parallel and perpendicular to the rubbing direction, respectively. Further on slight increase of electric field the structure was observed to change from the Dv.M type texture to the homeotropic texture [5]. A chiral nematic planar texture usually adjusts its pitch length slightly to satisfy the condition of the surface. Therefore, the direction of the stripes for cells with d/p = 0.62 is coming out the same as that for cells with d/p ½ as predicted by theory.

E_{th} [eq. (3.1)] depends on chiral dopant concentration and increases with increase in dopant concentration, as shown in fig. 3.10(a). It was seen that the response of the field was instantaneous for CLC1 system but, in other samples (CLC2, CLC3, CLC4), the molecular alignment was delayed to get aligned along the applied field direction to form stabilized fingerprint texture with polydomains. The chiral dopant effects shows time dependence depicted in Fig. 3.9. With increasing function of temperature at constant respective threshold voltages, the texture remained stabilized up to certain temperature range and thereafter, we observed undulations of the chiralization lines and the planar texture with oily streaks was observed under OPM (until the melting of mixture to its isotropic phase). The time period and the temperature range of the stabilization texture as a function of chiral dopant concentration are shown graphically in fig. 3.10(b).

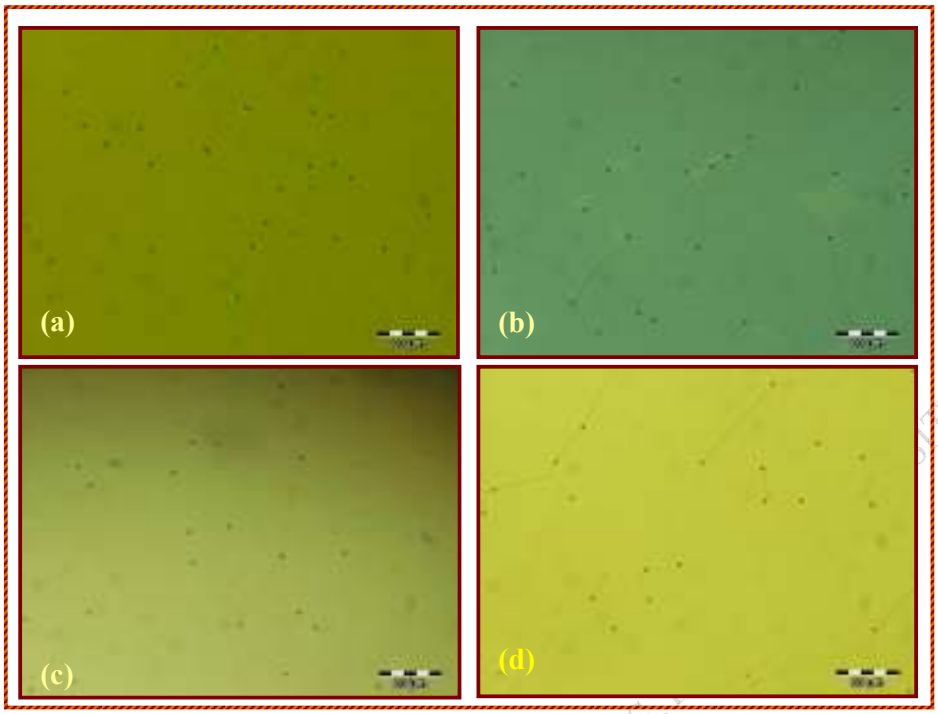

Fig. 3.7 Micrographs of the dynamic change of the patterns of the gratings at 0V for (a) CLC1 (b) CLC2 (c) CLC3 (d) CLC4

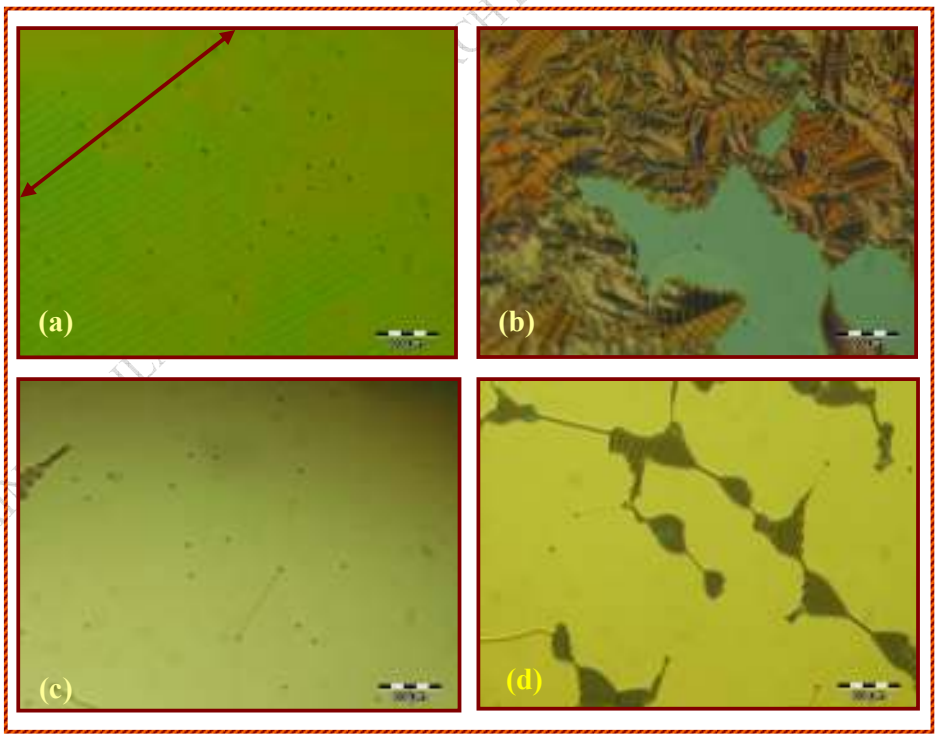

Fig. 3.8 Micrographs of the dynamic change of the patterns at onset of (a) 0.44V/µm (CLC1), showing Dv.M type texture, with strips parallel to rubbing direction represented by Black arrow (b) 0.72V/µm (CLC2) (c) 1.16V/µm (CLC3) (d) 1.50V/µm (CLC4) , showing the simultaneous growth of both Dv.M and Gr.M

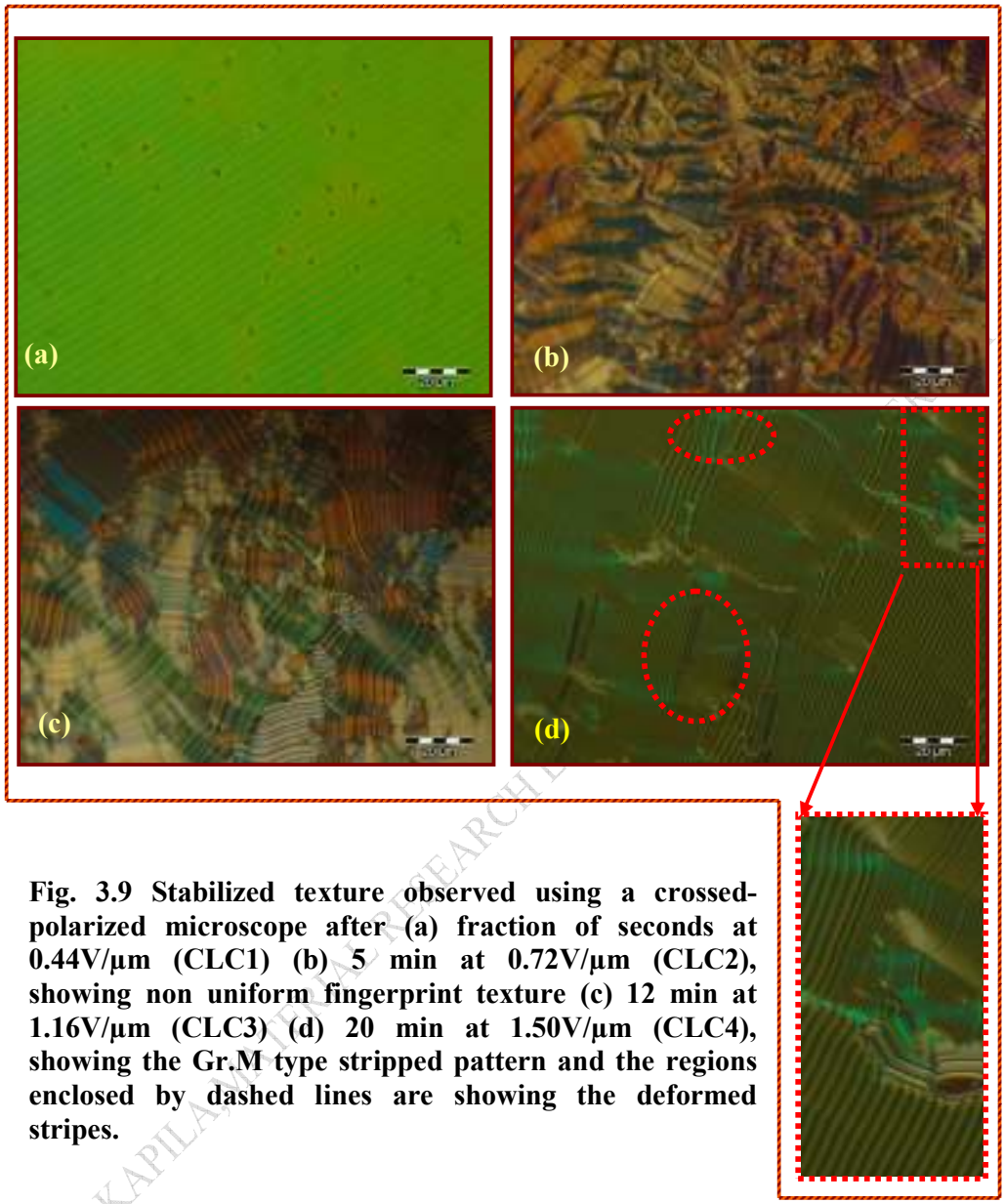

Fig. 3.9 Stabilized texture observed using a crossed-polarized microscope after (a) fraction of seconds at 0.44V/µm (CLC1) (b) 5 min at 0.72V/µm (CLC2), showing non uniform fingerprint texture (c) 12 min at 1.16V/µm (CLC3) (d) 20 min at 1.50V/µm (CLC4), showing the Gr.M type stripped pattern and the regions enclosed by dashed lines are showing the deformed stripes.

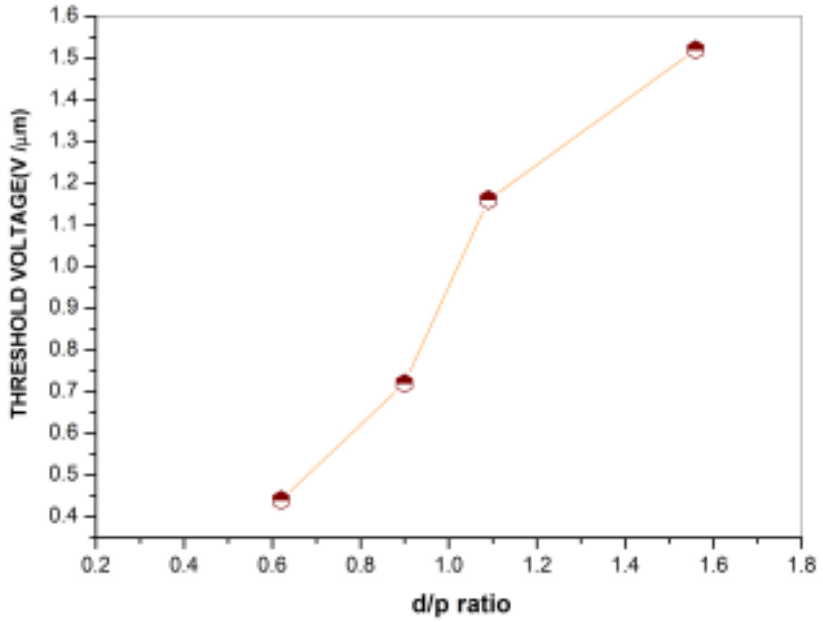

(a)

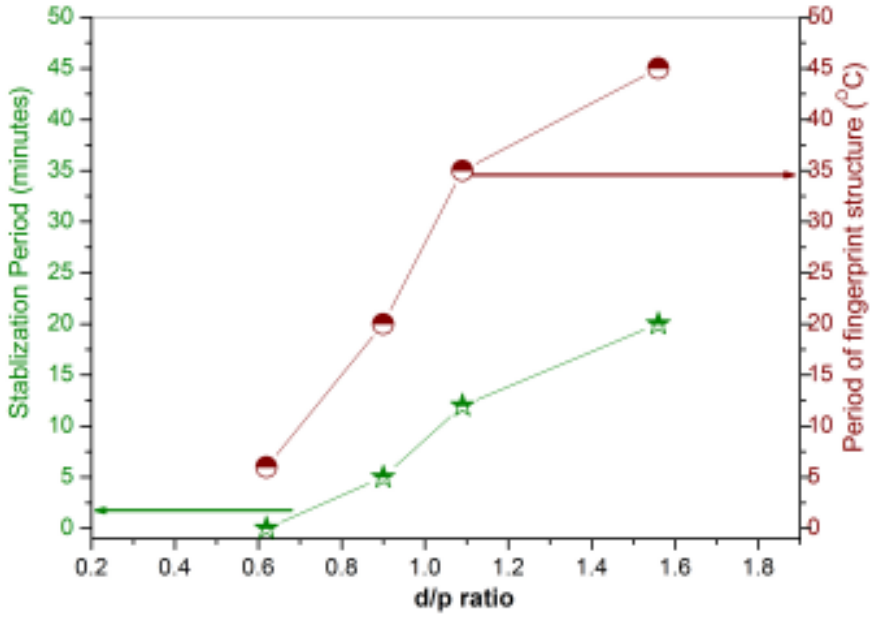

(b)

Fig. 3.10 (a) Threshold voltage for fingerprint orientation of helix (b) Stablization period and temperature duration of fingerprint structure at respective threshold voltages, as a function of thickness to pitch ratio, d/p in planer cells.

With increase in external field, the structure of CLC1 changed from the Dv.M type texture to the homeotropic texture, whereas for CLC4 the Gr.M type grating was seen to be unwounded progressively with increasing field, and finally turned into homeotropic texture at E_{uw} [5], given by

$$E_{uw} \quad (\ ^2 / p) \ \frac{4 \ k_{22}}{} \ ^{1/2} \tag{3.2}$$

Equating eq. (3.1) and (3.2) yields

$$E_{uw} / E_{th} \qquad \frac{k_{22}}{(2(6k_{22}k_{33})^{1/2}} \ ^{1/2} (d / p)^{1/2} \tag{3.3}$$

It is generally known that the exact value for k_{22} cannot be experimentally measured for our system BL036, nonetheless, using the experimentally obtained [20] value, that is k_{22}~6.18 x 10^{-12} N and substituting value of k_{33}= 27.0 x 10^{-12} N, eq (3) yields the estimated value of E_{uw}/E_{th} 0.77 for CLC1 and 1.22 for CLC4. This result explains why with the slightly increased external field, the structure changes from the Dv.M type texture to the homeotropic texture for CLC1. A cholesteric planar texture with a larger pitch required a smaller threshold E_{uw} to transition into the homeotropic state. Accordingly, for a cholesteric planar texture film with a small d/p ratio, E_{uw} is near or smaller than E_{th}. Thus, when an external field is applied to rotate the helical axis of a planar texture by 90^o, the cholesteric-nematic transition occurs for Dv.M type gratings almost immediately. For a sample with large d/p ratio, the E_{uw} is much larger than E_{th}. As a result, the Gr.M type fingerprint grating can be unwound progressively with increasing field, and finally completely unwound to become homeotropic.

3.2.3 Pitch:

A sample cell of 5 m thickness containing randomly dispersed spacer particles was filled with a nematic liquid crystal mixture and the same mixture was doped with chiral impurity and sandwiched between 5 m cells under similar conditions. The optical behaviour of these two cases yield interesting results as shown in fig.3.11 (a,b). In fig.3.11 (a) the disclination shrunk to become virtually linear between the spacer particles, in order to minimize the line tension associated with the disclination. Whereas the reverse twist lines were bowed with the smaller radius of curvature being associated with the shorter pitch length, consistent with nematic cell showing a virtually infinite radius of curvature as shown in fig. 3.11(b). We strongly feel that the bowing was caused by the introduction of the chiral dopant that favoured one sense of twist but was prevented from forming a single twist domain by pinning of the disclination lines. The disclination therefore increased its length and bows, driven by chirality, until equilibrium was reached. The pitch (P) was calculated by measuring radius of curvature (R) of the bowed disclination line [21], with the help of OLYSIA BioReport software, through the relation

$$P=2R \qquad (3.4)$$

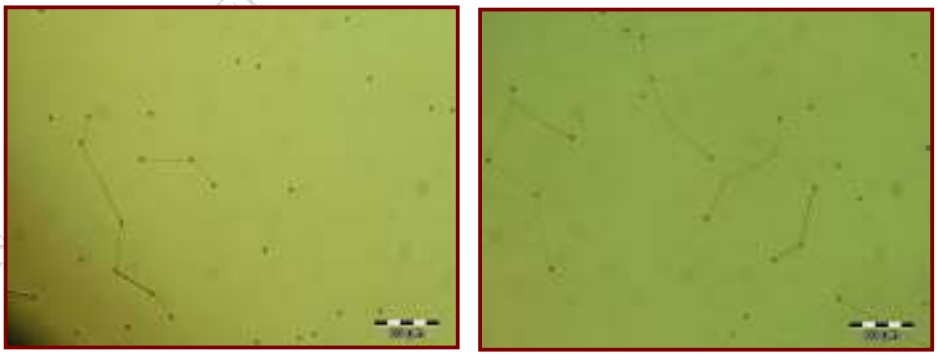

(a) (b)

Fig. 3.11 Cell containing (a) NLC and (b) CLC1 under crossed polarizers.

The pitch of the CLC sample is found to be decreasing with the increasing temperature, and is explained by the equation [2]

$$1/p = (HTP)\ XcT \tag{3.5}$$

Where p = pitch of chiral nematic liquid crystal, HTP = helical twisting power of chiral dopant, Xc = concentration of chiral dopant, T = temperature of the sample.

Fig. 3.12. shows a typical variation of helix pitch as a function of temperature.

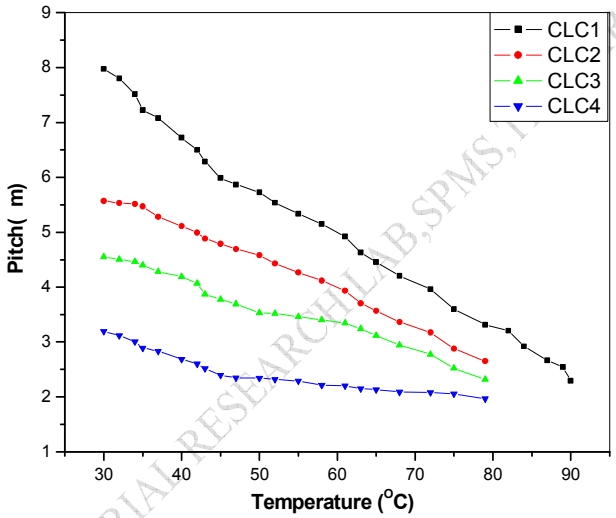

Fig. 3.12 Helical pitch as a function of temperature for CLC samples

3.2.4 Electro-optic Analysis:

3.2.4. (a) Transmission profile

The electrooptic response profile of the NLC and CLC samples as a function of applied voltage (at 50 Hz), is shown in fig. 3.13(a). We noticed that the chirality induced liquid crystal mixture shows lower transmission and higher threshold. At lower applied field, the transmission shows fluctuations, possibly due to ionic effects. The transmission remained constant for the lower temperature, but as the temperature increases, we observed the increase in transmission. Although the trend observed for all the five samples was same, but at higher temperatures the difference among the

NLC and CLC samples is quite low in comparison to lower temperatures, as is clearly seen in fig. 3.13(b).

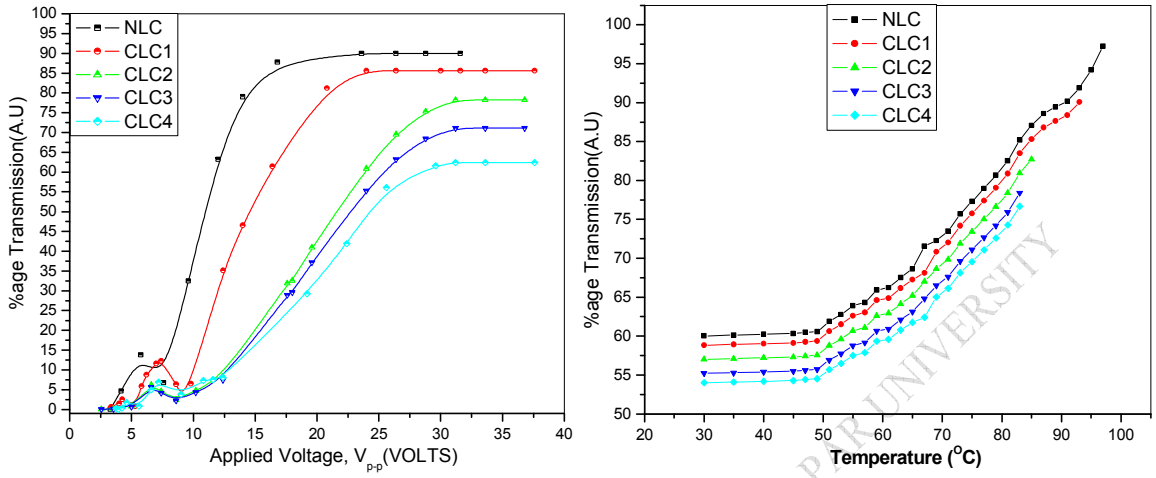

(a) (b)

Fig. 3.13: Electro-optic response of chiral nematic liquid crystal as a function of (a) applied field and (b) temperature

3.2.4. (b) Response time:

The optical response time allow us to define not only the electro-optical properties of the condensed materials but also their performance for practical applications. [The rise time τ_r is taken as time required to get transmission change from 10 to 90% upon switching ON the cell. Similarly, decay time τ_d has been taken as time required for transmission intensity to fall from 90–10%]. Response time of nematic liquid crystal mixture is influenced by the torques associated with viscosity, elasticity and external field. It is also affected by the inertia of nematic liquid crystal molecules and surface anchorage effects [22-23]. For simplicity and convenience we assume that the contributions from the surface elasticity and inertial effects are very small and thus negligible in comparison to the viscosity. The rise time of a nematic liquid crystal mixture can be expressed as

$$r \quad \frac{1}{E^2} \tag{3.6}$$

Where, τ_r = response time, γ_1 = rotational viscosity, ε= dielectric anisotropy, E= external electric field

Experimental results are in perfect agreement with the theory, and the rise time is decreasing with the increasing field strength and temperature. At about temperatures 10^oC below T_{NI}, it is having lowest value; it may be due to the smallest value of ratio $\frac{1}{}$ near the T_{NI} [24]. The response time is generally found to be much faster then the decay time. The electric field induces an external torque on each molecule, but when the field is removed or reduced, interactions between liquid crystal molecules provide the dominant restoring forces. These interactive forces are relatively weaker than the torque caused by an external field, which leads to slower decay time [5].

The CLC sample shows the similar behavior as a function of temperature and voltage changes, however a modification was noticed obviously due to the presence of optically active dopant (OAD), that exerts the torque on the molecules and helps in their rotation, thus decreasing the response time. The approximate relation for the response and decay times for the field induced changes in CLC sample can be expressed as [25]:

$$r \quad \frac{1}{{}_0 | \quad | E^2 \quad k_{22}{}^2 / P^2} \tag{3.7}$$

$$d \quad \frac{{}_1 P^2}{k_{22}{}^2} \tag{3.8}$$

where τ_r and τ_d = response time and decay time respectively, γ_1 = rotational viscosity, k_{22} = Elastic constant, ε= dielectric anisotropy, P = pitch of CLC, E= external electric field.

It is obvious from the above relation that response time of the CLC sample is supposed to be faster in comparison to that of pure nematic liquid crystal mixture that explains the trend in the response time for our mixtures, showing almost 2 fold and 2.5 fold decrease in rise time and decay time respectively for CLC4 w. r. t NLC as is shown in fig. 3.14 and 3.15. There is significant decrease in decay time with increasing chiral dopant concentration, likely due to the increased elastic energy from helical structure, at higher chiral concentration the decay of the transmittance is dominated by twisting due to helical structure.

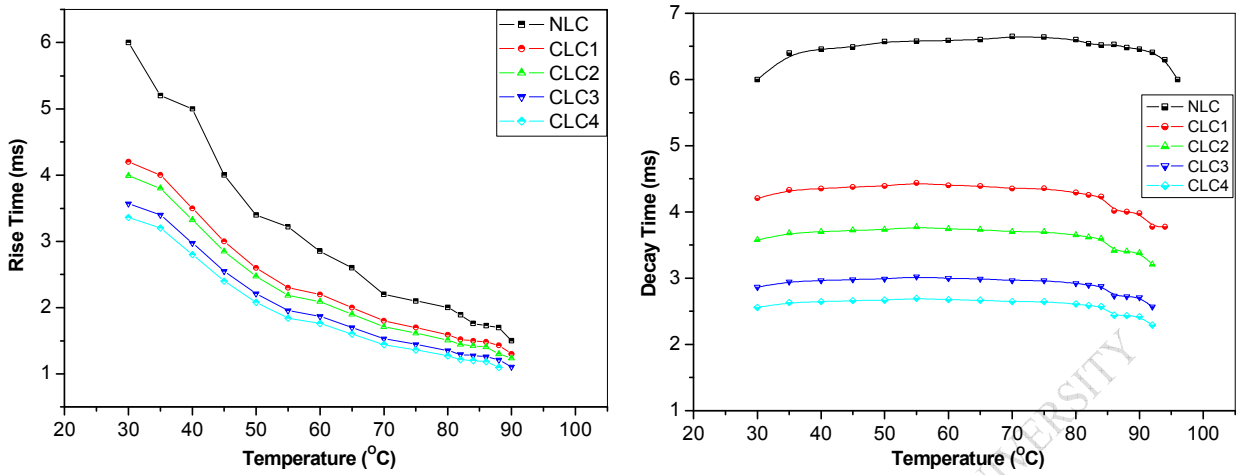

(a) (b)

Fig. 3.14 Response time as a function of temperature (a) the rise time and (b) the decay time

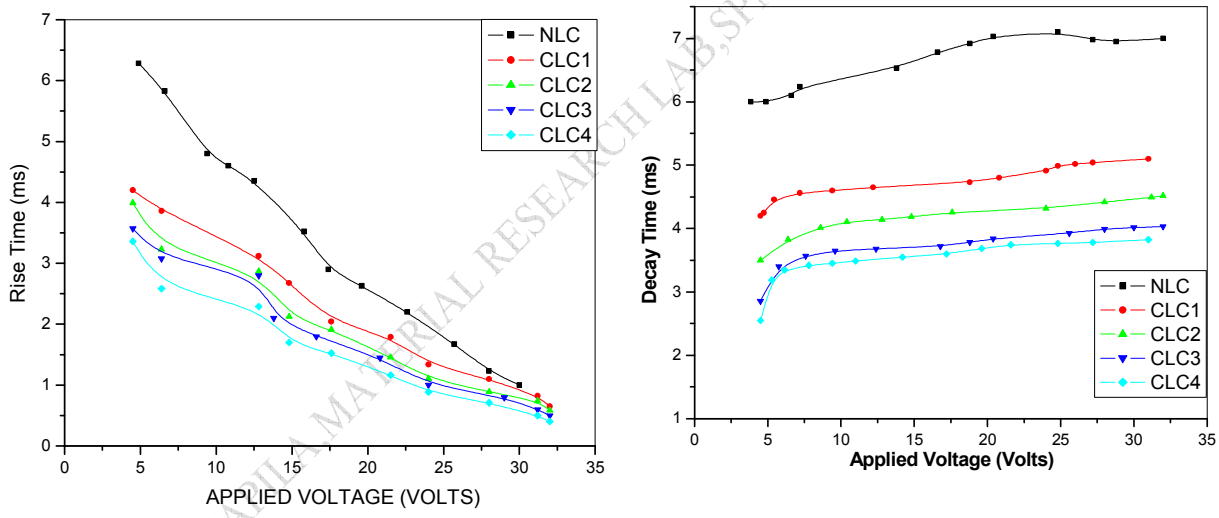

(a) (b)

Fig. 3.15 Applied voltage dependence of (a) the rise time and (b) the decay time

3.2.5. Thermochromic response

The optical properties of chiral nematic liquid crystals and their mixtures make them ideal materials for sensor devices. These are sensitive to physical changes like temperature, pressure, electric and magnetic field and this sensitivity has been greatly exploited for their potential application as thermal mapping in the medical field and industrial testing [26-29]. In the recent past, their use in research and testing has become increasingly widespread e.g. in flow visualization and heat transfer studies, temperature fields and thermal mapping etc [30-32].

The temperature range over which the cholesteric liquid crystal shows sensitivity to colour variations is its active range in which sensor characteristics are dominant [32-35]. In this range, cholesteric liquid crystal molecules align to form a helical structure, where pitch is a function of external stimulation (like temperature, pressure and electrical field). At different temperatures, the pitch changes, so does the wavelength of light either reflected or transmitted [1, 2, 36].

Light reflection has been used in thermochromic liquid crystal temperature measurements but its main disadvantage is that the correlating equation for temperature is sensitive to light intensity, lighting type and viewing angle [37-38]. In addition, while the CLC materials display colour over its entire active range, the reflection calibration generally utilizes only 25–50% of this range [33].

The light transmission properties of liquid crystals are used extensively in liquid crystal display technology [39], however, little work has been done to characterize and understand the effects of temperature on the light transmission properties of induced CLCs for sensing applications. Diankov et al. [40] reported measurements of the light transmitted through polymer stabilized and polymer dispersed cholesteric liquid crystals. They observed a modulation in the intensity of transmitted monochromatic light with temperature change and showed that this activity occurs over a wide range (outside the active range) of the liquid crystals. More recently, Roth et al. have studied the transmission characteristics of thermochromic liquid crystals in detail and reported larger calibration range and less sensitivity to lightning effects [33, 41].

In this section we are going to discuss the effects of chiral dopant in room temperature nematic liquid crystal mixture on its thermo-chromic responses in terms of Red, Green, Blue (RGB), hue and intensity of transmitted beam.

3.2.5. (a) Experiment

A room temperature nematic liquid crystal mixture, 4-pentyl-4'-cynobiphenyl and optically active dopant CB15 (M/S E-Merck, Darmstadt, Germany) were used. Small concentrations of chiral dopant at different wt/wt% have been diffused in the nematic liquid crystal, 4-pentyl-4'-cynobiphenyl, to induce chirality in it. The sample cells, prepared as explained in chapter 2, were placed on a temperature programmer cum hot stage (Linkam TP92-THMS600, UK) with an accuracy of ±0.1^{o}C. For thermochromic analysis, the measurements were conducted by slowly heating the sample@1^{o}C/min and acquiring thermal images of the sample cell on heating between crossed-polarizers through polarizing microscope (OLYMPUS BX51P) fitted with digital camera (DP12) with the help of OLYSIA BioReport software at different temperatures. Each image was analyzed using the OLYSIA BioReport software to determine the amount of red, green, and blue in a specified region of the image (generally consisting of ~10,000 pixels).

3.2.5. (b) Uncertainty Estimates

All temperature measurements used calibrated thermocouples with an uncertainty of ±0.1°C. The OLYMPUS DP12 is a 12 bit camera, which yields a resolution of 1/4095 (in arbitrary unit, (au)) on the measured RGB signals. We performed five tests on the same CLC sample cells over the period of one month, to test the repeatability of the sample cells. For all the four concentrations of chiral dopant, we measured a maximum variation in the temperature calibration curve of ~0.15°C.

3.2.5. (c) Thermochromic analysis:

The samples were calibrated for thermochromic response in RGB (red-green-blue) and HSI (Hue-Saturation-Intensity) model space for colour. The RGB model is a model used for describing colours generated additively, as is the case on a monitor screen. RGB images, also referred to as true-colour image, can contain up to 16,777,216 (=256 x 256 x 256) different colours via the additive mixing of the three primary colours red, green and blue. HSI is another model for describing colour values. HSI values of a colour originate from RGB values via coordinate transformation. The HSI colour space can be shown as in fig. 3.16(a). The central axis is the intensity, the distance from the axis is the saturation and the angle corresponds to the hue. The colour wheel (Fig. 3.16(b)), is a two dimensional projection of the HSI colour space. The saturation

increases towards the outer limits. The hue, saturation and intensity values are automatically calculated and generated by the OLYSIA BioReport software.

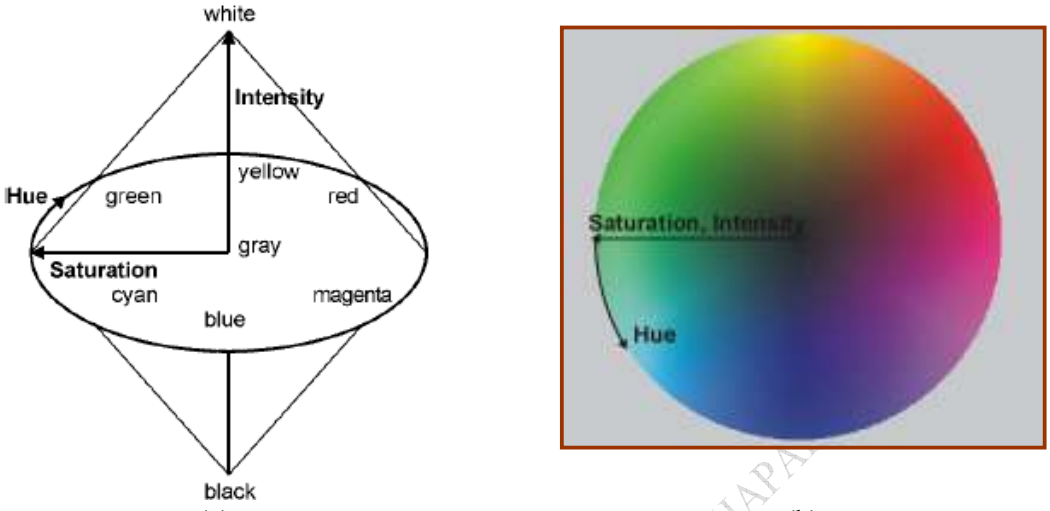

(a) (b)

Fig. 3.16 (a) Hue-Saturation-Intensity colour space (b) colour wheel (Hue-Saturation-Intensity model)

The variation in hue as a function of temperature for all the four chiral induced samples is shown in fig. 3.17 [42]. We observed that for CLC1, the hue varied rapidly beyond 35^{o}C for CLC1 whereas variation is not steep in other cases. Hue is maximum for CLC4 over wide temperature range but attains a plateau. For sensing applications, CLC1 sample showed better response in comparison to other three samples.

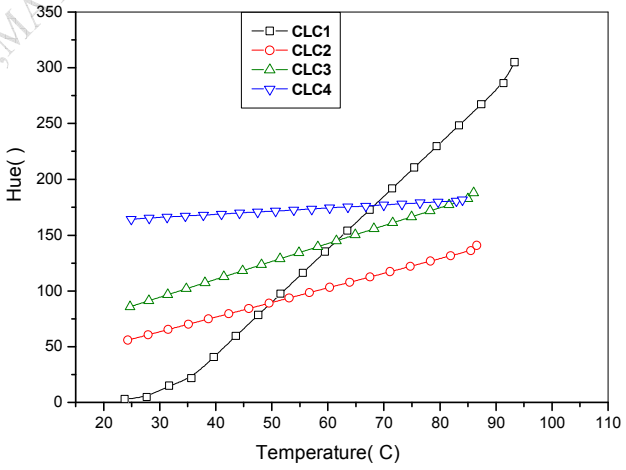

Fig. 3.17 Variations in displayed Hue with change in surface temperature for chirality induced nematic liquid crystal samples.

The RGB variations as a function of temperature for CLC1 are shown in fig. 3.18. The variation in average standard deviation with change in temperature of CLC1 for red, green, blue and hue values is shown in fig. 3.19. The hue values are showing almost 69% less average standard deviation than red and green and 48% less average standard deviation than blue. So we calculated the colour response in HSI model. Also the HSI model is easier to understand than the RGB model because its parameters are more in line with one's own intuitive description of a colour.

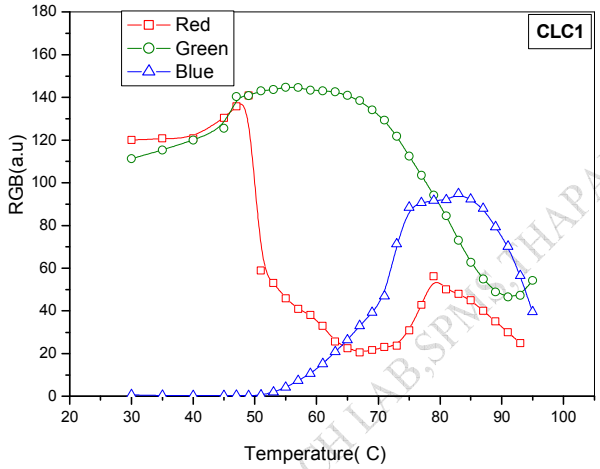

Fig. 3.18. Red-green-blue variation with respect to temperature for CLC1

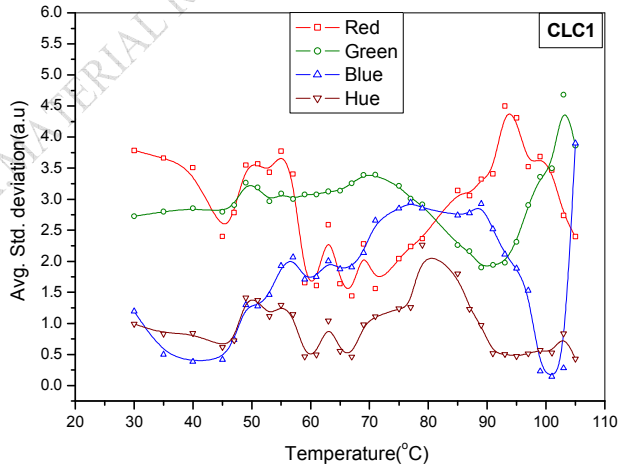

Fig. 3.19. Variation in average standard deviation of thermochromic data of CLC1, with change in temperature

The hue, saturation and intensity variation in CLC1 with change in temperature thus obtained are as depicted in fig. 3.20. As is clear from the fig. 3.20, the CLC1 sample showed the typical liquid crystal response, red at lower temperature limit of the bandwidth passing through yellow, green, blue and violet at the elevated temperature, thus having wide colour bandwidth starting from 30°C to 94°C, suggestive of its use as sensor over wide temperature range.

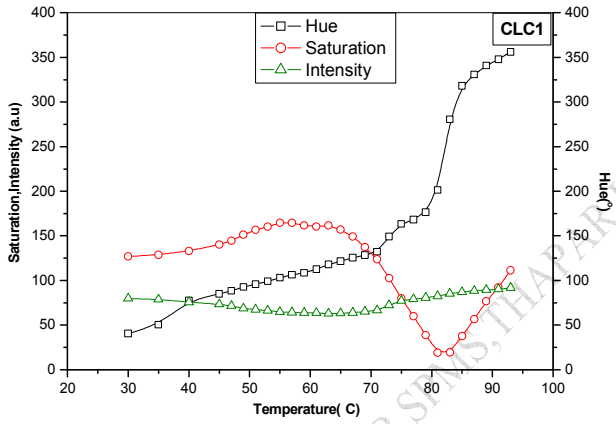

Fig. 3.20. Thermochromic response of CLC1 in terms of Hue-Saturation-Intensity model as a function of temperature

3.2.5. (d) Ageing effect:

The stability of the samples for colour and performance was tested and analysed over the period of two years. The variations thus obtained for sample CLC1 are shown in fig. 3.21. The average change in the value of hue, saturation and intensity was found to be very small, 2%, 3%and 2% respectively. This indicates the chemical stability of the sample for long period.

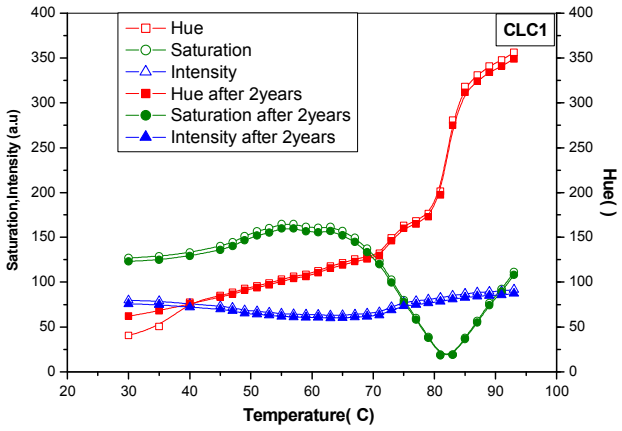

Fig. 3. 21. Ageing effect of CLC1 in Hue-Saturation-Intensity model over period of 2 years

References

[1] H. S. Kitzerow and C. Bahr, *Chirality in Liquid Crystals*, Springer (1996)

[2] P. G. de Gennes, *The Physics of Liquid Crystal*, Oxford University Press (1975)

[3] P. J. Colling and M. Hird, *Introduction to Liquid Crystal: Chemistry and Physics*, Taylor and Francis Ltd (1997)

[4] S. Chandrasekhar, *Liquid Crystal 2nd Edn. Cambridge*: Cambridge University Press (1992)

[5] L. M. Blinov and V. G. Chigrinov, *Electrooptic Effects in Liquid Crystal Materials*, Springer-Verlag (1994)

[6] P. S. Pershan, *Structure Of Liquid crystal Phases*, World Scientific publishing Co. Pt. Ltd. (1988)

[7] E. Lueder, *Liquid Crystal Displays*, John Wiley and Sons, Ltd. (2001)

[8] D. K.Yang, *J. Display Technology*, 2, (2006)32

[9] H. Qi and T. Hegmann *J. Mater. Chem.,* 16, 4197(2006)

[10] S. W. Choi, S. I. Yamamoto and Y. Haseba, H. Higuchi and H. Kikuchi , *Appl. Phys. Lett*., 92, 043119(2008)

[11] L. N. Lisetski, S. S. Minenko, A. V. Zhukov, P. P. Shtifanyuk, and N. I. Lebovka, *Mol. Cryst. Liq. Cryst.,* 510, 43/ 1177 (2009)

[12] W. Helfrich, *Appl. Phys. Lett.,* 17, 531 (1970)

[13] D. Subacius, P. J. Bos and O. D. Lavrentovish, *Appl. Phys. Lett.,* 71, 1350 (1997)

[14] D. Subacius, S. V. Shiyanovskii, P. Bos and O. D. Lavrentovish, *Appl. Phys. Lett*., 71, 3323 (1997)

[15] O. D. Lavrentovich, S. V. Shiyanovskii and D. Voloschenko, *Proc. SPIE,* 149, 3787(1999).

[16] F. Rondelez and J. P. Hulin, *Solid State Commun.,* 10, 1009 (1972)

[17] M. J. Park, O Ok Park , *Microelectronic Engineering*, 85, 2261 (2008)

[18] E. P. Raynes, *Liq. Cryst.* 2006, **33**, 1215 – 1218

[19] B. R. Acharya, K. W. Baldwin, R. A. MacHarrie, and J. A. Rogers, C. C. Huang and R. Pindak, *Appl. Phys. Lett.*,81, 5243 (2002)

[20] H. Takahasi, J. E. Maclennan, and N. A. Clark, *Jpn. J. Appl. Phys*., 37, 2587 (1998)

[21] S. T. Wu, *Appl. Phys. Lett.* , 57, 986 (1990)

[22] E. Jakeman, E.P. Raynes, *Phys. Lett. A*, 39, 69(1972)

[23] J. Stasiek, A. Stasiek, M. Jewartowski, M.W. Collins, *Optics and Laser Technology,* 38 (4–6), 243 (2006)

[24] M. Bharara, J. E. Cobb, D. J. Claremont, *The International Journal of Lower Extremity Wounds,* 5(4), 250 (2006)

[25] K. Azar, D. J. Farina, *Electronics Cooling Magazine,* 1, 3 (1997)

[26] D. J. Farina, Electronics Cooling Magazine, 1, 2 (1995)

[27] E. J. Klein, *AIAA*, 68, 376(1968)

[28] V. U. Kakade, G. D. Lock, M. Wilson, J. M. Owen, J. E. Mayhew, *Int. J. Heat Fluid Flow* (2009) article in press

[29] J. Vejrazka, Ph. Marty, *Heat Transfer Engineering*, 28(2), 154(2007)

[30] T. B. Roth and A. M. Anderson, *ASME J. Heat Transfer*, 129(3), 372(2007)

[31] J. L. Hay and D. K. Hollingsworth, *Exp. Therm. Fluid Sci.,* 12, 1(1996)

[32] S. Bakrania and A. M. Anderson, *Proceedings of IMECE'02:2002 ASME* l, November 2000, New Orleans

[33] C. R. Smith, D. R. Sabatino and T. J. Praisner, *Exp. Fluids*, 30, 190(2001)

[34] D. J. Farina, J. Hacker, R. J. Moffat and J. K. Eaton, *Exp. Therm. Fluid Sci.,* 9, 1(1994)

[35] R. Wiberg and N. Lior, *Rev. Sci. Instrum*., 75(9), 2985(2004)

[36] H. Birecki and F. J. Kahn, *J. Appl. Phys*., 51(4), 1950(1980)

[37] G. Diankov, H. Naradikian and T. Angelov, *J. Mater. Sci.: Mater. Electron*, *14(10)*, 831(2003)

[38] T. B. Roth and A. M. Anderson, *ASME J. Heat Transfer*, 130(1), 014503(1) (2008)

[39] S. Kapila and K. K. Raina, *Int. J of Mod. Phy B,* (at press)

Overview

The chapter discusses the experimental findings on effects of doping chiral molecules on electro-optic response of side chain liquid crystal polysiloxanes. Three step reactions for synthesis of novel side chain chiral liquid crystal polymers of high molecular weight has been discussed in detail and the results of influence of chiral doping introduced in the liquid crystal polysiloxanes on phase sequence and electro-optic properties presented. The optical transmission increased with increase in temperature and doping concentration. The liquid crystal polymer showed chiral nematic phase from room temperature to 67^{o}C and further chiral doping results in decrease in melting point of the material. The refractive indexes of the materials were found to be in the range of most commercial polymers suitable for switchable windows.

4.1 Introduction

Thermotropic liquid crystalline polymers (LCP) have been the subject of much interest for both fundamental and applied research, due to their ability to combine the properties of low molecular mass liquid crystal and those of a polymer. Liquid crystal polymeric materials benefit over their small molecule LC counterparts from the mechanical integrity that the polymer component provides to the system [1-5]. Although LCP are a subject of intense research, but until 1956 all known examples of LC were only low molecular weight compounds. Robinson was the first to identify the liquid crystallinity in an LCP, as an explanation for a birefringent solution of a polymeric material, poly-γ-benzyl-L-glutamate in chloroform, previously observed by Elliott and Ambrose [6, 7]. Chemists then discovered that LCP may be readily synthesized by covalently stitching small mesogenic units (rigid monomers) together into a chain using flexible spacers, usually small carbon chains. Main chain LCP (MCLCP) may be formed by incorporating the mesogens directly into the polymer backbone while side chain LCP (SCLCP) may be formed by using flexible spacers to attach mesogen as pendant groups to polymer backbone [8, 9] (Fig. 4.1).

Liquid Crystal Polymer	Macromolecular Representation	Remarks
MCLCP		MCLCP are usually classed with construction materials. 1: mesogenic unit , 2: spacer
SCLCP	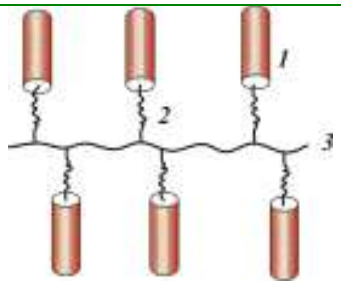	SCLCP are called functional materials; 1: mesogenic unit, 2: spacer, 3: main chain

Fig. 4.1 Schematic representation of macromolecules of liquid crystal polymers [10].

In a manner analogous to low molecular weight liquid crystals, liquid crystal polymers show the nematic structure characterized only by the orientational order, the smectic structure accompanied by formation of the layered structure (Fig. 4.2) and the chiral nematic helical structure, which appears when chiral moieties are present in macromolecules (dark brown rods in fig. 4.2). The latter structure is interesting from the viewpoint of its unique optical characteristics, in particular selective reflection of light in certain spectral regions. The LC state is attained in the temperature interval between glass transition temperature T_g (or melting T_m, if a polymer crystallizes) and the isotropic temperature T_{iso}, above which the LC polymer looses its LC properties and transforms into an isotropic melt. In this temperature interval the LC polymer behaves as a low molecular mass liquid crystal and gives rise to N, Sm or N* mesophases [10].

Structural Representation of LCP Mesophase

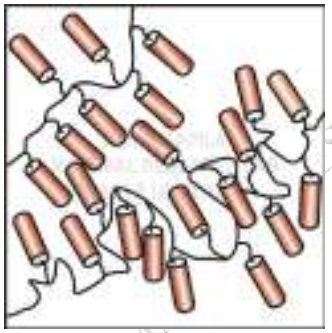

Nematic structure , with orientational order

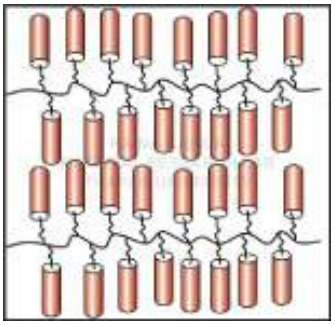

Smectic structure with characteristic layered structure.

Chiral nematic mesophase charcterized by a

supramolecular structure with helix pitch P corresponding to the turn of the director at an angle of 2 and a period of change in optical properties of d = P/2

Fig. 4.2 The types of mesophases of liquid crystal polymers [10].

Side chain liquid crystal polymers (LCPs) are quite peculiar systems combining the characteristic features of classical polymers with the rich phase behaviour and the structural diversity of low molecular weight LCs and that's why although being first introduced in late 70's only, several thousand SCLCPs have been synthesized. Side chain polymer liquid crystals exhibit better mechanical and electro-optic properties for applications in optically nonlinear devices including optical wave-guides and electro-optic modulators in poled polymeric slab wave-guides, optically addressed spatial light modulators, tunable notch filters, optical amplifiers and laser beam deflectors. SCLCP displays have also a number of advantages over low molar mass liquid crystal systems like simple and minimal fabrication cost and high flexibility [11-13].

The first SCLCPs were synthesized by Finkelmann et.al. using a polymethacrylate backbone [14-15]. These researchers discovered that liquid crystallinity could be maintained within a side group LC polymer if a flexible spacer is used to decouple the mesogen from the backbone. In addition to enabling LC behaviour of polymers, the flexible spacer and the degree of decoupling dictates the type and speed of responses that external fields induce. This discovery of Finkelmann started a flurry of research activity into the area of SCLCP. The outcome is that several thousand SCLCP have been synthesized, many different types of mesogens have been attached to variety of different polymers and many types of LC mesophases have been realized in polymer LC. To date the most common backbone for SCLCPs include polyacrylates, polymethacrylates and polysiloxanes. These comb like LCPs have been interested for their mesophase properties caused by the low molecular weight liquid crystalline side chain and the excellent mechanical properties offered by the polymeric backbone. Provided that long enough spacers are inserted between the polymer backbone and the mesogenic side groups, nematic order can persist despite the steric constraints imposed by the polymer chain in the side chain liquid crystal polymer systems. Much of the research focus has been on the polysiloxanes since they are known to be low glass transition temperature (T_g) substituted materials because of the flexibility of the backbone and thus desirable in electro optic applications [16-19].

Due to their special physical properties and potential technical applications, chiral mesophases have grown to be a central topic in liquid crystal research [20-22]. Until now most liquid crystals with chiral mesophases have incorporated a centre of chirality. Only a few examples of mesogenic compounds and dopants that possess an axis or a plane of chirality have been reported [23-24].

In this chapter we represent the experimental results of the influence of chiral doping on the physical properties of the liquid crystal polymers. Our preliminary results indicate the chiral doping enhances the range of applications of the synthesized liquid crystal polymer.

4.2 Experimental

Dichloro silanes were procured from M/s Fluka (99% purity), 5-bromo 1-pentene of 99% purity was procured from M/s Sigma-Aldrich. Solvents (toluene, diethyl ether, butanone, tetra hydro furan and ethanol of AR grade) were procured from M/s Sd fine chemicals, India. The catalyst for hydrosilylation (hexa chloro platinnic acid) was procured from M/s Sigma-Aldrich. Plasticizer dibutyl tin dilaurate was procured from M/s Sd fine chemicals and chiral dopant C15 was procured from E-Merck, Darmstadt, Germany.

All other chemicals like sodium chloride, potassium carbonate and potassium hydroxide were procured from M/s Sd fine and M/s Ranbaxy chemicals, India. All the chemicals received were used as received without further purification.

The liquid crystal polymers were synthesized and for characterization sample cells were prepared as given in detailed method in chapter 2 of this thesis.

4.3 Results and Discussion

4.3.1 poly (hydrogen methyl) siloxanes

4.3.1 (a) Synthesis

Poly(hydrogen methyl) siloxanes were synthesized by controlled hydrolytic condensation of di chloro(hydrogen methyl) silanes (M/s Fluka) using saturated solution of sodium chloride in water in 1:2 ratio(v/v) at 0-5^{o}C over a period of 2 hours in inert nitrogen atmosphere. The reaction mixture was kept at room temperature for 4-5 hours to attain the desirable viscosity. The polymer was extracted with diethyl ether and dried over anhydrous sodium sulfate [24]. Vacuum treatments were carried out to remove traces of solvent and impurities. The synthetic route for the preparation of the polymer is given in scheme 4.1.

Scheme 4.1

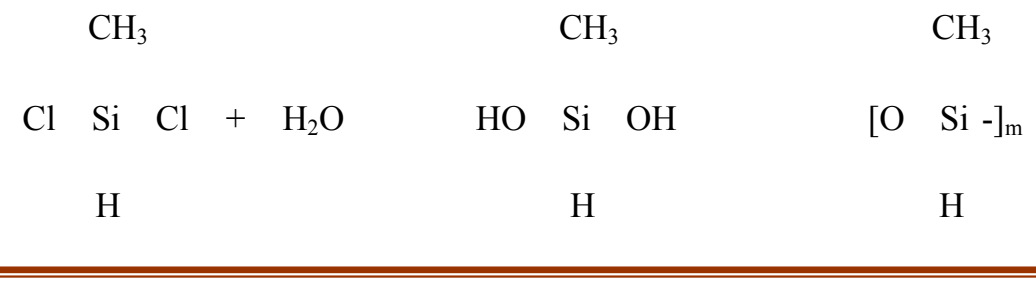

4.3.1 (b) Characterization

Viscosity:

The solution viscosity of polysiloxanes was measured using Ubbelohde viscometer at 30 0.5oC in toluene. The value of intrinsic viscosity [ ] was calculated by plotting a graph between $_{sp}$/C (specific viscosity/concentration) and concentration (C) and is found to be 0.06dl/g.

Infrared Spectroscopy:

Poly (hydrogen methyl) siloxanes synthesized in the present study have been analyzed using Perkin –Elmer Infrared spectrometer (Model FTIR 1720X). In this spectrum, there was no peak at 666 cm^{-1} due to Si-Cl confirming the complete hydrolysis of silanes to form poly (hydrogen methyl) siloxane. Further presence of Si-O-Si, Si-C, Si-H and C-H peaks in IR spectrum of poly (hydrogen methyl) siloxane is in conformity with the reported literature [25].

4.3.2 Mesogenic unit (4-pentenyloxy-4'-cyano biphenyl)

4.3.2 (a) Synthesis

The liquid crystal mesogens were synthesized using well known reaction method. The mesogens are synthesized by reacting equimolar quantities of 5-bromo-1-pentene and 4-hydroxy-4'-cyano biphenyl in dry butanone in presence of potassium carbonate. From the reaction mixture, the organic layer is separated and is washed with 5% potassium hydroxide followed by distilled water several times. The liquid crystalline material 4-pentenyloxy-4'-cyano biphenyl was extracted by evaporating the solvent

under reduced pressure. The resulting liquid crystal materials were extracted and purified using repeated recrystallization of these materials in ethanol. The synthetic route for the preparation of these mesogens is given in scheme 4.2. These materials were then characterized using IR spectroscopy.

Scheme 4.2

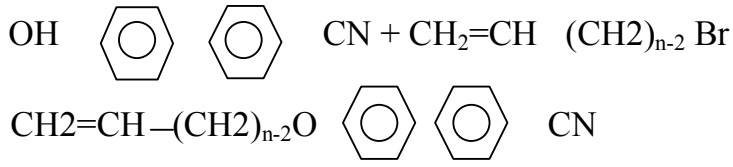

4.3.2 (b) Characterization

IR spectroscopy:

The liquid crystal mesogens were characterized using Perkin–Elmer Infrared spectrometer (Model FTIR 1720X). In these spectra, the characteristic peaks due to the functional groups, C N, C-H, were observed and confirmed the preparation of these liquid crystalline moieties.

4.3.3 Side chain siloxane liquid crystal polymers

4.3.3 (a) Synthesis

The liquid crystal polymers were synthesized by reacting polysiloxanes and pentenyloxy cyano biphenyl in presence of hexa chloro platinnic acid catalyst in toluene medium at 60^{o}C. The liquid crystal polymers were extracted and purified, we term it as SCLCP (A). The liquid crystal polymer obtained was further doped with mixture of plasticizer dibutyl tin dilaurate and chiral dopant C15 and we term it as SCLCP (B). The plasticizer increases the interchain distance of polymers and induces the proper mixing of the chiral dopant in LCP. The increase in the intermolecular distance induces the free rotation of the groups in the polymer chain and reduces the phase transition temperatures (both glass transition and liquid crystal phase transition). The resulting SCLCPs were characterized using differential scanning calorimeter and

polarizing microscopic textures. They show higher flexibility due to the flexibility of siloxane backbone and addition of plasticizers and higher liquid crystalline range due to the low glass transition temperature of polysiloxanes. The synthetic route for the synthesis of liquid crystal polymers is given in scheme 4.3.

Scheme 4.3

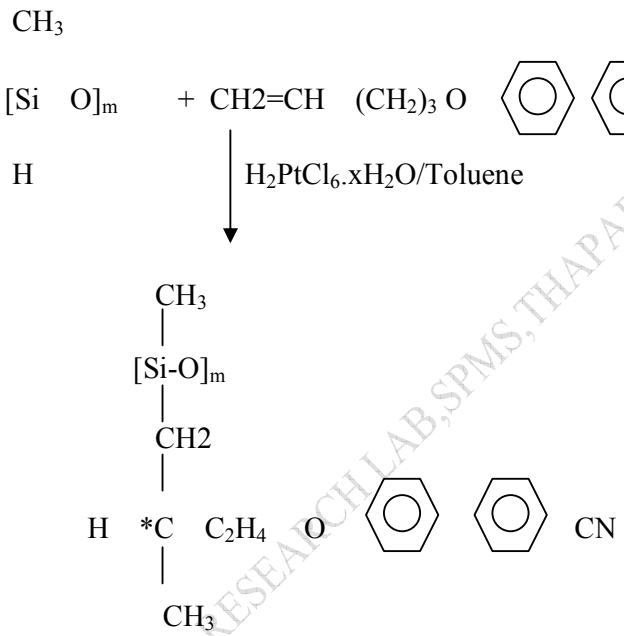

4.3.3 (b) Characterization

IR Spectra:

The absence of the Si-H bond at 1050cm^{-1} and the functional groups due to the CH3, CH2 and CN bonds near 2200cm^{-1} confirm the formation of the polysiloxane based side chain liquid crystal polymers.

Optical polarizing microscopy:

The optical textures of SCLCP (A) and SCLCP (B) observed under crossed polarizers using Olympus polarizing microscope (model BX51P) are shown in fig. 4.3. The materials were found to show the chiral nematic phase as is visible through the typical fingerprint texture of both the samples.

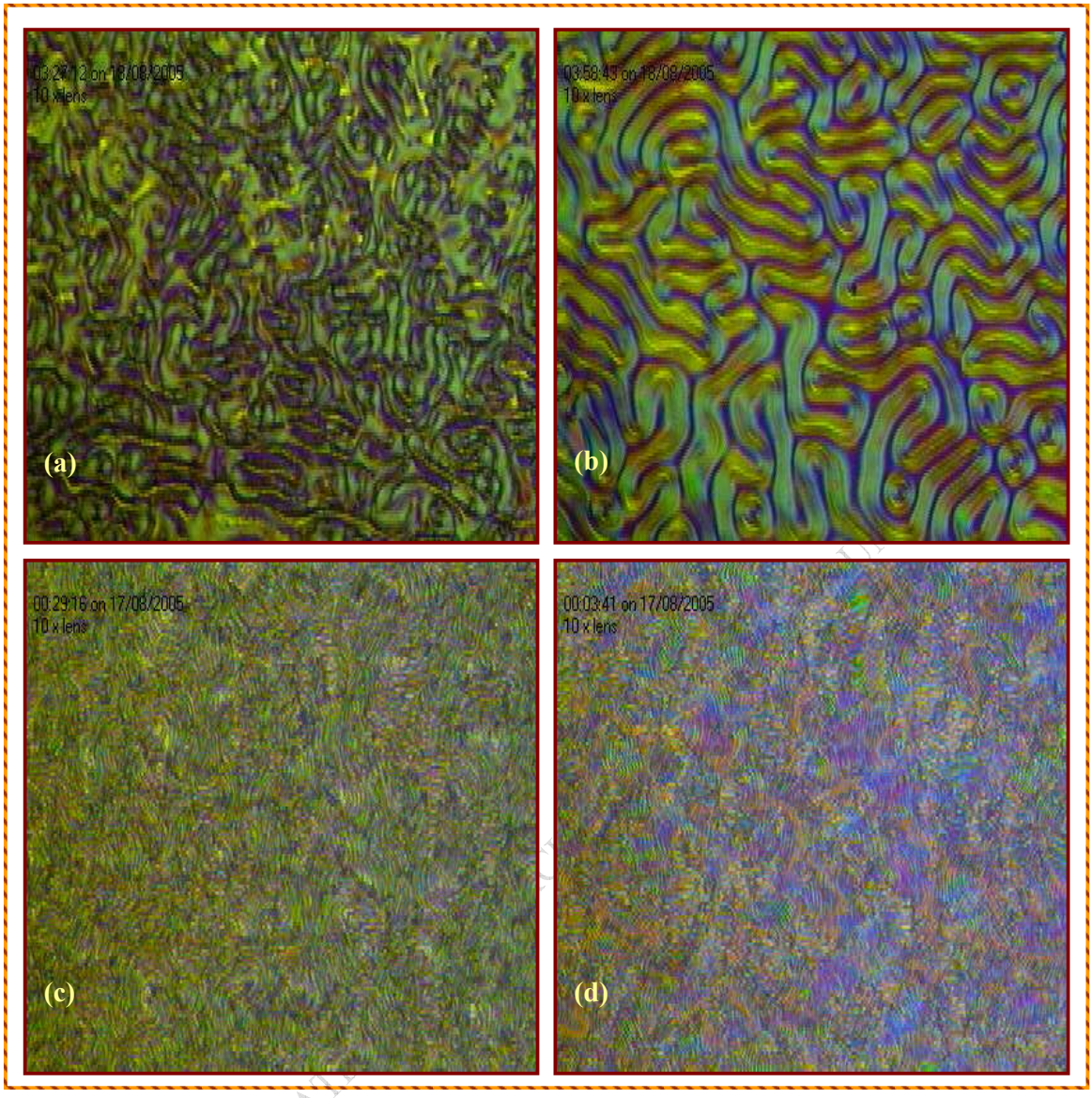

Fig. 4.3 Micro texture of SCLCP samples at (a) 35^{o}C and (b) 60^{o}C of SCLCP(A) (c) 35^{o}C and (d) 60^{o}C of SCLCP(B) at 10X [26,27]

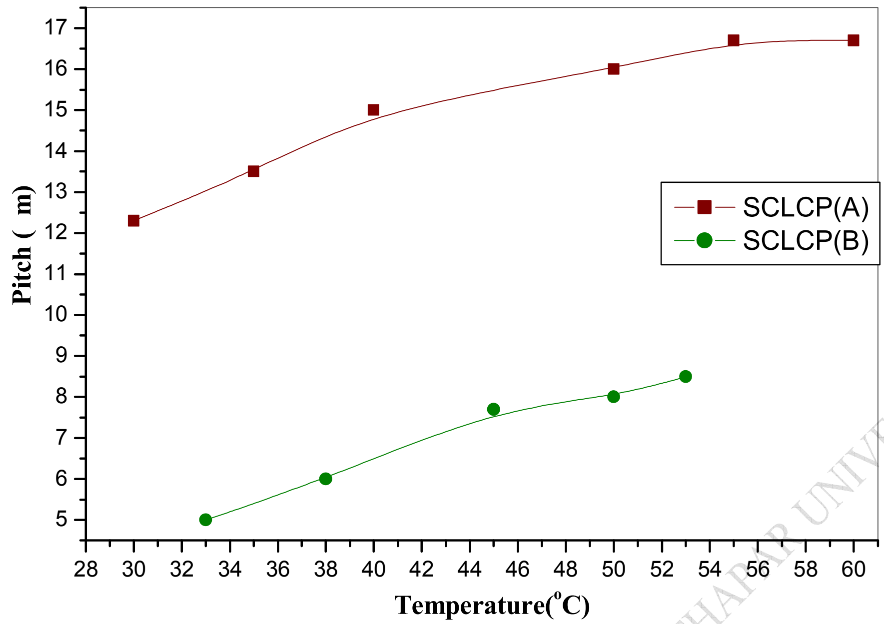

Fig. 4.4. The temperature dependence of pitch for SCLCPs

As it is clear from the micro-textures, the pitch of the materials is observed to be temperature dependant. The pitch of the SCLCPs were measured over the liquid crystalline range using Linksys software and it was found that unlike most of the chiral nematic liquid crystals, the pitch of the synthesized chiral nematic liquid crystal polymers of high molecular weight show the increase with the temperature. This may be due to the dynamic motion of the polymer with the increase in the temperature. As the temperature is increased, the polymer molecules which are coiled may be getting uncoiled changing the average shape of the molecules and increasing the pitch of the materials. The pitch of the material is decreased around 2-2.5 fold by doping with the chiral material. The dependence of Pitch with the temperature is plotted as shown in fig. 4.4.

Differential scanning calorimetry

The siloxane based liquid crystal polymers were characterized by differential scanning calorimetry which is a complementary technique to the polarizing microscopy. The phase transitions observed by polarizing optical microscopy were also observed in DSC confirming the phase transitions. The chiral doping thermally stabilizes the phase

at 49°C as indicated by increase in enthalpy from 7.37 J/g to 11.69 J/g. The melting point of the polymer also reduced from 68°C to 61°C with addition of chiral dopant and plasticizer. It may be due to the increase in the flexibility of the system. The thermographs of both the SCLCPs are shown in fig. 4.5.

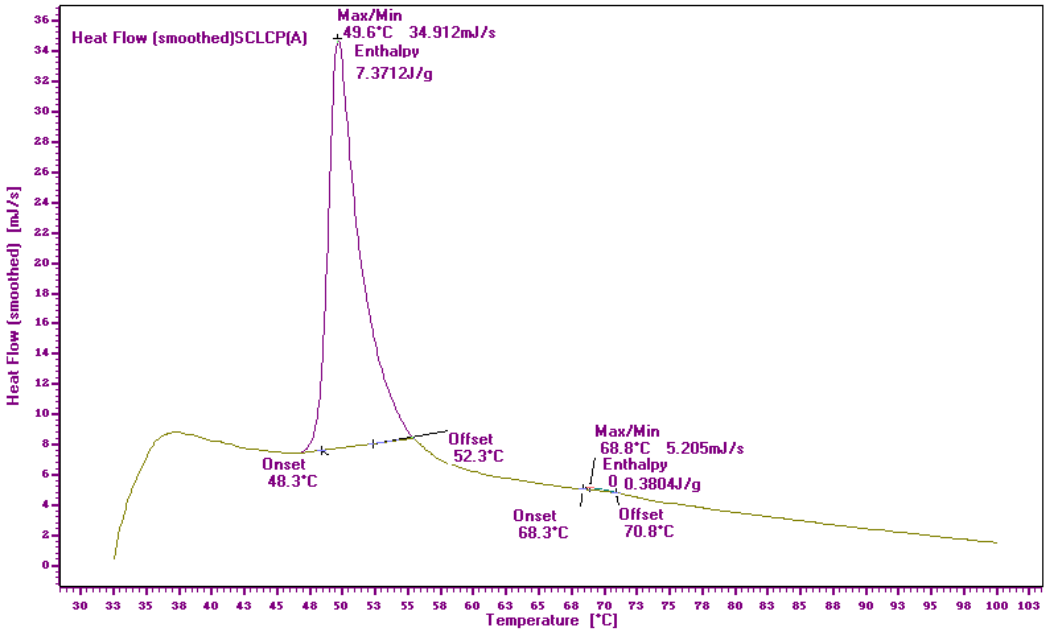

(a)

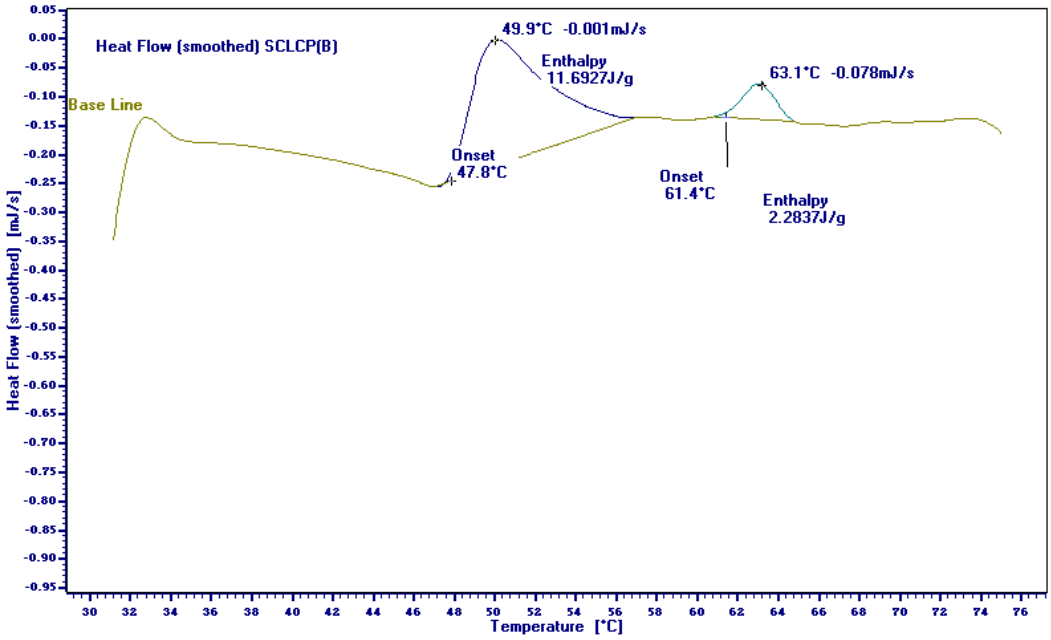

(b)

Fig. 4.5 Thermal profile of (a) SCLCP (A) and (b) SCLCP (B)

Refractive Index Measurements

Refractive Index of the SCLCPs with and without chiral impurity (A and B respectively) was studied using Abbe's Refractometer. The refractive index of SCLCP (A) was found to be 1.63 whereas the refractive index of SCLCP (B) was found to be 1.57. The refractive index of both Liquid crystal polymers are in the range of refractive index of so many commercial polymers making the possibility to use in Polymer dispersed liquid crystal systems enhancing the range of applications.

4.4 Electro-optic properties

The voltage dependence of the output transmission at different temperatures for Liquid crystal polymer of high molecular weight with and with out chiral impurity is shown in fig. 4.5. It depicts that as temperature increases, the transmission increases and slightly shifts to higher applied voltage. Primarily it may be due to the decrease in order parameter with an increase in temperature. Another possible reason for increasing the transmission with temperature may be due to decrease in anchoring energy of liquid crystal polymer network.

It was also found that the doping of chiral material influences the output transmission. At lower temperatures, the transmission increases around 1.3-1.5 folds, whereas, at higher temperature, very negligible change was observed. This may be due to the dynamic motion of the polymer with the increase in the temperature, leading to suppression of the difference between chirality doped and undoped samples.

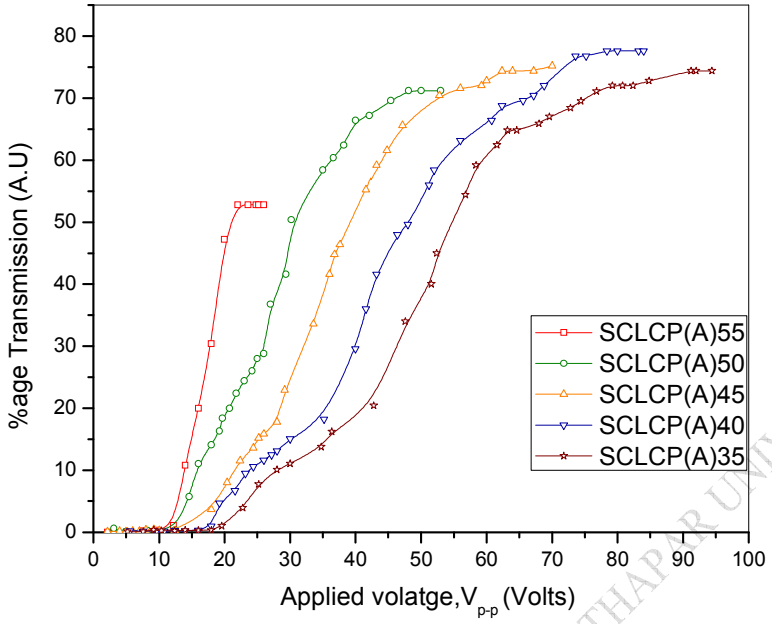

(a)

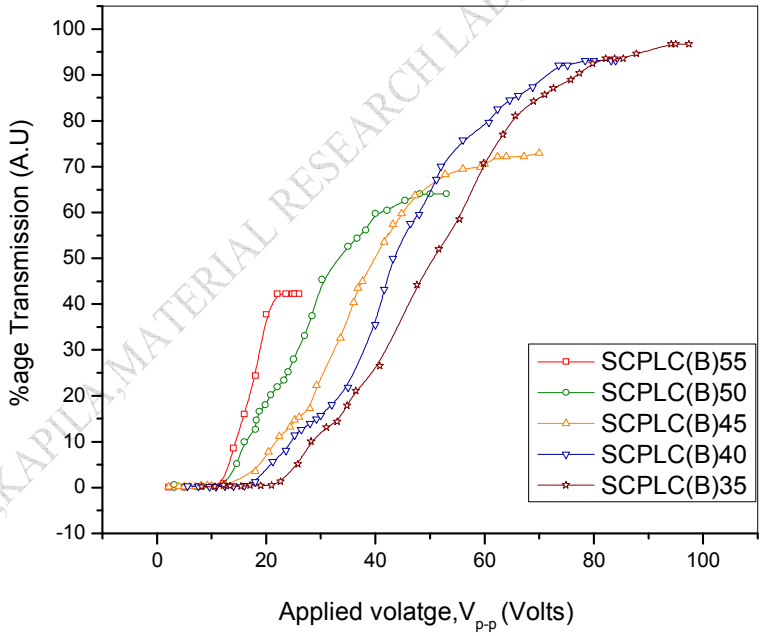

(b)

Fig. 4.6 Output transmission as a function of applied voltage of SCLCPs (a) without Chiral doping (b) with chiral doping, at different temperatures

References:

[1] P. J. Colling and M. Hird, *Introduction to Liquid Crystal: Chemistry and Physics*, Taylor and Francis Ltd (1997)

[2] P. J. Colling, *Liquid Crystal: Nature's Delicate Phase of Matter,* Pricenton: University Press (1990)

[3] S. Chandrasekhar, *Liquid Crystal 2nd Edn. Cambridge*: Cambridge University Press (1992)

[4] A. M. Donald, A. M. Windle, and S. Hanna, *Liquid Crystalline Polymer. Cambridge:* Cambridge Univ. Press (2006).

[5] H. Huang, J. Geng, S. He, B. Li, C. Ouyang, Y. Yin, H. Cao, L. Wang, M. Hai, G. Wang, H. Yang, *Liquid Crystals*, 34: 8, 949(2007)

[6] C. Robinson, *Trans. Faraday Soc.,* 52, 571(1956)

[7] E. Ambrose, *Faraday Soc. Discussions*, 9, 246(1950)

[8] A. Cifferi, W. R. Krigbaum, R. B. Meyer, *Polymer Liquid Crystals*, Academic Press: New York (1982)

[9] C. B. Mcardle, *Side Chain Liquid Crystal Polymer*, Champan and Hall: New York (1989)

[10] V. P. Shibaev, *Polymer Science*, *Ser. A*, 51, 1131(2009)

[11] H. Finkelmann, Phil. Trans. R. Soc. Lond. A , 309, 105(1983)

[12] Chain-Shu Hsu, Progress in Polymer Science, 22, 829(1997)

[13] G.W.Gray, C.Hogg and D.Lacey., *Mol.Cryst. Liq.Cryst*., 67, 657 (1981)

[14] H. Finkelmann, H. Ringsdorf, J. H. Wendroff, *Makromol. Chem.,* 179, 273 (1978)

[15] H. Finkelmann, M. Happ, M. Portugall, H. Ringsdorf, *Makromol. Chem.,* 179, 2541 (1978)

[16] G. Kossmehl, H.I. Nagel, W.Hasse, J. Mayer, *J. Acta Polymer*, 45, 21(1994)

[17] S. Meyer, R. Zentel, *Current Opinion in Solid States and Materials Science*, 6, 545(2002)

[18] G. Sumana, K. K. Raina, J. App. Poly. Sci., 94, 159 (2004)

[19] G. Sumana, K. K. Raina, Current App. Phy., 5, 277 (2005)

[20] D. Dardas and W. Kuczyñski*, Opto-electronics Review 12(3), 277–280 (2004)

[21] H. R. Brand , H. Pleiner, Mol.Cryst.Liq.Cryst. 292, 141 (1997)

[22] Y. Zhao, Li Guan, Liquid Crystals, 30, 181 (2003)

[23] K. Robbie, D. J. Broer, M. J. Brett, *Nature*, 399, 764 (1999)

[24] G. Sumana , K. K. Raina, *J. Polym. Mater*. , 19, 281(2002)

[25] D. H Williams, I. Fleming, *Spectroscopic methods in Organic Chemistry*, 5th edition, Mc Graw Hill, Maidenhead (1995)

[26] G. Sumana, S. Kapila and K. K. Raina , *Seminar on "Recent Trends in Liquid Crystal Research", India-United Kingdom science networks, Raman Research Institute,* Bangalore, India (2005)

[27] G. Sumana, S. Kapila and K. K. Raina , *Electroactive polymers : materials & devices, Vol II : Proc. 2nd International Conference on Electroactive Polymers* Goa, India, 189(2007)

Overview

This chapter describes the experimental results on the morphological, opto electronic and opto dielectric responses in chiral smectic C liquid crystal mixture, containing low concentration of carbon nanotubes. The results indicate increase in optical transmission and reduction of threshold voltage by about 40% with the CNT dispersion. We observed that embedding the CNTs in LC matrix results in the increase of dielectric constant (by about 27%). Relaxation peaks at 300Hz and 500 kHz were observable that corresponds to Goldstone mode and Soft mode respectively for undoped chiral smectic C liquid crystal. On CNT dispersion the relaxation frequency corresponding to goldstone mode shifts to 400Hz where as soft mode frequency was unchanged and with high bias field (10V) the domain mode is observed corresponding to relaxation peak at 500Hz.

5.1. Introduction

Chiral Smectic C (SmC*) liquid crystal (LC) phases with tilted structure exhibit interesting physical properties [1-2]. Due to lower symmetry, they possess spontaneous polarization and thus show ferroelectric behaviour in liquid crystals. The possibility of this phase was first envisaged by A. Saupe [1] and experimentally demonstrated by R. B. Mayer et.al. [2]. Over the years, lot of focus in liquid crystal physics and device properties concentrated on these materials [3-6] because of their fast electro-optic responses.

In the recent past, many researchers have explored the possibility of improving the performance of opto-electronic LC devices by dispersing low concentration of nano-particles into a LC matrix [7-10]. Among them the carbon nanotube (CNT)-LC composite is a unique assemblage of an anisotropic dispersion (CNTs) in an anisotropic media (LC) making it multifaceted composite to study the physical properties and morphology [11-15].

The earlier work on CNT-LC composites is reported with nematic liquid crystal (NLC) systems [16-18] and only few researchers have studied the properties of CNT-SmC* composites [19-22]. Some reports suggest a faster response time and reduced threshold voltage with CNT dispersion but there is scarcity of collective dielectric studies indifferent SmC* based materials. Arora et al. [22] reported about 0.01% CNT dispersed in SmC* had decreases the dielectric permittivity in comparison to undoped system and increase in at lower frequency for bias measurements. Prakash et al. [21] reported increase in conductance due to increase of by about one order of magnitude with 0.5% CNT. Podgornov et al. [19] observed a decrease in spontaneous polarization, dielectric permittivity. They reported increase in Goldstone mode (GM) relaxation frequency with 0.01% single walled CNT (SWCNT).

In this chapter, we present the experimental findings, in the opto-electronic and opto-dielectric behaviour of a chiral liquid crystal material containing low concentration of carbon nanotubes. We observed that embedding the CNTs in LC matrix results in the increase of dielectric constant and enhancement of optical transmission, which we believe could be due to the strong interaction between respective systems.

5.2 Carbon Nano Tubes

Carbon nanotubes, made of pure carbon, are regular and symmetric as crystals. These exquisitely thin, impressively long macromolecules have been the object of intense scientific study ever since their discovery in 1991 by Iijima [23]. The bonding in CNTs is sp^2, with each carbon atom joined to three neighbouring atoms, and forms a hexagon, as in graphite. If one of the graphitic sheets of carbon atoms is rolled up into a cylinder a mere millionth of a millimeter across, a nanotube is formed as shown in fig. 5.1. There are two main classes of CNTs with high structural perfection, single walled carbon nanotube (SWCNT) which has a single cylindrical wall and multi-walled carbon nanotube (MWCNT) composed of several such concentric cylinders nested within one another. The lengths of both types vary largely, depending on the way they are made, and are generally microscopic rather than nanoscopic, i.e. greater than 100 nanometers. These are usually produced by three main techniques, arc-discharge, laser ablation and chemical vapour deposition (CVD) methods [24-30].

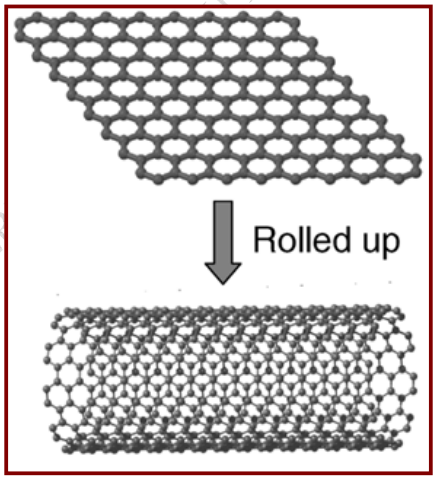

Fig. 5.1 A sheet of carbon atoms covalently bonded in hexagonal arrays, rolled into a hollow cylindrical SWCNT [27].

Single-walled carbon nanotubes

Most single-walled carbon nanotubes (SWCNT) have a diameter close to 1 nanometer, with a tube length that can be many thousands of times longer. It is generated when a

graphene sheet of a certain size is wrapped in a certain direction. The way in which the grapheme sheet is rolled affects the conductance of the nanotube, its density, its lattice structure, and other properties.

Multi-walled carbon nanotubes

Multi-walled carbon nanotubes (MWCNT) consist of multiple layers of graphite rolled in on them to form a tube shape. There are two models which can be used to describe the structures of multi-walled nanotubes. In the Russian Doll model, sheets of graphite are arranged in concentric cylinders, e.g. a (0, 8) within a larger (0, 10) SWCNT as shown in fig. 5.2. In the Parchment model, a single sheet of graphite is rolled in around itself, resembling a scroll of parchment. The interlayer distance in MWCNTs is close to the distance between graphene layers in graphite, approximately 3.3 A. MWCNTs are typically 100 times longer than their width and have outer diameters mostly in the tens of nanometers, typically in the range of 5 nm to 50 nm [31-33].

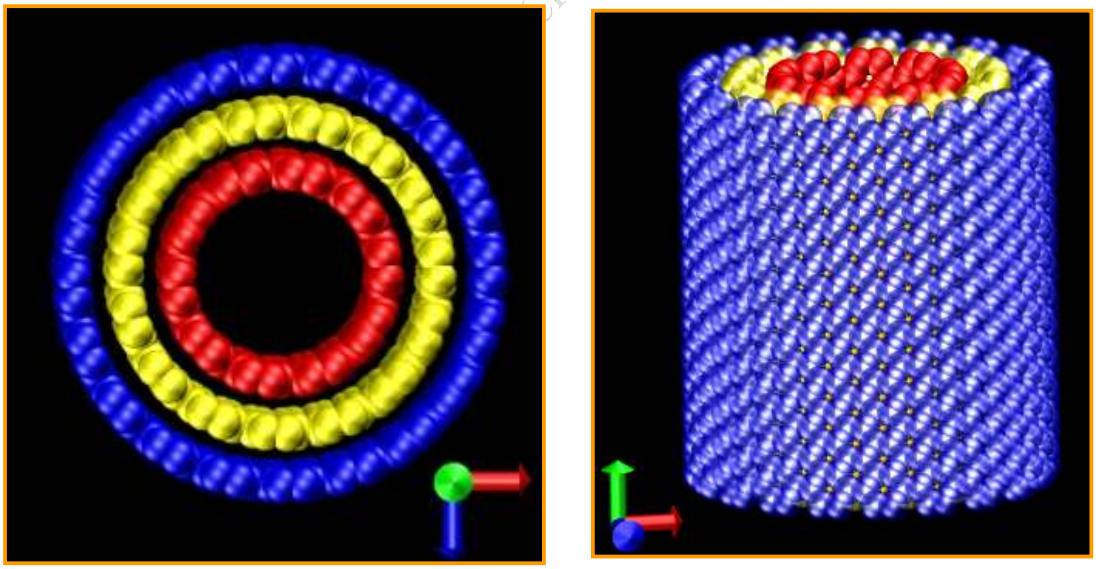

Fig. 5.2 Structure of Russian Doll model MWCNT (a) Front view and (b) Side view [34].

5.3 CNT-liquid crystal composites:

The CNT composite has become one of the fascinating research areas for technological applications as the performance of host materials improves significantly by an addition of a small amount of CNTs. It is possibly due to unique atomic and electronic structure of one dimensional carbon nanotubes. Among various CNT composites, the liquid crystal LC composite attract special interest of researchers because of the unique assemblage of anisotropic media. [35-38].

As an essential prerequisite for realizing the technological applications it is crucial to obtain a uniformly dispersed CNT suspension. The one of the most challenging tasks is to homogeneously disperse the CNTs into the liquid crystal host, as CNTs have a tendency to aggregate into networks and fibrils (MWCNTs) within the dispersion due to the van der Waals interaction between the nanotubes [27]. To overcome this, the CNT-liquid crystal composites were normally prepared by ultrasonification of an initially homogeneous solution of liquid crystal (LC) and nanotubes. Fig. 5.3(a) shows optical textures of the SmC* mixture with 0.1%CNT prepared manually by shaking the compound. Optical micrograph shown in fig. 5.3(b), exhibiting 0.1%CNT dispersed through sonification is suggestive of a finer dispersion of nanotubes in the liquid crystal matrix. The detailed procedure is described in chapter 2 of this thesis.

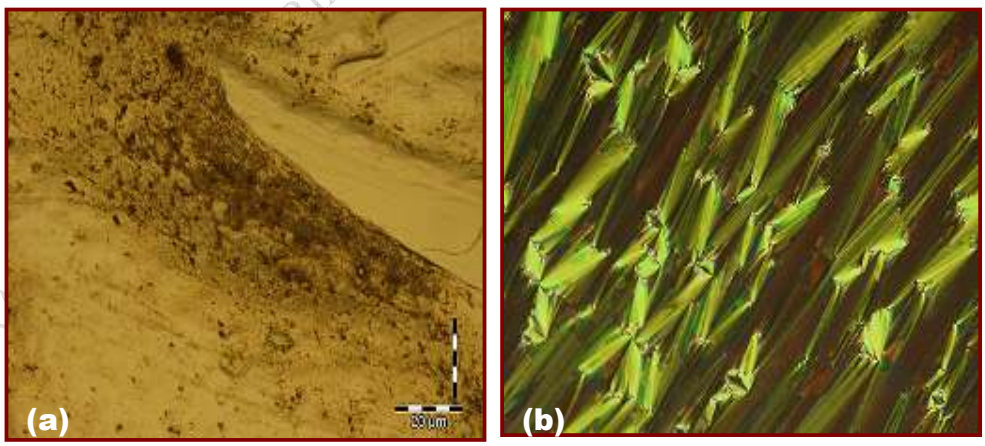

Fig. 5.3 Optical micrographs (10X) of 0.1% MWCNT in SmC* (a) with manual shaking (b) after sonification at reduced temperature (ΔT= -30°C).

5.4 Dielectric Relaxations in Chiral Smectic Liquid Crystals:

In this section the possible relaxation processes in the chiral liquid crystal phases have been discussed. Both types of molecular processes i.e collective and non-collective exists in chiral liquid crystal phases. Different relaxation processes in chiral smectic phases are shown in fig. 5.4.

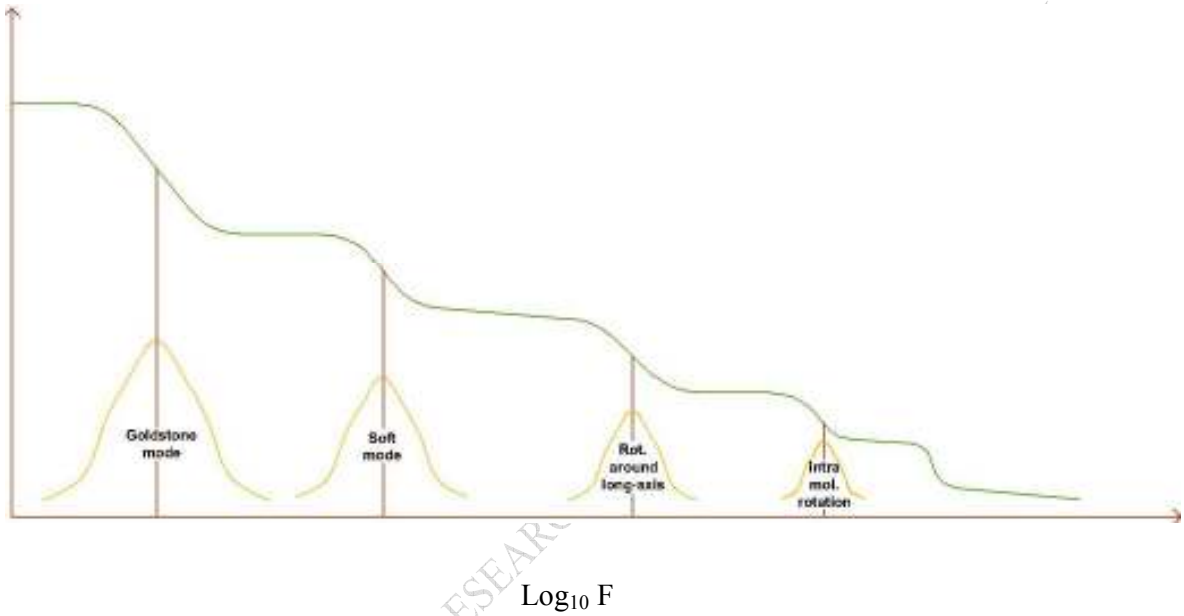

Fig. 5.4 Frequency dependence of the perpendicular component of the complex dielectric permittivity in chiral smectic phases. The spectrum exhibits relaxation processes of collective and non-collective modes.

The chirality of molecules has two effects on the system in the tilted phase. First, the tilt locally breaks the mirror symmetry w.r.t. the plane of tilt and normal to the smectic layers. Therefore, a transverse spontaneous polarization is induced locally, which is perpendicular to tilt direction and is normal to the layers. Second, because of the chiral character of the molecules, the tilt is not homogeneous. The molecules within one layer are tilted uniformly but the direction of tilt precesses around the normal to the smectic layers as one goes from one smectic layer to another. Together with the tilt, the transverse electric polarization, which remains locally perpendicular to the tilt, forms a helicoidal structure (SmC* phase) [39-41].

The projection of molecules into the smectic phases (which are taken to be parallel to the XY plane) is described by an order parameter

$$_1\hat{x} \quad _2\hat{y} \tag{5.1}$$

The induced transverse in plane polarization perpendicular to the direction of tilt (Fig. 5.5(a)) is given by

$$P \quad P_X\hat{x} \quad P_Y\hat{y} \tag{5.2}$$

Denoting the wave vector of helical pitch p_0, as $q = 2 /p_0$, for small tilt angles we can write

$$\begin{aligned} &_1 \quad n_x n_z \quad _0 Cos(qZ), \qquad _2 \quad n_x n_z \quad _0 Sin(qZ) \\ &P_X \quad P_0 \; Sin(qZ) \qquad\qquad P_Y \quad P_0 Sin(qZ) \end{aligned} \tag{5.3}$$

Where Z = co-ordinate normal to the smectic planes. $_0$ and P_0 are the magnitude of tilt angle and spontaneous polarization respectively [42].

It has been seen that even if the system exhibits a local net polarization, the macroscopic average of this will be zero. Applying an electric field of magnitude E parallel to the smectic layers will however disturb the helix in such a way that an average macroscopic polarization $<P_i>$ is induced. Here it has been assumed that the field acts in the X-direction. On the other hand, there exists a quadratic field effect, which originates in the dielectric anisotropy of molecules. The dielectric anisotropy is defined as

$$= _{||} - \tag{5.4}$$

This describes the tendency of electric field to align the molecules with their axis of the largest dielectric susceptibility in the direction of field [40-41, 43-44].

The disturbance of equilibrium order parameter, when an electric field is applied to the system (parallel to the smectic layers) can be divided into two parts.

i) Amplitude changes (change in the magnitude of tilt $_0$ and polarization P_0)

ii) Phase changes (i.e. changes in the direction of tilt and the polarization)

Hence, dielectric response of the system will consist of four parts (apart from the high frequency electronic response), two of that are connected to director reorientation and two connected to reorientation of the polarization. Denoting the amplitude changes by

$_1$ and P_1 and the phase changes by $_2$ and P_2 (Fig. 5.5 (b,c)), we can express order parameter as

$$\begin{matrix} _1(t) & _0\,Cos(qZ) & _1(t)\,Cos(qZ) & _2(t)\,Sin(qZ) \\ _2(t) & _0\,Cos(qZ) & _1(t)\,Sin(qZ) & _2(t)\,Cos(qZ) \\ P_x(t) & P_0\,Sin(qZ) & P_1(t)\,Sin(qZ) & P_2(t)\,Cos(qZ) \\ P_y(t) & P_0\,Cos(qZ) & P_1(t)\,Cos(qZ) & P_2(t)\,Sin(qZ) \end{matrix} \qquad (5.5)$$

Linear combinations of the director reorientation modes are commonly denoted by the soft (amplitudon) mode *"SM"* and the Goldstone (phason) mode *"GM"*.

Linear combinations of the polarization reorientation modes are the polarization soft mode "*PSM*", and the polarization Goldstone mode "*PGM*", the relaxation frequency (f_r) of which has been reported to be of the order of 500MHz. These two modes appear due to the molecular rotation around long axis of the molecule.

For each mode at a given temperature contribution to the dielectric constant decreases with increasing frequency of the field from the low frequency value ($f<<f_i$) to zero. This value is adopted when the value of the applied electric field is so high ($f>>f_i$) that the mode cannot follow the electric field, where f_i is the characteristic relaxation frequency of that mode. The difference between the low and high frequency contributions of the mode to the total dielectric constant is called the dielectric strength of the i^{th} mode and is denoted by $_i$ (T).

$$= _0 - \qquad (5.6)$$

Where and $_0$ are the infinite frequency and static relative dielectric constants respectively. The dielectric strength is related to the average induced polarization as

$$_a \quad _i(T) \quad \lim_{E \to 0} \frac{P_i}{E} \qquad (5.7)$$

where E is the magnitude of a static applied electric field and $_a$ being the permittivity of free space.

Several relaxation mechanisms, each of which is connected to a characteristic relaxation frequency contributes to complex dielectric constant *(, T), given by

$$*(\ ,T) \quad (\ ,T) \quad i\ "(\ ,T) \tag{5.8}$$

Where = 2 f is the angular frequency of applied field and T is the temperature of the system. (, T) is the real part and (, T) is the imaginary part of the dielectric constant respectively [45-46].

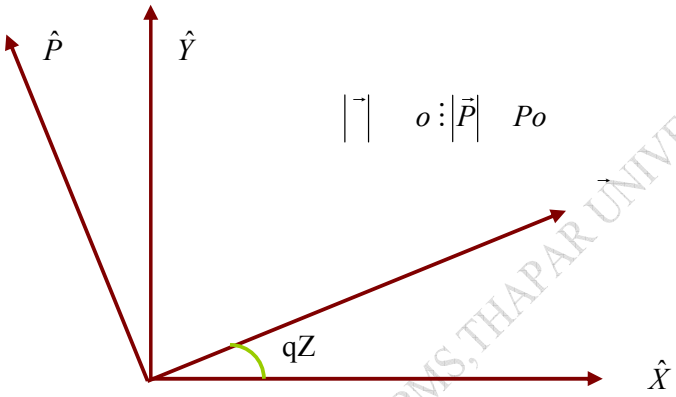

(a)

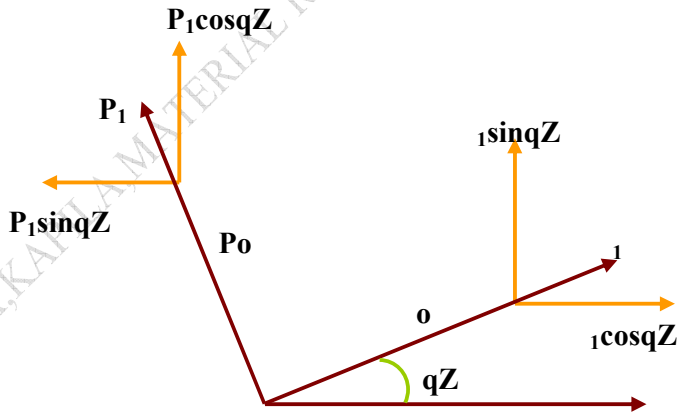

(b)

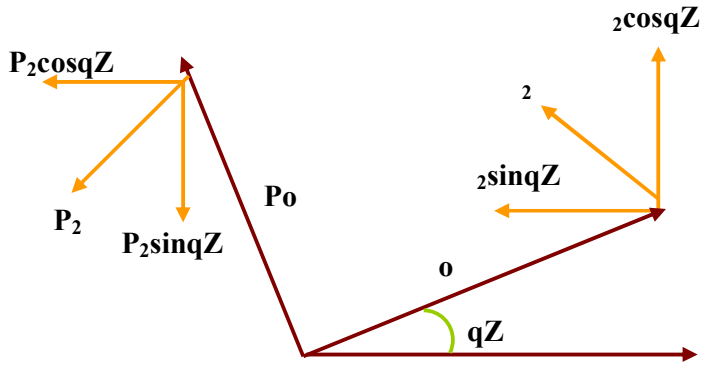

(c)

Fig. 5.5 Introduction of the order parameter and P and their changes due to the application of an electric field to the system. The amplitude changes connected to the SM are denoted by $_1$ and P_1 while the phase changes connected to the GM are denoted by $_2$ and P_2. (a) order parameters (b) amplitude changes (SM) (c) phase changes (GM)

5.4.1a Debye Type Relaxation: On application of an electric field to some medium, polarization of the medium approaches its equilibrium value exponentially with time. Decay function (t) is defined by

$$(t) \quad \exp(\ t/\ ) \qquad (5.9)$$

Where is the relaxation time, which is independent of time, but depends on temperature. This type of relaxation is known as Debye type relaxation.

Thus, with the assumption that relaxation behaviour of each mode is characterized by one single relaxation frequency (Debye relaxation), we can write the complex dielectric constant of the SmC* phase as

$$*(\ ,T) \quad \frac{_i(T)}{1\ \ i\ \ _i} \qquad \frac{^0}{1\ \ i\ \ _i} \qquad (5.10)$$

Where $_i$ (T) is the dielectric strength and $_i$ =1/2 f_i is the relaxation frequency of the corresponding mode. The generalization of the Debye formulation describes a dielectric process with a discrete distribution of relaxation times associated with a single dielectric process. On comparing Eq. (5.8) and Eq. (5.10), we obtain

$$(\quad) \qquad \frac{^{0}}{1 \quad ^{2} \; ^{2}} \tag{5.11}$$

$$(\quad) \qquad \frac{^{0}}{1 \quad ^{2} \; ^{2}} \tag{5.12}$$

is also known as the dielectric loss factor. D the dissipation factor i.e. the dielectric loss is given by

$$D \quad \frac{(\quad)}{(\quad)} \tag{5.13}$$

Eq. (5.11) and Eq. (5.12) are Debye equations. Debye type relaxation is best visualized by Cole-Cole plot as shown in fig. 5.6[47-48].

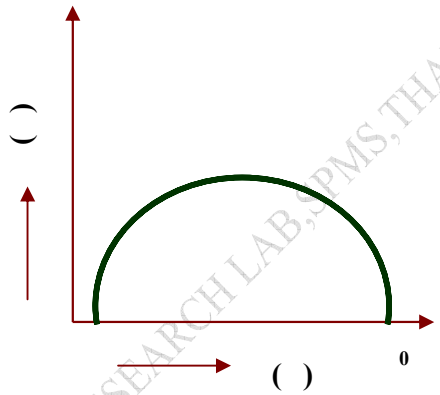

Fig. 5.6 Cole-Cole plot for a Debye dielectric relaxation

5.4.1b Distribution of Relaxation Times: Majority of LCs show a distribution of relaxation times. One can also assume that the relaxation time has a continuous distribution of dielectric relaxation times and is due to the superposition of several types of absorption. Eq. (5.11) and Eq. (5.12) are modified to

$$\frac{G(\quad)}{1 \quad ^{2} \; ^{2}} \; d \tag{5.14}$$

Where G( ) is the distribution function for relaxation times

$$\frac{G(\quad)}{1 \quad ^{2} \; ^{2}} \qquad d \tag{5.15}$$

Cole-Cole suggested an empirical distribution about a mean relaxation time $_{0}$, leading to complex permittivity as

$$*(\quad) \qquad \frac{0}{1 \quad (i \quad _i)^{1 \quad i}} \tag{5.16}$$

Where $_i$ is the distribution parameter i.e. the spreading factor for a particular reorientation process. The value of $_i$ lies between 0 and 1. $_i = 0$ corresponds to a single relaxation time; while $_i$ close to 1 corresponds to an infinite distribution of relaxation time. Here also Cole-Cole plot provided an elegant method of finding out whether a system has a single relaxation time. This plot is also useful for the characteristics of different types of distribution function and is widely applied [48].

By splitting Eq. (5.16) into its real and imaginary parts, we get

$$\frac{1}{2}(\quad _0 \qquad) \; 1 \quad \frac{Sinh(1 \qquad) \ln \quad _0}{Cosh(1 \qquad) \ln \quad _0 \quad Sin\frac{1}{2}} \tag{5.17a}$$

and

$$\frac{1}{2}(\quad _0 \qquad) \quad \frac{Cosh\frac{1}{2} \quad _0}{Cosh[(1 \qquad) \ln \quad _0] \quad Sin\frac{1}{2}} \tag{5.17b}$$

5.4.1c Distribution of Relaxation Times in Chiral SmC Liquid Crystals: As discussed, the dielectric response of the system in ferroelectric SmC* LCs consists of four modes (apart from the usual electronic order parameter). Two high frequency modes and two modes of lower frequency connected to the reorientation of director (Fig. 5.7).

The frequency dependence of the * complex dielectric permittivity in the SmC* phase can be presented as (when an electric field is applied parallel to the smectic layers)

$$*(\quad) \qquad \frac{GM}{1 \quad (i \quad _{GM})^{1 \quad GM}} \quad \frac{SM}{1 \quad (i \quad _{SM})^{1 \quad SM}} \quad \frac{PGM}{1 \quad (i \quad _{PGM})^{1 \quad PGM}} \quad \frac{PSM}{1 \quad (i \quad _{PSM})^{1 \quad PSM}} \tag{5.18}$$

Here the second term is connected with *GM*, third with the *SM*. fourth and fifth term is connected with the molecular reorientation around their long and short molecular axes defined as the polarization modes due to the *PGM* and the *PSM*.

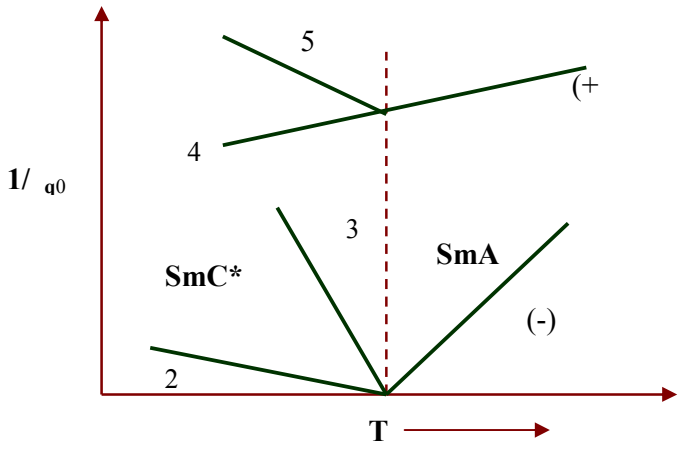

Fig.5.7 Schematic predicted temperature dependence of order parameter relaxation frequencies in SmC* at T_{C^*A}. Mode 2 is the *GM* and mode 3 *SM* of the SmC* phase.

In the SmA phase, $_0 = P_0 = 0$, so that only amplitude changes are present. The system thus exhibits a double degenerated soft director mode and a double degenerated high-frequency polarization mode. The complex dielectric constant in this case is written as

$$*(\quad) \qquad \frac{_{SA}(T)}{1 \quad (i \quad _{SA})^{1 \quad SA}} \quad \frac{_{PA}(T)}{1 \quad (i \quad _{PA})^{1 \quad PA}} \tag{5.19}$$

However for frequencies upto approximately 50MHZ the valid expression from Eq.(5.18) is

$$*(\quad) \qquad \frac{_{GM}(T)}{1 \quad (i \quad _{GM})^{1 \quad GM}} \quad \frac{_{SM}(T)}{1 \quad (i \quad _{SM})^{1 \quad SM}} \tag{5.20}$$

The *SM* contribution shows up practically in the vicinity of SmC*-SmA transition (T_{C^*A}). The term *SM* arises from the fact that, by approaching T_{C^*A}, the binding force or the corresponding elastic constant gets soft for a certain mode of vibration. Accordingly, we can say that any mode, when approaching T_{C^*A} characterized by

$$_0 \qquad \textit{and} \qquad 0 \tag{5.21}$$

is a soft mode. If the SmA phase is cooled down and allowed to approach T_{C^*A}, the elastic constant controlling the tilt fluctuations gets soft. Thus the fluctuation amplitude increases drastically and its susceptibility diverge at T_{C^*A}. The softening of this elastic constant means that the phase will lose its stability gradually until it becomes unstable and the molecules fluctuate collectively (Fig. 5.8 (a)). When a weak

electric field is applied in a direction perpendicular to the director it can easily perturb the tilt fluctuation depending on how close the system is to T_{C^*A}. The system becomes soft against these fluctuations. The mechanism is usually observed in the kHz range with strong temperature dependence. In other words, the molecules collectively oscillate around the smectic cone. This mode is called *GM* (Fig. 5.8 (b)). This process has a characteristic frequency, which varies in the range of a few kHz with weak temperature dependence. These modes are thermally activated. Both of them could be measured in the planar orientation [45, 49].

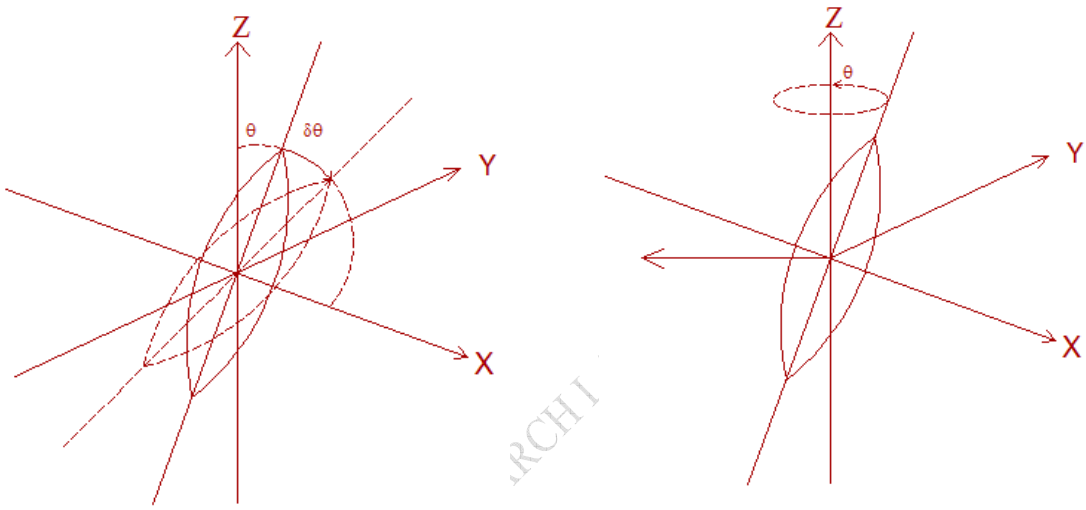

(a) **(b)**

(a)

Fig. 5.8 Geometry for the a) Soft mode contribution b) Goldstone mode contribution

5.4.2 Effect of Bias voltage:

A bias electric field is one of the important parameters that strongly affect the dielectric properties of chiral smectics. The researchers [49] have reported on the appearance of periodical structure on the application of d.c bias on the GM. It suppresses the GM and at certain bias (higher than the critical field) a new modulated structure gives rise to a domain mode "DM". The effect of bias field on the dielectric increment and relaxation frequency of the GM have been studied by many authors [50-53].

5.5 Dielectric measurements:

(a) Measurement technique

The evaluation of experimental data is much facilitated by Cole-Cole plot or arc plot [48]. For a dielectric with a single relaxation time the Cole-Cole plot is semicircle. A simple evaluation of the Debye Eq. (5.11) and Eq. (5.12) shows that the equation between the real (( )) and imaginary part (( )) of the dielectric constant is the equation of a circle

$$( ) \quad \frac{s}{2} \quad ^2 \quad (\quad ( ))^2 \quad \frac{1}{4}(\quad _s \quad)^2 \qquad (5.22)$$

The Cole-Cole plot provides therefore an elegant method of finding out whether a system has a single relaxation time. This plot is also useful for the characterization of different types of distribution function, and is widely applied.

The arc plot of a dielectric with a single relaxation time is shown in fig. 5.9. A given point on the semi-circle corresponds to the frequency while the summit corresponds =1. The plot has the disadvantage that the does not appear in it. Any material with a single relaxation time characterized by $_S$ and gives the same arc plot.

The plot in Fig 5.9(a) can be considered in cartesian co-ordinates but its treatment is mathematically more elegant in the complex plane. A point on the semi-circle defines two vectors U and V.

By virtue of the construction U - V = $_0$ - , while U = ( ) - + i ( ) by definition

If the Debye equations apply

$$V \quad Ui \qquad (5.23)$$

Which signifies that the two vectors are at right angles to each other, since multiplication by i signifies rotation by /2 in the complex plane.

Cole and Cole generalized the representation of a Debye dielectric by a circular arc plot in the complex plane so that it applies to a certain type of distributions of relaxation times (Fig.5.9 (b)) and it is defined as

$$\frac{V}{U} \quad (\quad)^{1} \tag{5.24}$$

Where and are the constants defined as the relaxation time (=1/2 f_i) and the distribution parameter of the corresponding relaxation mode. f_i is the relaxation frequency of the relaxation mode. For any point on the arc defined by plotting ( ) as a function of ( ) the angle between U and V is (1-) /2. This is the case for two secants of a circle, where the radii drawn from the center of circle subtend an angle (1-) as shown in Fig.5.9(b) and the construction of the circle follows the diagram. The corresponding dielectric constant has already been explained in Eq. (5.16). Where

$$V \qquad (0) \qquad (\ )^{2} \qquad (\ )^{2} \quad ^{1/2} \tag{5.25a}$$

$$U \qquad (\ ) \qquad (\ )^{2} \qquad (\ )^{2} \quad ^{1/2} \tag{5.25b}$$

( ) = Real dielectric constant at a particular frequency

( ) = Imaginary dielectric constant at that frequency

(0) = Low frequency dielectric constant where the Cole-Cole plot cut the abscissa axis at the lower frequency side.

( ) = High frequency dielectric constant where the Cole-Cole plot cut the abscissa axis at the higher frequency side.

The difference of (0) and ( ) from the Cole-Cole plot gives the dielectric strength of that mode. A plot of $\log_{10}$(V/U) versus $\log_{10}$f gives a straight line. The intercept on the abscissa corresponds to f_r and the slope gives the distribution parameter . The data points may deviate from the straight line because at low frequencies, the value of (V/U) is very small, as V is small and at high frequencies (V/U) is large, as U is small. This makes the value of $\log_{10}$ (V/U) very sensitive to the choice of C (0) and C ( ) [54].

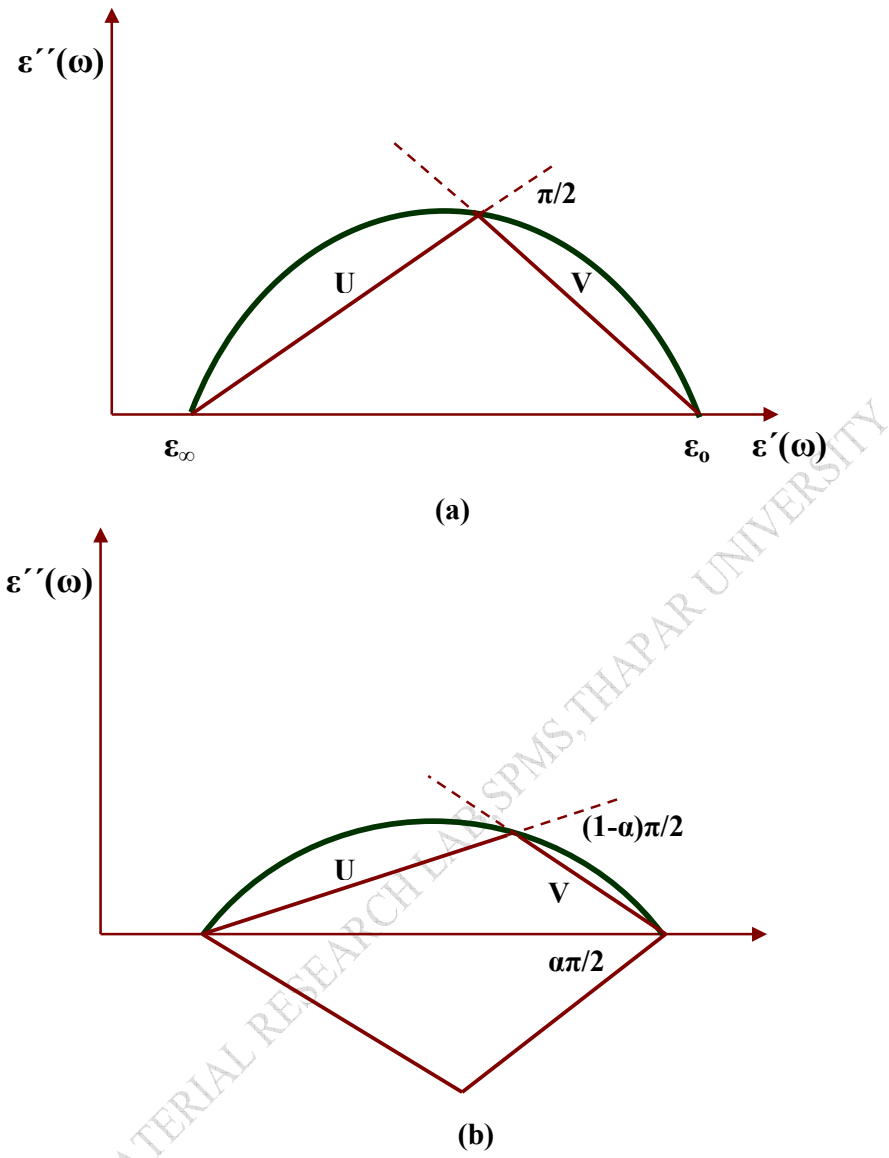

Fig. 5.9 Arc plot for (a) Debye dielectric (b) dielectric with a Cole-Cole distribution characterized by the parameter

(b) Low and high frequency correction

The quantitative evaluation of the dielectric measurements in the frequency range up to 10MHz is relatively straight forward. However, there are at least two sources of systematic errors:

- ✧ At low frequency, due to freely moving ions
- ✧ At high frequency due to resistance of ITO conducting layer and lead inductance.

Therefore corrections are needed to get correct value from measured data. It is however, possible to subtract the background from the spectrum to get the correct contribution, through fitting the experimental data to some function.

Liquid crystal mixtures are not ideal dielectrics i.e. there are certain concentration of charge carriers, which can move freely in the mixture on the application of the electric field. In the low frequency dielectric measurement, if the dc conductance due to ionic charges of the sample is comparable to the ac conductance, the effect of electrode polarization is observed in such a way that measured values are very large. Ionic conductance and associated electrode capacitance have profound effect on measured data in liquid crystal mixtures at frequencies less than 10 KHz. In this regard an admittance model was proposed by Srivastava et.al. [55], according to this model C (dc) is a frequency dependent function, increasing with frequency as a $(f)^{1/2}$. Therefore measured dielectric spectrum in low frequency region has a contribution from dipolar orientation and the freely moving charges that can be written with Cole-Cole eq. (5.16) as

$$\varepsilon^{*} \quad \varepsilon' \quad j\varepsilon'' \quad \varepsilon'(\quad) \qquad {}_{i} \frac{(\Delta\varepsilon)_{i}}{1 \quad (j\omega\tau_{i})^{(1 \quad {}_{i})}} \quad \frac{A}{\omega^{n}} \quad j\frac{(dc)}{\varepsilon_{0}} \quad {}^{k} \qquad (5.26)$$

Where $'(\infty)$ is the high-frequency limiting value of the relative dielectric permittivity and (dc) is the ionic conductivity. Δ , τ and are dielectric strength, relaxation time and distribution parameter ($0< <1$) respectively, A, n and k are fitting parameters and value of k is usually 1 for dc conductivity, $_0$ (=8.85 pF/m) is the free-space permittivity. Second term in above equation is Cole-Cole term for relaxation modes present in the dielectric spectrum where i represent number of relaxation modes.

In the high frequency region above 100 KHz, the contribution from the freely moving ions becomes negligibly small. However, the loss of energy due to the resistance of the ITO layer becomes dominating resulting in a pronounced increase in absorption with increasing frequency. Gouda et al. [56] have proposed a high impedance model to account for ITO effect in which cut-off frequency of the cell is given by the inverse of $R_{ITO}C$, where R_{ITO} is the resistance due to ITO coating on glass electrodes. Thus in order to diminish the effect of ITO layer by shifting it to high frequency it is important to use glass electrodes of very low resistive layer. An additional imaginary term B^{m} is

added in the imaginary part of Cole-Cole eq. (5.16) to partially account for ITO effect, where B and m are constants as far as correction terms are small.

$$'' \quad B^{\,m} \quad \mathrm{Im}\{ '(\ ) \quad {}_i \frac{(\ )_i}{1 \quad (j \quad {}_i)^{(1 \quad {}_i)}}\} \tag{5.27}$$

Generally one may get a dielectric spectrum with pronounced background from both low and high frequency effects. On adding eq. (5.26) and (5.27) we get

$$\varepsilon^* \quad \varepsilon' \quad j \quad '' \quad \varepsilon'(\ ) \quad {}_i \frac{(\Delta\varepsilon)_i}{1 \quad (j\omega\tau_i)^{(1 \quad {}_i)}} \quad \frac{A}{\omega^n} \quad j\frac{(dc)}{\varepsilon_0 \quad {}^k} \quad jB\omega^m \tag{5.28}$$

Thus by fitting the frequency dependence of the dielectric spectrum to a proper function, it is possible to correct for the background in the dielectric spectrum at low and high frequencies in order to correctly characterize the dielectric parameters.

In the present work, the dielectric parameters of all the relaxation modes present in the chiral liquid crystal mixtures have been calculated by fitting eq. (5.28) on the experimentally obtained results, with the Origin software. The software finds the mean deviation of the dielectric spectrum from the measured values minimizes it and finds the optimum parameters and also displays the fitted curve relative to the experimental curve.

5.6. Results and discussion

5.6.1 Phase transitions and morphological behaviour of CNT dispersed SmC LC*

The phase sequence and transition temperature of undoped SmC* material, were

$$\text{Cryst} \xrightarrow{-20^oC} \text{SmC*} \xrightarrow{61^oC} \text{SmA} \xrightarrow{73^oC} \text{N*} \xrightarrow{83^oC} \text{Isotropic}$$

And the variation in phase transition temperatures after dispersing 0.05% and 0.1% CNT respectively, as observed through optical polarizing microscopy and thermal studies through DSC (fig. 5.10), was found to be

$$\begin{array}{lllllll} \text{SmC*} & \xrightarrow{62^oC} & \text{SmA} & \xrightarrow{75^oC} & \text{N*} & \xrightarrow{95^oC} & \text{Isotropic} \\ \text{SmC*} & \xrightarrow{68^oC} & \text{SmA} & \xrightarrow{80^oC} & \text{N*} & \xrightarrow{105^oC} & \text{Isotropic} \end{array}$$

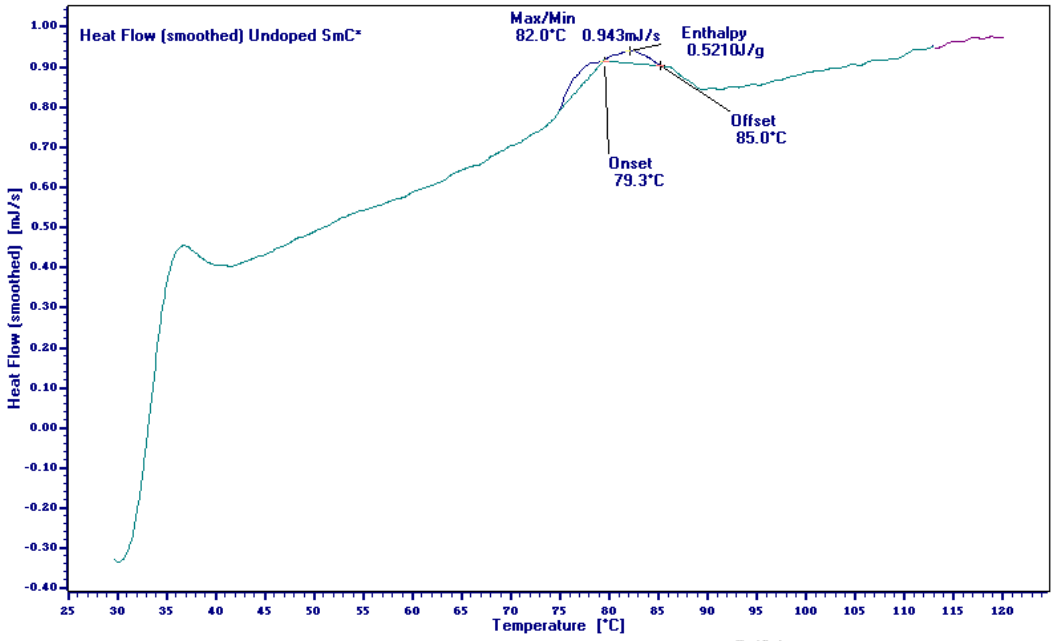
Heat Flow (smoothed) Undoped SmC*
Max/Min
82.0°C 0.943mJ/s
Enthalpy
0.5210J/g
Offset
85.0°C
Onset
79.3°C
Heat Flow (smoothed) [mJ/s]
Temperature [°C]

(a)

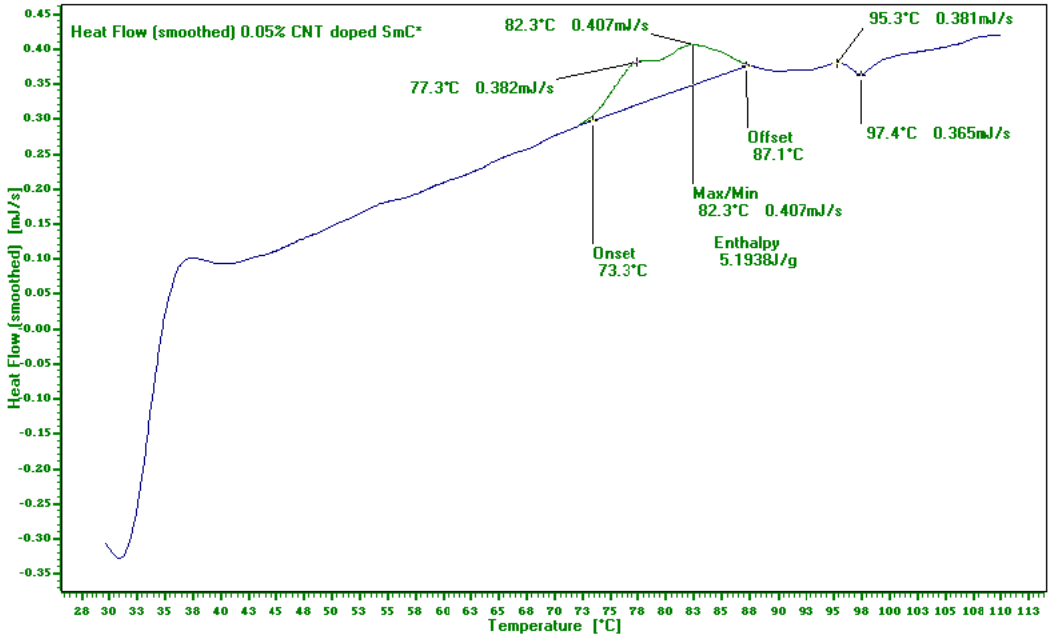
Heat Flow (smoothed) 0.05% CNT doped SmC*
82.3°C 0.407mJ/s
95.3°C 0.381mJ/s
77.3°C 0.382mJ/s
Offset
87.1°C
97.4°C 0.365mJ/s
Max/Min
82.3°C 0.407mJ/s
Enthalpy
5.1938J/g
Onset
73.3°C
Heat Flow (smoothed) [mJ/s]
Temperature [°C]

(b)

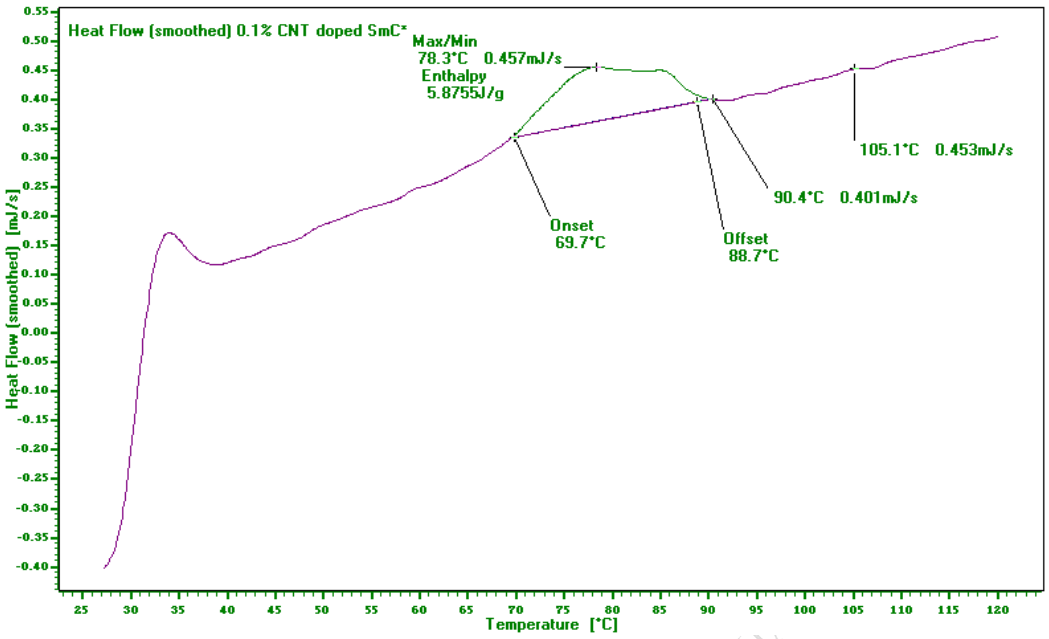

(c)

Fig. 5.10 DSC thermograms for (a) undoped SmC* (b) 0.05% (wt/wt) CNT-SmC* composite (c) 0.1% (wt/wt) CNT-SmC* composite

The geometry of the molecular structure in a SmC* phase and its modified behaviour with CNT dispersion is shown in fig. 5.11(a,b). We expected the effective SmC* molecule-CNT coupling in the layers as depicted. The corresponding optical textures of the SmC* mixture with 0.1%CNT dispersed in SmC* after sonification. We observed that the focal conic SmC* texture is retained and CNT has got uniformly dispersed.

Fig. 5.11 shows evolution and growth of liquid crystal texture with 0.05% CNT while cooling the sample from isotropic phase to room temperature under crossed polarizer. The micro texture at 92^0C was dark suggesting that the CNT-SmC* mixture is in the isotropic phase. On cooling, birefringent domains appeared at 90^0 C, which continue to grow, stabilize and then coalesce at about 82 ^{0}C. The preferential alignment after domains was observed in the SmC* phase fig. 5.12[d, e]. Similar behaviour was seen after dispersing 0.1% CNT in the liquid crystal matrix.

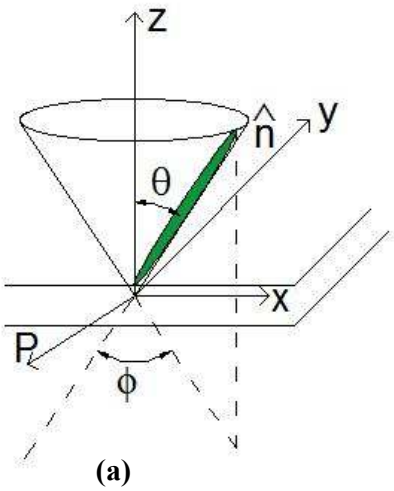

(a)

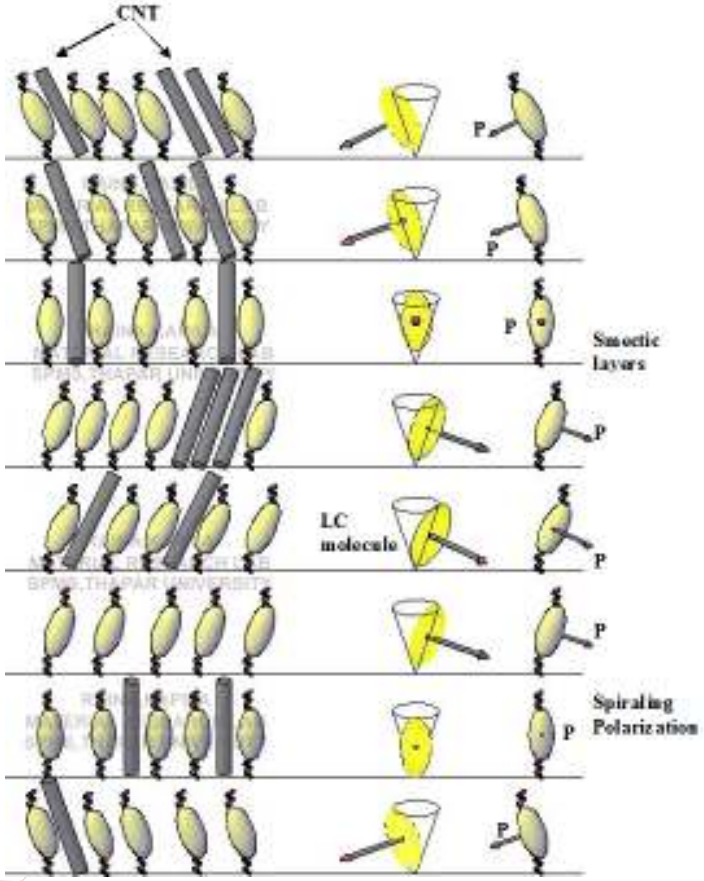

(b)

Fig. 5.11 (a) Basic geometry of undoped SmC* phase showing the spiraling of the director around z – axis (b) model representing the low concentration CNT dispersed SmC*. The ovals represent liquid crystal molecules and the cylinders CNTs.

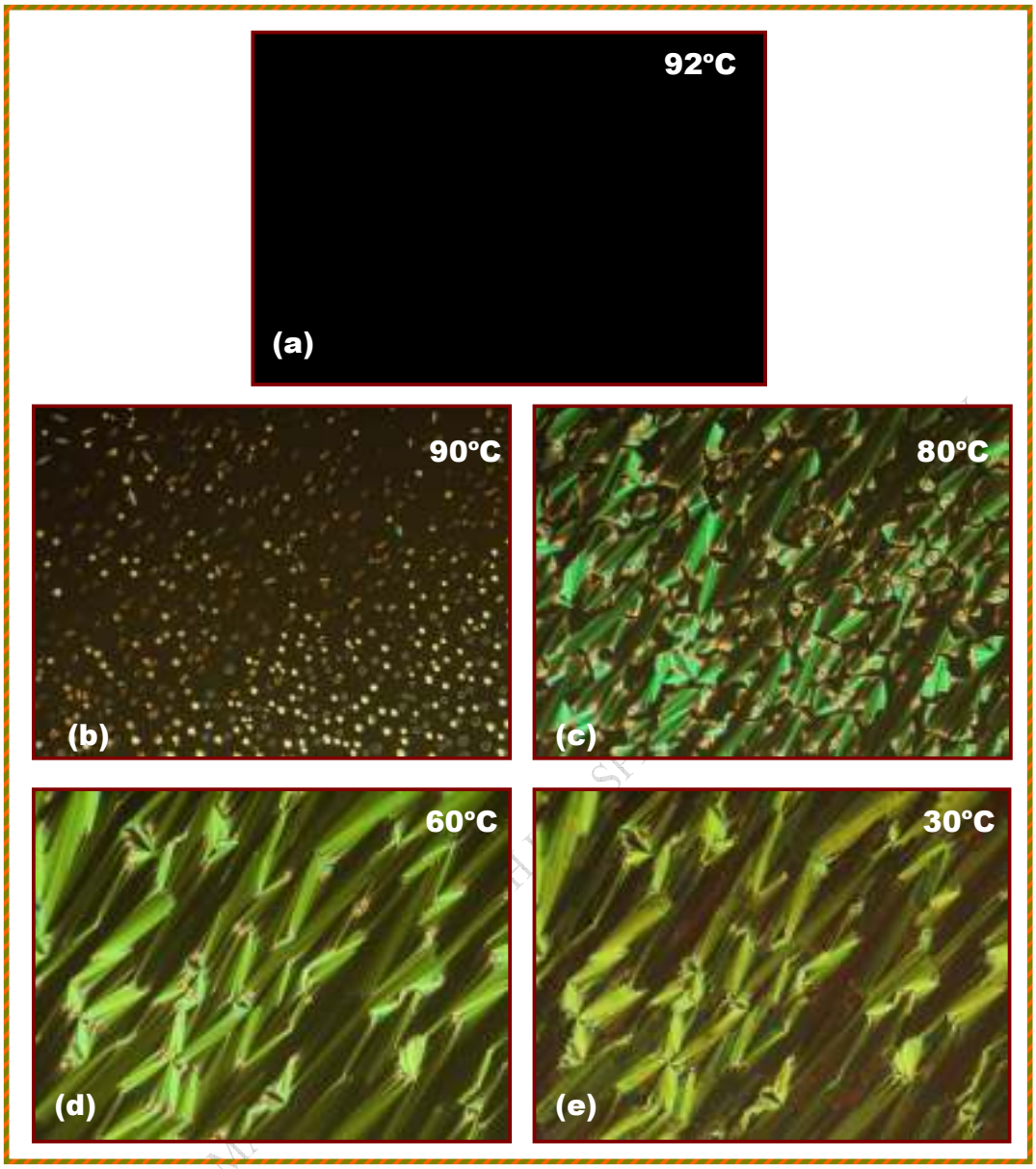

Fig. 5.12 Micrographs showing morphological evolution during cooling from the 90°C to 30°C for 0.05 % (wt/wt) CNT-SmC* composite

5.6.2. Opto-electronic responses of dispersed systems

The electro optic profile of pure and CNT doped SmC* liquid crystal samples at reduced temperature $\Delta T = -30^{o}C$ ($\Delta T = T - T_{C^*-A}$ where T_{C^*-A} is the temperature of SmC*- SmA phase transition) is shown in fig. 5.13. We noticed that the CNT doped liquid crystals showed higher transmission as compared to pure system. The switching voltage in CNT doped was 0.5 V/μm however for the pure material the switching voltage was about 0.9 V/μm. It shows that CNT doping can significantly reduce the threshold voltage (by about 40%).

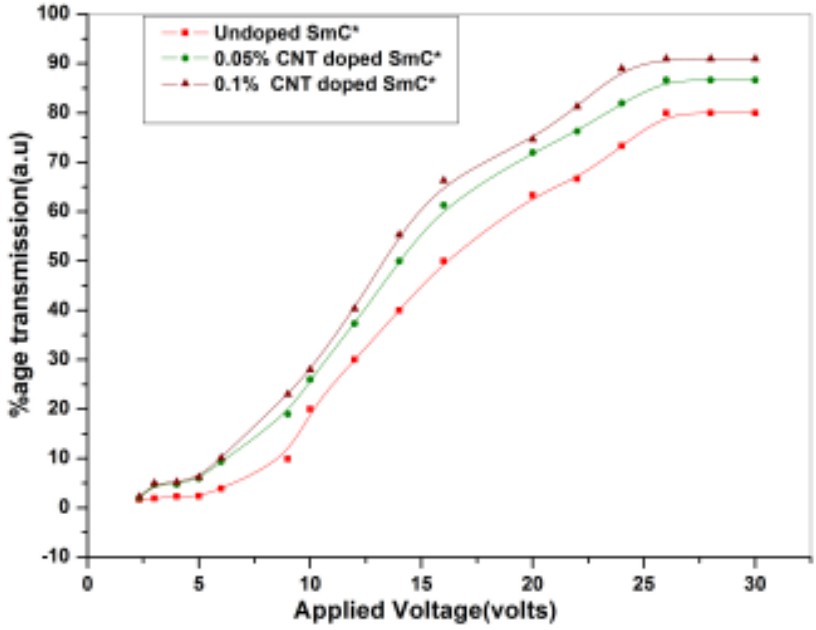

Fig. 5.13 Transmission as function of applied voltage at reduced temperature ($\Delta T = -30^{o}C$) for undoped SmC* and CNT dispersed SmC*

5.6.3. *Dielectric responses*

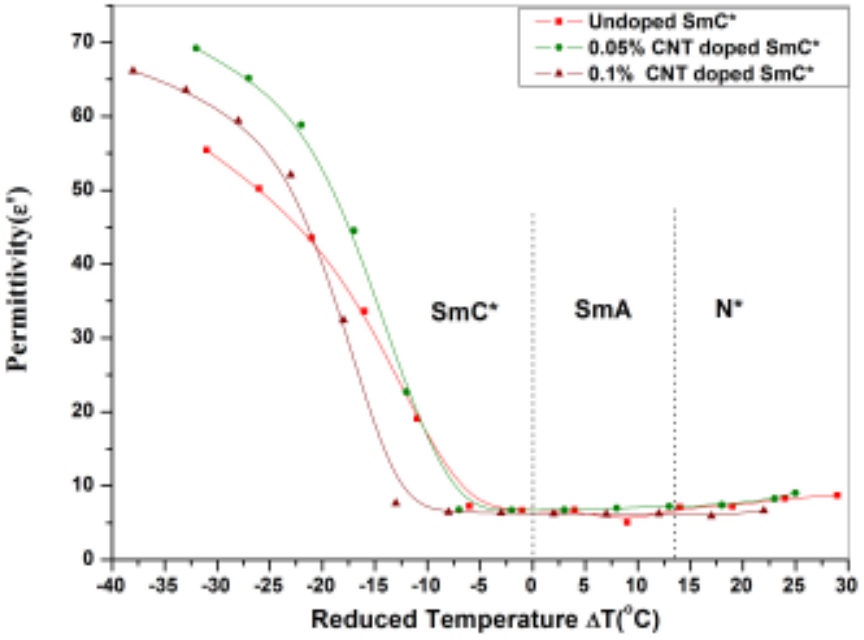

Fig. 5.14 Dielectric permittivity ε' as a function of reduced temperature (ΔT) for undoped SmC* and CNT dispersed SmC*, at 50 Hz.

Fig. 5.14 shows the variation of permittivity as a function of temperature in undoped and CNT doped sample. We observed that the permittivity of the composite was higher for 0.05% doped sample throughout the temperature range where as in the 0.1% doped sample the permittivity shows a crossover at $\Delta T = -20^{o}C$. It reflects on the response of CNT systems to the temperature. At high temperature, the thermal agitation likely became more dominant over intermolecular interactions which resulted in collisions between molecules and hence randomization of dipoles, resulting in decreased dielectric permittivity.

Similar behaviour was observed for the variation of as a function of frequency as in fig. 5.15. About 25% increase in was noticed after CNT dispersion at 100Hz and this change narrowed down at higher frequencies. This low frequency variation indicates the dominant gold stone mode (GM) behaviour of dielectric spectra.

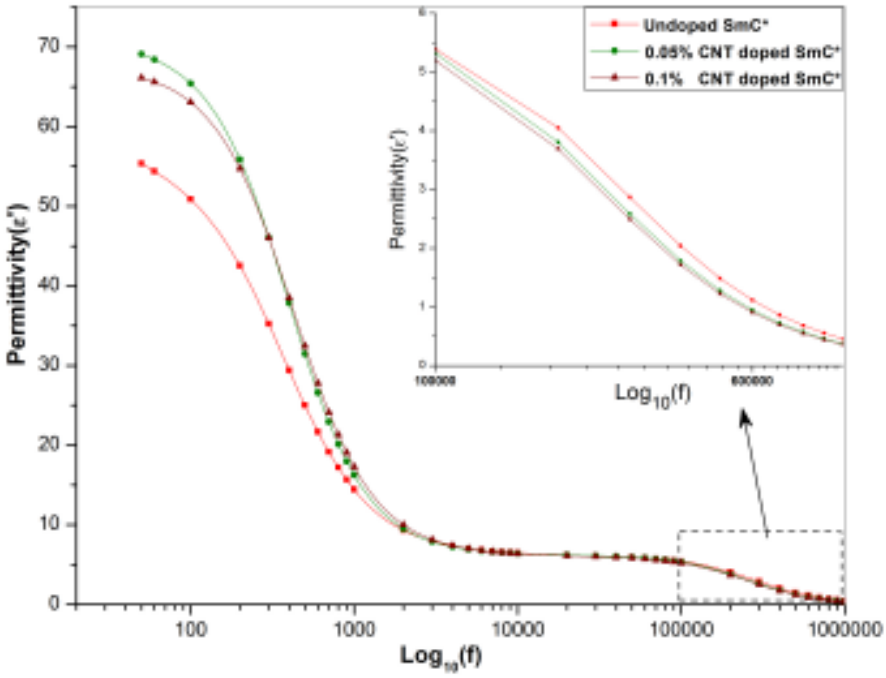

Fig. 5.15 Dielectric permittivity ε' as a function of frequency for undoped SmC* and CNT dispersed SmC*, at reduced temperature (ΔT= -30°C). Inset shows the high frequency relaxation process.

5.6.4 Effect of Bias voltage

The effects of bias voltage on the GM in the form of dispersion and absorption behaviour for undoped and 0.1%CNT doped SmC* are shown in fig. 5.16(a) and fig. 5.16(b) respectively. In SmC*, GM is due to the fluctuation of the azimuthal angle and soft mode is due to the suppression of tilt angle . The contribution of GM mode is maximum when the helix is undistorted, distortion of helix due to applied electric field (E) & polarization (P) coupling leads to the suppression of GM contribution and hence change in permittivity. We saw that the loss was highest without any bias (0V) voltage but decreased with increase in bias voltage (10V) in the 0.1% CNT dispersed SmC*. The coupling between chiral smectic c molecules and the CNTs also influence the suppression of GM contribution which in turn could affect the helix unwinding and results in loss. The residual permittivity also give rise to domain mode corresponding to relaxation peak at 500Hz and soft mode corresponding to 500 KHz as shown in fig. 5.16(b). The appearance of loss peak at high frequency is indicative of conductivity in

the high frequency region and is attributed by $_{AC}=\ _{o}\ (\ )$, where o is the electric constant, ( ) is dielectric loss at given frequency and is the cyclic frequency, resulting in dissipation.

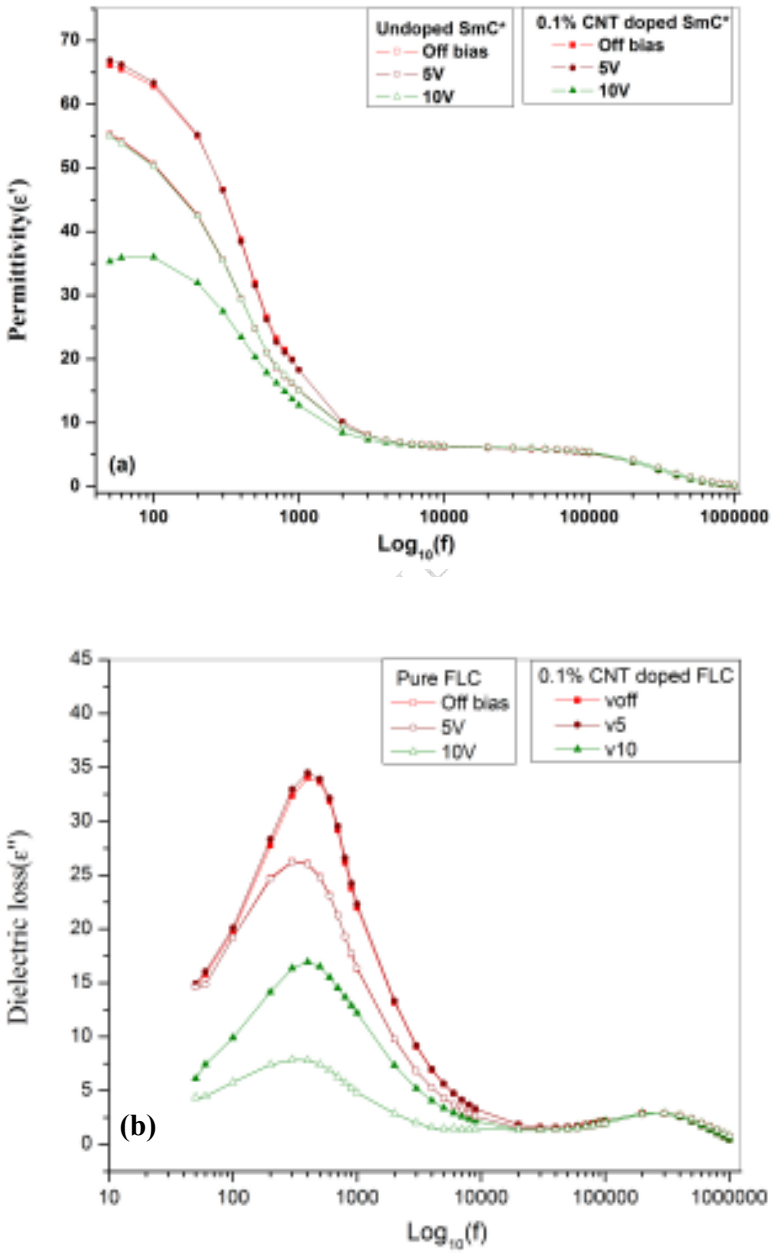

Fig. 5.16 Permittivity as a function of frequency at different bias voltages for undoped SmC* and 0.1% CNTs dispersed SmC* (a) dispersion (b) absorption curves

5.6.5 Relaxation spectra

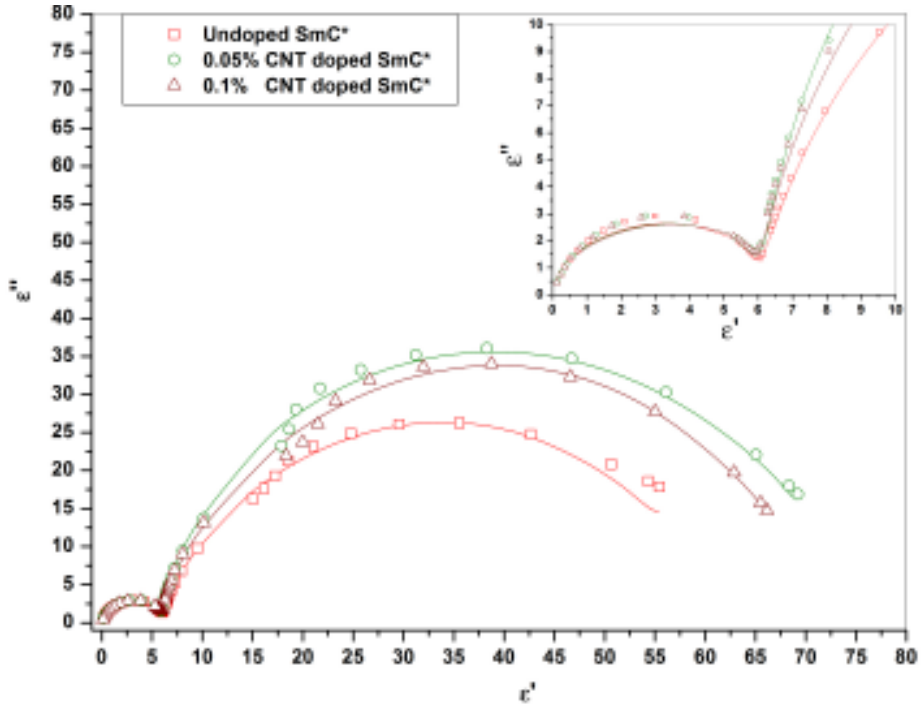

Fig. 5.17 Cole-Cole plots for the Goldstone Mode and Soft Mode at ΔT= -30°C for undoped SmC* and CNT dispersed SmC*. Open symbols represent experimental data and solid lines are the best fit corresponding to eq. (5.28) Inset shows the high frequency relaxation process.

The smaller semi- circle in the fig. 5.17 represents the relaxation due to the Soft Mode (SM) (inset) where as, bigger semi circle represents the contribution due to Goldstone Mode. In the vicinity of the Tc*-A, SM follow the Currie-Weiss law. It was found that dielectric strength for GM increased for CNT doped SmC*. The magnitude of relaxation frequency for GM was found to be 300Hz for Pure SmC* and 400Hz for CNT doped SmC*. It implies that the molecular motion responsible for the fluctuation of the azimuthal angle in the pure SmC* is slower than that of the CNT doped SmC*. It is a consequence of the fact that the presence of CNTs in SmC* layers hinder the azimuthal fluctuations.

References

[1] A. Saupe, Mol. Cryst. Liq. Cryst. **7**, 59 (1969)

[40] R. B. Meyer, L. Leibert, L. Strzelecki and P. Keller, *J. Phys. Lett. (Paris)* **36**, *LC* **69** (1975)

[41] K. K. Raina and Jasjit K. Ahuja, *Mol. Cryst. Liq. Cryst.* **325,** 157 (1998)

[42] G. Sumana and K. K. Raina *Curr. Appl. Phys.* **19,** 588 (2005)

[43] S. Khosla and K. K. Raina, *J. of Physics and Chemistry of Solids* **65(6)**, 1165 (2004)

[44] P. Malik and K. K. Raina, *Optical Materials* **27** , 613 (2004)

[45] E. Matsui and A. Yasuda, *Phys. Rev. E*, **56**, 600 (1997)

[46] S. Kaur, S. P. Singh, A. M. Biradar, A. Choudhary and K. Sreenivas, *Appl. Phys. Lett*., 91, 0231201 (2007)

[47] A. V. Koval'chuk, T.N Koval'chuk, *Mol. Cryst. Liq. Cryst.* **496(1),** 269 (2008)

[48] H. H Liang, Y. Z. Xiao, F. J. Hsh, C. C. Wu and J. Y. Lee, *Liquid Crystals*, **37(3)**, 255 (2010)

[49] J. P. F. Lagerwall and G. Scalia, *J. Mater. Chem.* **18**, 2890 (2008)

[50] I. Dierking, G. Scalia and P. Morales, *J. Appl. Phys.* **97**, 044309 (2005)

[51] M. Endo, T. Hayashi, Y. A. Kim and H. Muramatsu, *Jap. Journ. of Appl. Phys*, **45,** 4883 (2006)

[52] H. Y. Chen, N. A. Clark and W. Lee, *Appl. Phys. Lett*, **90**, 033510 (2007)

[53] S. Y. Jeon, S. H. Shin, S. J. Jeong, S. H. Lee, S. H. Jeong, Y. H. Lee, H. C. Choi and K. J. Kim, *Appl. Phys. Lett,* **90**, 121901 (2007)

[54] W. Lee, C. Yu. Wang, and Yu C. Shih, *Appl. Phys. Lett.* **85 (4)**, 513-515 (2004)

[55] C. Y Huang, C.Y. Hu, H. C. Pan and K. Y. Lo, *Jpn. J. Appl. Phys.* **44 (11)**, 8077-8081 (2005).

[56] In-Su Baik, S. Y. Jeon, S. H. Lee, K. A. Park, S. H. Jeong, K. H. An and Y. H. Lee, *Appl. Phys. Lett.* **87**, 263110 (2005)

[57] F. V. Podgornov, A. M. Suvorova , A. V. Lapanik , W. Haase, *Chemical Physics Letters* **479,** 206–210(2009)

[58] D. Sharma, S. Tyagi and K. K. Raina, *Advanced Materials Research Transtech* , Switzerland **67**,167-172(2009)

[59] J. Prakash, A. Choudhary, D. S. Mehta and A. M. Biradar, *Phys. Rev. E* **80**, 012701 (2009)

[60] P. Arora, A. Mikulko, F. Podgornov, W. Haase, *Mol. Cryst. Liq. Cryst.* **502**, 1 (2009)

[61] S. Iijima. *Nature*, **354**, 56 (1991)

[62] C. Dekker, *Physics Today*, **52**(5), 22(1999)

[63] J. W. Mintmire, B. I. Dunlap and C. T. White, *Phys. Rev. Lett.,* **68**, 631 (1992)

[64] R. Saito, M. Fujita, G. Dresselhaus and M. S. Dresselhaus, *Appl. Phys. Lett.,* **60**, 2204 (1992)

[65] M. Rahman and W. Lee , *J. Phys. D: Appl. Phys.* **42**, 063001(2009)

[66] M. Endo, K. Takeuchi, S. Igarashi, K. Kobori, M. Shiraishi, H. W. Kroto, *J. Phys. Chem. Solids,* , **54**, 1841(1993)

[67] D. T. Colbert, J. Zhang, S. M. McClure, P. Nikolaev, Z. Chen, J. H. Hafner, D. W. Owens, P. G. Kotula, C. B. Carter, J. H. Weaver, A. G. Rinzler, R. E. Smalley, *Science*, **266**, 1218(1994)

[68] P. Avouris, *Chemical Physics*, **281(2-3)**, 429 (2002)

[69] P. M. Ajayan and O. Z. Zhou, *Carbon Nanotubes*, **80**, 391(2001)

[70] G. Dresselhaus and P. Avouris, Carbon Nanotubes Synthesis, Structure, Properties and Applications, Springer Publication (1996)

[71] M. Dresselhaus, *Nature,* **432**, 959(2004)

[72] http://en.wikipedia.org/wiki/carbon-nanotubes

[73] H. Duran, B. Gazdecki, A. Yamashita and T. Kyu, *Liq. Cryst*. **32**, 815 (2005)

[74] S. Y. Jeon, Kyung Ah Park, In-Su Baik, S. J. Jeong, S. H. Jeong, Kay Hyeok An, S. H. Lee and Y. H. Lee, *Nano: Brief reports and reviews*, **2(1)**, 41 (2007)

[75] R. Basu and G. S. Iannacchione, *Appl. Phys. Lett.* **93**,183105 (2008)

[76] K K Raina, S. Kapila**,** S. Kumari, P Kumar , *International Liquid Crystals Conference (ILLC08) (June, 2008)* Jeju Island, Korea

[77] K. Yoshino, T. Uemoto, Y. Inuishi, *Jap. J. Appl. Phys*., **16**, 571 (1977)

[78] Ph. M. Lagarde, Ph.D. Thesis, University of Paris, Orsay (1982)

[79] T. Carlsson, C. Fillipic, I. Levstik and B. Zeks, *Physical Review A*, **35 (8)**, 3527 (1987)

[80] K. K. Raina, *Mol. Cryst. Liq. Cryst.,* **151**, 211 (1987)

[81] A. K. Gathania, B. Singh and K. K. Raina, *J. Phys. Condens. Matter*, **11**, 3813(1999)

[82] J. K. Ahuja, Ph.D Thesis, Thapar Institute of Engineering and Technology (2000)

[83] J. W. Goodby and N. A. Clark, *Ferroelectric Liquid Crystals*, Gordan and Breach, Science publishers-New York (1991)

[84] C. Fillipic, T. Carlsson, A. Levstik, B. Zeks and R. Blinc, *Physical Review A*, **38(1**1), 5833(1988)

[85] K. S. Cole and R. H. Cole, *J. Chem. Phys*., **9**, 341(1941)

[86] V. V. Daniel, *Dielectric Relaxations*, Academic Press, New York (1967)

[87] A. M. Birader, S. Wrobel and W. Haase, *Phys. Ev. A*, **39(5),** 2693(1989)

[88] S.Wrobel, S Hiller, M.Pfeiffer, M. Marzec, W. Haase, R. Twig and K. Betterton, *Liquid Crystal* , **18(1),** 21(1995)

[89] S. Hiller, A.M. Biradar, S. Wrobel and W. Haase, *Physical Review E*, **53(1),** 641(1996)

[90] K. K. Raina and J. K. Ahuja, *Jpn. J. Appl. Phys*., **39**,4076 (2000)

[91] R. Singh, V. K. Aggarwal, K. K. Raina and B. Bhadur, *Curr. Appl. Phys*,**5**,588 (2005)

[92] T. P. Majumder, S S Roy and S. K. Roy, *Mol. Cryst. Liq. Cryst*., **265**, 577, (1995)

[93] S. L. Srivastava and R. Dhar, *Indian J. Pure and Appl. Phys*., **29,** 745(1991)

[94] F. Gouda, K. Skarp and S. T. Lagerwall, *Ferroelectrics*, **113**, 165(1991)

Conclusion

This chapter summarizes the important findings and results obtained from chiral liquid crystal systems as discussed in chapter 3, 4 and 5. The future possibilities have been explored on the basis of above work for both basic and applied research point of view.

The chiral liquid crystal systems have been studied in detail and the main results thus concluded through the analysis of the experimental data on the chiral liquid crystal systems are summarized in brief as follows:

- The role of chiral dopant on helix dynamics under electric field has been studied in detail, via dynamic pattern formation and the results show that the gratings form in two distinct ways depending upon thickness to pitch ratio, d/p i.e. chiral dopant concentration. For a d/p = 0.62 the formed cholesteric gratings belong to the Dv.M type. For d/p = 1.56 the Dv.M and Gr.M types appear simultaneously but the latter, initiating near the edges and the surface defects, before elongating in the direction of rubbing dominated.

- It was noticed that with the induction of chirality, the response time of the chirality induced sample was faster in comparison to that of pure nematic liquid crystal mixture. The response time reduced by almost 2 fold with addition of about 10% chiral dopant.

- Thermochromic effects gave very good results. It was observed that about 1% chiral doping in nematic liquid crystal mixture showed active response over the wide temperature range 30^{o}C - 94^{o}C. It was shown that the system can sustain colour over the period of 2 years and these colours were stable during this period.

- Novel side chain chiral liquid crystal polymers of high molecular weight has been synthesized and found to show chiral nematic phase from room temperature to 67^{o}C. Chiral doping resulted in decrease in melting point of the material. The optical transmission of the polymers was found to increase with temperature and the addition of chiral doping. The refractive index of the materials (1.63 and 1.57) were found to be in the range of most commercial polymers suitable for switchable windows and the application range can be further enhanced by preparing polymer dispersed liquid crystal films.

- Our results on chiral smectic C liquid crystal mixture, containing low concentration of carbon nanotubes, indicate the increase in transition temperature of the virgin material by about 5^{o}C after CNT doping. CNT dispersion strongly influenced the optical transmission and reduced threshold voltage by about 40%. At lower temperature and frequency, permittivity increased by about 27% on dispersing CNT in chiral smectic c matrix. No significant variation in dielectric permittivity was noticed at high temperature and frequencies. The GM relaxation frequency was changed from 300 Hz to 400 Hz after CNT doping where as soft mode frequency was unchanged. On CNT dispersion with high bias field (10V) the domain mode is observed corresponding to relaxation peak at 500Hz.

List of publications:

Papers in referred Journals/Reviewed papers

a) Referred journals

1. Thermochromic behaviour of a novel nematic liquid crystal mixture: Effects of chiral doping, **Shikha Kapila** and K. K. Raina, Int. J of M Phy B, (accepted, at press).
2. Effects of CNTs opto electronic and opto dielectric responses in chiral smectic C liquid crystal, K K Raina and **Shikha Kapila** (communicated).
3. Dynamic pattern formation in novel chiral nematic liquid crystal mixture: Electric field effects, **Shikha Kapila** and K. K. Raina (communicated).
4. Morphological and electro-optical responses of novel chiral nematic liquid crystal mixture, **Shikha Kapila** and K. K. Raina (communicated).

b) Reviewed conference full papers

1. Synthesis and characterization of novel acrylate based side chain ferroelectric Liquid Crystal Polymers, G. Sumana, K. K. Raina, P. Malik, P. Kumar, **S. Kapila**, P. Sharma, A. Bubnov and Chandra Prakash, Ferroelectrics and Dielectrics: Proc. of XIII-National Symposium on Ferroelectrics and Dielectrics held at University of Delhi (Nov.04), 55-58, Eds. R. P. Tandon, Allied Publishers, 2004, ISBN 81-7764-701-6
2. Characterization of chirality induced liquid crystal mixture, **Shikha Kapila**, K.K. Raina, Advances in Technologically Important Crystals: Proc. of National Conference on Advances in Technologically Important Crystals (NC_ATIC) held at University of Delhi (Oct 06), 198-203, Eds. Binay kumar and R. P. Tandon, Macmillan India Ltd, 2006, ISBN 10: 1403-93152-6
3. Studies on the effect of chiral doping on synthesized side chain liquid crystal polysiloxanes , G.Sumana, **Shikha Kapila** and K.K.Raina , Electroactive polymers : materials & devices, Vol II : Proc. 2nd International Conference on Electroactive Polymers held at Goa (Feb 07), India 189-195,Eds. S. A. Hashmi, Amita Chandra and Amreesh Chandra, Allied Publishers, 2007, ISBN: 8184242468.

Conference / Proceedings (International/National)

1. Electro-optics of chirality induced nematic liquid crystal mixture , **Shikha Kapila**, K.K. Raina, International Conference on Liquid Crystals(ICLC06), 5-8 Dec 06, Mumbai University
2. Influence of chiral doping on the optical behaviour of a liquid crystal mixture: a key to colour sensor **Shikha Kapila**, K.K. Raina, NCETEM-2007,Thapar University ,India
3. Morphological and Dielectric behaviour of CNT dispersed FLC composite, K K Raina, Ms. **Shikha Kapila,** Ms. Simta K, and Dr. Pankaj Kumar , International Liquid Crystals Conference (ILLC08) (June, 2008) Jeju Island, Korea

4. Droplet orientation and its Morphology in polymer dispersed ferroelectric liquid crystal composite films. K K Raina and **Shikha Kapila**, International Conference on Advances in Polymer Technology-APT '08(Sept,08), CUSAT, Kochi, India
5. Chirality induced liquid crystal mixture as optical sensor, **Shikha Kapila** and K.K.Raina, International symposium on Nanostructured Materials (ISNM-09) (Oct 28-29) Kanya Maha Vidyalaya, Jalandhar (Punjab)

Conference/Symposium/Seminar Attended

1. National Seminar on Ferroelectrics and Dielectrics XIII, University of Delhi, New Delhi, Nov. 23-25 , 2004
2. Advanced Condensed Matter Physics, SPMS, TIET Patiala, Feb. 11-12, 2005
3. Seminar on "RECENT TRENDS IN LIQUID CRYSTAL RESEARCH", India-United Kingdom science networks, Raman Research Institute, Bangalore, Nov. 14-16, 2005
4. National Seminar on Recent Trends in Polymer Science and Technology, SLIET Longowal, Dec. 10-11, 2005
5. National Conference on Advances in Technologically Important Crystals (NC_ATIC), University of Delhi, New Delhi, Oct. 12-14 , 2006
6. International conference on Liquid Crystal, Uni. of Mumbai, Dec. 5-8, 2006
7. National conference on emerging trends in Engineering Materials, SPMS, TIET Patiala, Feb.1-3, 2007
8. International symposium on Nanostructured Materials (ISNM-09), Kanya Maha Vidyalaya, Jalandhar (Punjab), Oct. 28-29, 2009